

DISSERTATION

INTEGRATION OF GRAPHICAL, PHYSICS-BASED, AND MACHINE LEARNING METHODS FOR
ASSESSMENT OF IMPACT AND RECOVERY OF THE BUILT ENVIRONMENT FROM WIND HAZARDS

Submitted by

Stephanie F. Pilkington

Department of Civil and Environmental Engineering

In partial fulfillment of the requirements

For the Degree of Doctor of Philosophy

Colorado State University

Fort Collins, Colorado

Summer 2019

Doctoral Committee:

Advisor: Hussam Mahmoud

Bruce Ellingwood

John van de Lindt

Sammy Zahran

Therese McAllister

Sara Hamideh

Copyright by Stephanie F. Pilkington 2019

All Rights Reserved

ABSTRACT

INTEGRATION OF GRAPHICAL, PHYSICS-BASED, AND MACHINE LEARNING METHODS FOR ASSESSMENT OF IMPACT AND RECOVERY OF THE BUILT ENVIRONMENT FROM WIND HAZARDS

The interaction between a natural hazard and a community has the potential to result in a natural disaster with substantial socio-economic losses. In order to minimize disaster impacts, researchers have been improving building codes and exploring further concepts of community resilience. Community resilience refers to a community's ability to absorb a hazard (minimize impacts) and "bounce back" afterwards (quick recovery time). Therefore, the two main components in modeling resilience are: the initial impact and subsequent recovery time. With respect to a community's building stock, this entails the building damage state sustained and how long it takes to repair and reoccupy that building. In modeling these concepts, probabilistic and physics-based methods have been the traditional approach. With advancements in artificial intelligence and machine learning, as well as data availability, it may be possible to model impact and recovery differently.

Most current methods are highly constrained by their topic area, for example a damage state focuses on structural loading and resistance, while social vulnerability independently focus on certain social demographics. These models currently perform independently and are then aggregated together, but with the complex connectivity available through machine learning, structural and social characteristics may be combined simultaneously in one network model. The popularity of machine learning predictive modeling across multiple different applications has risen due to the benefit of modeling complex networks and perhaps identifying critical variables

that were previously unknown, or the mechanism behind how these variables interacted within the predictive problem being modeled.

The research presented herein outlines a method of using artificial neural networks to model building damage and recovery times. The incorporation of graph theory to analyze the resulting models also provides insight into the “black box” of artificial intelligence and the interaction of socio-technical parameters within the concept of community resilience. The subsequent neural network models are then verified through hindcasting the 2011 Joplin tornado for individual building damage and the time it took to repair and reoccupy each building. The results of this research show viability for using these methods to model damage, but more research work may be needed to model recovery at the same level of accuracy as damage. It is therefore recommended that artificial neural networks be primarily used for problems where the variables are well known but their interactions are not as easily understood or modeled. The graphical analysis also reveals an importance of social parameters across all points in the resilience process, while the structural components remain mostly important in determining the initial impact. Final importance factors are determined for each of the variables evaluated herein. It is suggested moving forward, that modeling approaches consider integrating how a community interacts with its infrastructure, since the human components are what make a natural hazard a disaster, and tracing artificial neural network connections may provide a starting point for such integration into current traditional modeling approaches.

ACKNOWLEDGEMENTS

I would like to express my sincerest gratitude to my advisor, Dr. Hussam Mahmoud, for his continued support, encouragement, and motivation during this research and the pursuance of my PhD. I will forever appreciate his generosity in providing me with the opportunity to work within this topic area, while allowing me the creative and intellectual freedom to explore new ideas. I would also like to express my thanks to my additional committee members, Dr. Bruce Ellingwood, Dr. John van de Lindt, Dr. Sammy Zahran, Dr. Therese McAllister, and Dr. Sara Hamideh for their support and contributions in the progression of this research.

I greatly appreciate and sincerely thank Dr. Andrew Curtis and Dr. Steve Smith for their assistance with the Joplin data. The hindcasting analysis could not have been completed without their generosity in sharing their gathered data.

I would like to also personally thank my family and friends for their unwavering support and reassurance in this endeavor. I am truly fortunate to have such inspirational parents who will continually support me in pursuance of difficult goals and to have a brother in my life that is always willing to lend a hand. Without these individuals, I would not be where I am today.

TABLE OF CONTENTS

ABSTRACT ii

ACKNOWLEDGEMENTS iv

LIST OF TABLES viii

LIST OF FIGURES x

CHAPTER 1 INTRODUCTION 1

 1.1 STATEMENT OF PROBLEM 1

 1.2 OBJECTIVES AND SCOPE OF RESEARCH 2

CHAPTER 2 BACKGROUND AND LITERATURE REVIEW 6

 2.1 NATURAL HAZARDS 6

 2.1.1 *Natural Hazards as Disasters* 6

 2.1.2 *Meteorology of Severe Weather* 10

 2.2 THE SOCIO-TECHNICAL ASPECT OF DISASTERS 13

 2.2.1 *Engineering and Construction parameters Contributing to Disasters* 14

 2.2.2 *Social parameters Contributing to Disasters* 18

 2.3 COMMUNITY RESILIENCE 23

 2.3.1 *Conceptual Background* 23

 2.3.2 *Current Modeling Approaches* 26

 2.4 PHYSICS-BASED APPLICATIONS IN IN-CORE FOR MODELING COMMUNITY IMPACT
AND RECOVERY FROM NATURAL HAZARDS 29

 2.4.1 *Modeling Building Damage State* 29

 2.4.2 *Modeling Building Recovery* 33

 2.5 MACHINE LEARNING APPLICATION 35

2.5.1	<i>Conceptual Overview</i>	36
2.5.2	<i>Current Applications</i>	37
2.6	COMPLEX NETWORKS.....	39
2.6.1	<i>Conceptual Overview</i>	39
2.7	SUMMARY	42
CHAPTER 3 MEANS AND METHODS		44
3.1	ARTIFICIAL NEURAL NETWORKS	44
3.1.1	<i>Using Mathematical Principles to Teach Machines</i>	46
3.1.2	<i>Proposed Variations</i>	50
3.1.3	<i>Data Collection</i>	56
3.1.4	<i>Conclusion</i>	68
3.2	GRAPH THEORY	68
3.2.1	<i>Overview</i>	69
3.2.2	<i>Analytical Concepts</i>	70
3.2.3	<i>Conclusions</i>	72
3.3	VALIDATING MODEL RESULTS THROUGH HINDCASTING.....	72
3.3.1	<i>Assigning Building Data to Joplin Community</i>	73
3.3.2	<i>Data Assimilation of Known Results from the Joplin Tornado</i>	75
CHAPTER 4 RESULTS AND MAIN OBSERVATIONS		81
4.1	SYNOPSIS	81
4.2	IMPACT MODELING	81
4.2.1	<i>Training Algorithm Variations</i>	82
4.2.2	<i>Input Variable Variations</i>	87
4.2.3	<i>Graphical Network Analysis</i>	90
4.2.4	<i>Hindcasting Damage from the 2011 Joplin Tornado</i>	97

4.3	RECOVERY	103
4.3.1	<i>Training Algorithm Variations</i>	104
4.3.2	<i>Input Variable Variations</i>	108
4.3.3	<i>Graphical Network Analysis</i>	112
4.3.4	<i>Hindcasting Recovery from the 2011 Joplin Tornado</i>	118
4.4	THE JOPLIN DATA	120
4.5	SUMMARY	129
CHAPTER 5 IMPLICATIONS OF RESULTS		131
5.1	THE USE OF ARTIFICIAL NEURAL NETWORKS FOR MODELING SOCIO-TECHNICAL INTERACTIONS	131
5.2	THE USE OF GRAPH THEORY TO ANALYZE ARTIFICIAL NEURAL NETWORKS	133
5.3	SOCIO-TECHNICAL ASPECTS OF THE 2011 JOPLIN TORNADO DATA AS IT RELATES TO THE ANN ANALYSES	138
5.4	SUMMARY OF FINDINGS AND LIMITATIONS.....	140
CHAPTER 6 CONCLUSION AND FUTURE RESEARCH.....		146
6.1	SUMMATION	146
6.2	CONTRIBUTION TO COMMUNITY RESILIENCE AND INTERPRETING ARTIFICIAL NEURAL NETWORKS	147
6.3	FUTURE APPLICATIONS.....	148
6.4	FUTURE RESEARCH.....	149
REFERENCES		151
APPENDIX A: ARTIFICIAL NEURAL NETWORK VARIABLES.....		161
APPENDIX B: ITERATIVE ANALYSIS RESULTS FOR MODIFYING TRAINING ALGORITHM AND MODEL INPUTS		167

LIST OF TABLES

Table 2-1 Frequency of Hazards (Bryant 2005; Centre for Research on the Epidemiology of Disasters 2018).....	7
Table 2-2 Worldwide Cost of Natural Hazards in USD at the end of relevant time frame (Bryant 2005; Centre for Research on the Epidemiology of Disasters 2018).....	7
Table 2-3 Deaths Resulting from Natural Hazards (Bryant 2005; Centre for Research on the Epidemiology of Disasters 2018)	8
Table 2-4 The Enhanced Fujita Scale (McDonald 2002).	9
Table 2-5 The 11 SoVI variables (Cutter et al. 2003).	20
Table 2-6 The 15 Social Vulnerability census variables (Flanagan et al. 2011).	22
Table 2-7 Community building portfolio archetypes (Memari et al. 2018).....	30
Table 2-8 REDiTM (Almufti and Willford 2013) Placards following a disaster an approximate corresponding damage state (Memari et al. 2018)	33
Table 3-1 Learning Algorithm Variations for updating weights and biases.	50
Table 3-2 Conjugate Gradient Based Training Algorithms	53
Table 3-3 List of variables and associated models that contain each. (Blue shading indicates current factors considered and green indicates new factors to combine. Key images are various forms of clipart (CanStockPhoto n.d.; ClipartXtras n.d.; Emojipedia n.d.; GalleryYoPriceVille n.d.)).....	56
Table 3-4 Windstorm Damage States for Buildings and EPN.....	58
Table 3-5 Potential Input Variables.....	59
Table 3-6 Recovery States defined by (Curtis and Fagan 2013).....	65
Table 3-7 Additional Input Variables for Recovery ANNs	66
Table 3-8 Cross-Identification of 19 Building Archetypes and ANN Descriptors.....	74

Table 3-9 Cross-Identification of 19 Building Archetypes and ANN Descriptors.....	76
Table 3-10 Converting TIS ranking to DS for wood and steel buildings (Curtis and Fagan 2013; Memari et al. 2018).....	77
Table 3-11 Converting TIS ranking to DS for masonry and concrete buildings (Curtis and Fagan 2013; Memari et al. 2018).....	78
Table 4-1 Total buildings damaged as recorded by Jasper County, MO and the United States Army Corps of Engineers (USACE) with comparison to physics-based fragilities and DM8 ANN results.....	99
Table 4-2 Summation by Building Archetype.....	101
Table 4-3 List of variables for damage and recovery models.....	104
Table 4-4 RM8 and RM2 results by building archetype.....	120
Table 4-5 Summary of BG Recovery by select demographics.....	129
Table 5-1 Calculated importance (I) values for the variables used in DM8, RM8, and RM2 ANNs.....	143
Table A-1 Building code (surface roughness and occupancy) key for ANN inputs.....	161
Table A-2 Building materials and shapes key for ANN inputs.....	165

LIST OF FIGURES

Figure 2-1 Deaths by natural hazard type in the U.S; after: (Borden and Cutter 2008)	8
Figure 2-2 Disaster declarations by type; data from (FEMA n.d.)	9
Figure 2-3 Photograph of SJRMC damage following the 2011 Joplin Tornado, taken by Tiffany Kelley Photography (Kelley 2011).	10
Figure 2-4 Radar images, taken using RadarScope™, of (a) convection structure of a straight-line wind event, (b) radar estimated wind velocity (green color represents motion towards radar tower, and red represents motion away from tower) of a straight- line wind event, (c) convection structure of a tornado-warned (red box) supercell, and (d) wind speed with rotation signature for a tornado warned supercell.	13
Figure 2-5 Instantaneous and simplified external pressure distribution on a low-rise building along with the static load distribution for a bending moment in association with the applied wind load (top corner C); after: (Holmes and Syme 1994).	14
Figure 2-6 Internal pressure of building with a large/dominant opening and how this differs with location of the opening relative to wind direction.	15
Figure 2-7 Neighborhood layout for assessing wind damage; after: Yau et. al. (2011).	17
Figure 2-8 Hazards-of-Place Model of Vulnerability; after: (Cutter 1996)	20
Figure 2-9 Typical resilience curve with its defined characteristics.	24
Figure 2-10 Conceptual relationships between vulnerability, resilience, and adaptive capacity within the concept of hazards, from (Cutter et al. 2008).	25
Figure 2-11 Disaster Resilience of Place Model layout, after (Cutter et al. 2008).	27
Figure 2-12 Building damage state fragilities for (a) light industrial buildings (T7) and (b) heavy industrial building (T8) from Memari et. al. 2018.	32
Figure 2-13 Mean conditional building level restoration process from Lin and Wang (2017b). ...	35

Figure 2-14 Typical multi-layer feed-forward neural network structure with up to ℓ hidden layers.
.....37

Figure 2-15 Visual differences between a (a) lattice structure and (b) a graph (either random or small-world).39

Figure 2-16 Process for creating a network from human brain data (Bullmore and Sporns 2009).
.....41

Figure 3-1 Overall process to build an Artificial Neural Network (MSE stands for Mean Square Error, and is discussed in detail in the following sections).....46

Figure 3-2 Parameters contributing to the relationships between neurons and where those “act” within the network structure (m is the number of inputs, p the number of hidden neurons, and n the number of outputs).....47

Figure 3-3 Relationships of weights and biases between a network’s neurons.....48

Figure 3-4 Example structure feature and the U.S. block group data of where it is located.62

Figure 3-5 Damage State 1 structure with example ANN input values.....63

Figure 3-6 Damage State 2 structure with example ANN input values.....63

Figure 3-7 Damage State 3 structure with example ANN input values.....64

Figure 3-8 Damage State 4 structure with example ANN input values.....64

Figure 3-9 Example Google Earth images and corresponding recovery states over time for (a) DS2 residential building that decided to rebuild from June 1, 2013 tornado event and (b) DS1 office building (windows were blown out) that wasn’t reoccupied until August 2017 following June 1, 2013 tornado event (circles show indications of building in use).67

Figure 3-10 Example image of a RS 3.2 building as seen when using video player to review recovery data. Red dot indicates location within Google Maps.79

Figure 4-1 ANN structure for relating hazard, structural, and sociological inputs to building damage state. (Photos are from NWS damage surveys (National Weather Service 2018).

Input images are various forms of clipart(CanStockPhoto n.d.; ClipartXtras n.d.; Emojipedia n.d.; GalleryYoPriceVille n.d.).....	82
Figure 4-2 (a) Percent error for MSE performance, (b) Percent error for SSE performance, (c) training performance for MSE performance and (d) training performance for SSE performance for the explored training algorithms.	84
Figure 4-3 Explored algorithms' (a) FNR, (b) FPR, (c) TNR, and (d) TPR for MSE performance.	85
Figure 4-4 Explored algorithms' (a) FNR, (b) FPR, (c) TNR, and (d) TPR for SSE performance.	86
Figure 4-5 Resulting percent error data ranges from 80+ ANN builds for (a) LM, (b) RP, and (c) BR training algorithms (Key images are various forms of clipart(CanStockPhoto n.d.; ClipartXtras n.d.; Emojipedia n.d.; GalleryYoPriceVille n.d.)).....	88
Figure 4-6 Final Ensemble ANNs' build percent error and how that error occurred through the training process as shown by respective confusion matrices.	89
Figure 4-7 ROCs for ensemble ANNs (a) DM3-C and (b) DM8-E.	90
Figure 4-8 Shortest path relative values for DM3 (a) combined ANNs and (b) averaged results from each ANN.	93
Figure 4-9 Shortest path relative values for DM8 (a) combined ANNs and (b) averaged results from each ANN.	94
Figure 4-10 DM3 (combined ANN structure) centrality scores as closeness versus degree.	95
Figure 4-11 DM8 (combined ANN structure) centrality scores as closeness versus degree.	96
Figure 4-12 (a) May 22, 2011 Joplin tornado track, (b) resulting damage path(Missouri Spatial Data Information Service n.d.), (c) Model 8 ANN determined damage path over actual satellite image, and (d) Model 8 ANN damage path over local tenure demographics(U.S. Census Bureau 2018).....	98

Figure 4-13 Results in matching individual buildings damage state to that modeled from physics-based and ANN methods..... 100

Figure 4-14 Results in matching individual buildings damage state to that modeled from DM3 and DM8. 102

Figure 4-15 (a) Percent error for MSE performance, (b) Percent error for SSE performance, (c) training performance for MSE performance and (d) training performance for SSE performance for the explored training algorithms in modeling recovery time. 106

Figure 4-16 Explored algorithms' (a) FNR, (b) FPR, (c) TNR, and (d) TPR for MSE performance in modeling recovery..... 107

Figure 4-17 Explored algorithms' (a) FNR, (b) FPR, (c) TNR, and (d) TPR for SSE performance. 108

Figure 4-18 Resulting percent error data ranges from 50+ ANN builds for (a) BR and (b) LM, training algorithms, with identifiers for RM2, which doesn't include structural characteristics, and RM8, which negates race. 109

Figure 4-19 Final Ensemble ANNs' build percent error and how that error occurred through the training process as shown by respective confusion matrices. 110

Figure 4-20 ROCs for ensemble ANNs (a) DM3-C and (b) DM8-E. 111

Figure 4-21 Shortest path relative values for RM2 (a) combined ANNs and (b) averaged results from each ANN. 113

Figure 4-22 Shortest path relative values for RM8 (a) combined ANNs and (b) averaged results from each ANN. 115

Figure 4-23 RM2 (combined ANN structure) centrality scores as closeness versus degree. ... 116

Figure 4-24 RM8 (combined ANN structure) centrality scores as closeness versus degree. ... 117

Figure 4-25 Actual recovery time for select buildings within Joplin and the percent errors from hindcasting with RM2 and RM8 for the exact match approach and a +/- 6-month error buffer..... 119

Figure 4-26 Distribution of buildings categorized as being in damage states 0 through 4, recovery time, and how many buildings in each damage state corresponded to each recovery time. 122

Figure 4-27 Neighborhoods containing structures that were recovered by (a) 1 year, (b) 1.5 years, (c) 2 years, or (d) structures that had not recovered by 2 years. 123

Figure 4-28 Census block group designation (a) for structures with recovery data (Curtis and Fagan 2013; U.S. Census Bureau 2018) and (b) by school district (Joplin Schools 2019). 124

Figure 4-29 Building damage state distribution by census block group. 125

Figure 4-30 Percent of each damage state’s buildings corresponding to each recovery time by census block group. 126

Figure 4-31 Building recovery and corresponding census block group by (a) the structures’ median year built and (b) per capita income. 127

Figure 4-32 Block groups that tended towards quicker recovery times by (a) median age, (b) percentage of individuals who do not have access to a vehicle, and (c) percentage of individuals who neither rent nor own. 128

Figure 5-1 3D Force directed graphs of combined network ensembles for (a) DM3 and (b) DM8. 134

Figure 5-2 The effect of increasing the amount of structures in a neighborhood classified as “other tenure” on resulting damage states and the distribution across tornado alley with satellite image examples of highly forested and high housing density areas. 135

Figure 5-3 3D Force directed graphs of combined network ensembles for (a) RM2 and (b) RM8. 136

Figure 5-4 Census Block Group distribution of (a) single female head of household with children (SFHwC), (b) renting tenure, (c) Hispanic population, (d) extractive industry employment,

(e) African American population, and (f) service industry employment for the state of Missouri.	139
Figure B-1 DM explored algorithms' (a) percent error with MSE, (b) percent error with SSE, (c) training performance of MSE, and (d) percent error of SSE.	167
Figure B-2 DM explored algorithms' with MSE (a) FNR, (b) FPR, (c) TNR, and (d) TPR.	168
Figure B-3 DM explored algorithms' with SSE (a) FNR, (b) FPR, (c) TNR, and (d) TPR.	168
Figure B-4 Various DMs' percent error for (a) BR, (b) LM, and (c) RP training algorithms.	169
Figure B-5 Various DM (a) FNR, (b) FPR, (c) TNR, and (d) TPR for BR.	169
Figure B-6 Various DM (a) FNR, (b) FPR, (c) TNR, and (d) TPR for LM.	170
Figure B-7 Various DM (a) FNR, (b) FPR, (c) TNR, and (d) TPR for RP.	170
Figure B-8 RM explored algorithms' (a) percent error with MSE, (b) percent error with SSE, (c) training performance of MSE, and (d) percent error of SSE.	171
Figure B-9 RM explored algorithms' with MSE (a) FNR, (b) FPR, (c) TNR, and (d) TPR.	171
Figure B-10 RM explored algorithms' with SSE (a) FNR, (b) FPR, (c) TNR, and (d) TPR.	172
Figure B-11 Various RMs' percent error for (a) BR and (b) LM training algorithms.	172
Figure B-12 Various RM (a) FNR, (b) FPR, (c) TNR, and (d) TPR for BR.	173
Figure B-13 Various RM (a) FNR, (b) FPR, (c) TNR, and (d) TPR for LM.	173

CHAPTER 1 INTRODUCTION

1.1 STATEMENT OF PROBLEM

Natural hazards are an inevitability that affect communities across the world. Instead of trying to forcibly work against nature, community resilience proposes that communities and individuals be able to avoid disasters then minimize loss and recover quickly, as well as learn from the events so that they may recover stronger and therefore more able to absorb future events. Building resilient communities includes evaluating our engineering materials, mitigation strategies, preparedness, and socio-economic structures. Part of this would involve being able to model community wide impact and recovery from hypothetical and oncoming events. In doing so, the community can improve its mitigation and preparedness strategies. Once models are established, changes in engineered infrastructure could also be evaluated for how they would minimize damage and impact, further improving recovery time.

Within these models, social, economical, and engineering components must interact across a community's infrastructure networks. For example, monetary resources may be a variable in dictating how and when an individual may be able to rebuild a structure. A community's monetary resources may also dictate the recovery of public utilities. Additionally, the rebuilding of a school may be critical to a population moving back to a location following an event. The research presented herein will evaluate the use of machine learning applications for potentially modeling the impact and recovery of a community's building stock, specifically from wind hazards. Additionally, this research will attempt to track patterns through a machine learning structure to assist in further identifying the socio-technical (social demographics and engineered infrastructure) contributions to both impact (damage) and recovery (rebuilding).

1.2 OBJECTIVES AND SCOPE OF RESEARCH

With advances in the area of Artificial Intelligence (AI) and Machine Learning (ML), an interesting opportunity in modeling the complex socio-technical interactions, with respect to a community's resilience, has become available. While current and past research well highlight the potential contributions of social parameters to the resulting building damage, it has proven difficult to model cohesively, which is where the application of ML may be able to assist. This research serves to evaluate the applicability, limitations, and areas for improvement of ML modeling applications in this context. Additionally, by combining the use of Artificial Neural Networks (ANNs) with graph theory, tracing artificial neural pathways may provide additional insight into the social and engineering interactions in such respects. Such ANNs will also be verified within this work through hindcasting the May 2011 Joplin, MO Tornado event.

In order to accomplish this objective, the following tasks and subtasks will be accomplished:

- **Task 1**: Conduct a Comprehensive Literature Review
 - Evaluate disaster literature for gaps in methodological approaches to modeling resilience.
 - Evaluate existing physics-based approaches to modeling building damage and recovery times.
 - Assess current applications of machine learning for predictive modeling, specifically Artificial Neural Networks (ANNs), across related and unrelated disciplines.
 - Identify previous studies in which graph theory was used to evaluate neural pathways.
- **Task 2**: Data Collection and Data Set Builds

- Determine which data are applicable for modeling resilience and which of those data are accessible.
- Create a key to communicate visual/subjective variables to an ANN.
- Gather data for model building that is also relative to data availability from an existing event or one that may occur in the future.
- **Task 3:** Build an ANN for Wind Hazard Impacts in terms of Damage State
 - Assemble a list of potential ANN training algorithmic theories for this task and Task 4..
 - Determine various ANN model structures in which different input variables are incorporated.
 - Evaluate the performance of each training and model option.
 - Determine the most relevant (lowest percent error from the build process) ANN training algorithm and model to use for the subsequent tasks.
- **Task 4:** Build an ANN for Building Recovery/Rebuilding from Wind Hazards
 - Determine various ANN model structures in which different input variables are incorporated.
 - Evaluate the performance of each training and model option.
 - Determine the most relevant (lowest percent error from the build process) ANN training algorithm and model to use for the subsequent tasks.
- **Task 5:** Conduct Graphical Analysis of Damage ANNs
 - Chose two ANN types: (1) most relevant and (2) a poorer performing build option.
 - Build multiple ANNs of each type for modeling and evaluation.
 - Combine these multiple ANNs together to form one conglomerated network.

- Trace the shortest path from network inputs to outputs (damage state) for each individual ANN and the combination network.
- Determine centrality of each ANN neuron within the individual ANNs and the combination network.
- **Task 6:** Conduct Graphical Analysis of Recovery ANNs
 - Chose two ANN types: (1) most relevant and (2) a poorer performing build option.
 - Build multiple ANNs of each type for modeling and evaluation.
 - Combine these multiple ANNs together to form one conglomerated network.
 - Trace the shortest path from network inputs to outputs (recovery time) for each individual ANN and the combination network.
 - Determine centrality of each ANN neuron within the individual ANNs and the combination network.
- **Task 7:** Simulate the 2011 Joplin Tornado
 - Gather existing data on the resulting building damage states and time to rebuild and reoccupy those buildings following the 2011 Joplin, MO EF5 Tornado. This will be used for comparison against the ANN modeling outputs.
 - Use the final multiple ANNs to model individual building damage state given the tornado path, wind speed, community demographics, and building stock characteristics.
 - Compare these results to that of physics-based methods in determining building damage state.
 - Compare both ANN and physics-based results to actual data for validation

- Use the final multiple ANNs to model individual building rebuild and re-occupancy times given the tornado path, wind speed, community demographics, and building stock characteristics.
- Compare recovery results to actual for evaluation.
- **Task 8:** Discuss Implications of Results, Conclusions, and Future Work
 - Outline which socio-technical variables may be considered critical for evaluating building damage states and recovery time, and therefore are recommended to be recorded for building future ANNs with this objective.
 - Conclude applicability of using ANNs in modeling community resilience.
 - Discuss further research needed and how individual building data could be used on the community scale.

The following chapters will outline influential research completed prior to this work, the methods in using ANNs, methods in applying graph theory, results of building damage and recovery ANNs, the 2011 Joplin data, and further discussion on the implications of such results. This research is intended to be a starting point within the application of AI for modeling impacts and recovery from natural hazards. Therefore, discussion will be given for how such methods could be expanded and improved upon.

CHAPTER 2 BACKGROUND AND LITERATURE REVIEW

2.1 NATURAL HAZARDS

2.1.1 NATURAL HAZARDS AS DISASTERS

Worldwide, natural hazards lead to destruction, economic losses, mass displacements of populations, and in some cases, loss of life. These events can be both climatological, covering situations ranging from extreme temperatures to tropical cyclones, and geological, covering landslides to movement of tectonic plates. All of these events are highly location-dependent based on proximity to fault lines, coastal areas, and specific atmospheric conditions. Eastern Asia is an example of a location subject to tropical cyclone conditions and tectonic plate activity. This locale (including Japan, the Philippines, Indonesia, and China), along with India, had the most natural hazard events in the world (Bryant 2005). According to Bryant (2005) tornadoes, which primarily occur within the U.S., were the most commonly occurring event in the world in the 20th century, as shown in Table 2-1. However, this did not make them the costliest (Table 2-2) or deadliest (Table 2-3). Those titles belonged to earthquakes and flooding, respectively. According to The Centre for Research on the Epidemiology of Disasters (2018) the average number of deaths for the 2000s and 2010s currently places earthquakes and “storms” (extreme weather such as thunderstorms, tornadoes, and tropical cyclones) as the deadliest natural hazards so far this century (Ritchie and Roser 2018).

Table 2-1 Frequency of Hazards (Bryant 2005; Centre for Research on the Epidemiology of Disasters 2018)

Hazard Type	# of Events in the 20th Century	# of Events from 2000 to 2018
Tornadoes (US)*	9476	
Extreme Weather		1891
Flood	2389	3029
Tropical Cyclone	1337	
Tsunami	986	
Earthquake	899	517
Wind (other)	793	
Drought	782	318
Landslide	448	351
Wildfire	269	222
Extreme Temperature	259	411
Temperate Winter Storm	240	
Volcano (Volcanic Activity)	168	97
Tornadoes (non-US)	84	
Famine	77	
Storm Surge	18	

* Tornadoes in the US are for F2-F5 tornadoes 1950-1995

Table 2-2 Worldwide Cost of Natural Hazards in USD at the end of relevant time frame (Bryant 2005; Centre for Research on the Epidemiology of Disasters 2018)

Hazard Type	Total Costs in the 20th Century	Total Costs from 2000 to 2018
Earthquake	\$248,624,900,000	\$530,581,604,000
Flood	\$206,639,800,000	\$514,976,464,000
Tropical Storm	\$80,077,700,000	
Wind Storm	\$43,890,000,000	
Extreme Weather		\$983,525,368,000
Wildfire	\$20,212,800,000	\$63,471,687,000
Drought	\$16,800,000,000	\$104,052,476,000
Cold Wave	\$9,555,000,000	
Heat Wave	\$5,450,000,000	
Extreme Temperatures		\$44,265,193,000
Total	\$631,250,200,000	\$2,240,872,792,000

Table 2-3 Deaths Resulting from Natural Hazards (Bryant 2005; Centre for Research on the Epidemiology of Disasters 2018)

Hazard Type	Associated Deaths in the 20 th Century	Associated Deaths from 2000 to 2018
Floods	6,851,740	99,606
Earthquakes	1,816,119	719,962
Tropical Cyclones	1,147,877	
Volcano (Volcanic Activity)	96,770	1,543
Landslides, avalanches, mud flows	60,501	16,854
Extra-Tropical Storms	36,681	
Heat Wave	14,732	
Drought		21,182
Extreme Temperature		162,616
Tsunami	10,754	
Cold Wave	6,807	
Tornado	7,917	
Extreme Weather		195,639
Wildfires	2,503	1,397
Total	10,052,401	1,218,799

Even though most media coverage encompasses hurricane and tornado deaths, the biggest contributor to loss of life in the U.S. has historically been heat and drought followed by cold weather, as shown in Figure 2-1 (Borden and Cutter 2008). However, according to the U.S. Federal Emergency Management Agency (FEMA), most disaster declarations in the U.S. are categorized under severe weather, flooding, and fire (Figure 2-2).

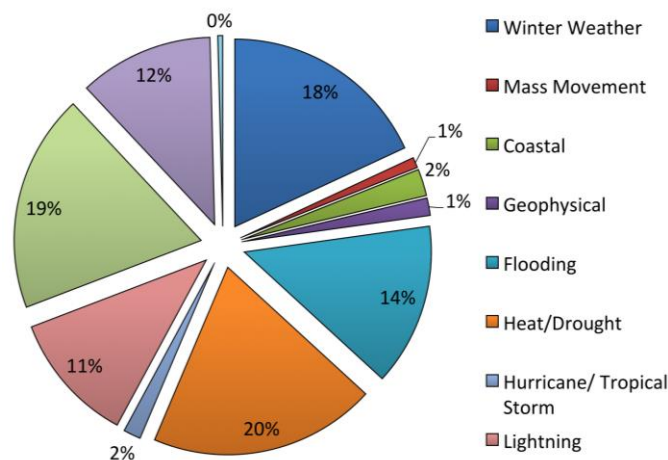


Figure 2-1 Deaths by natural hazard type in the U.S; after: (Borden and Cutter 2008)

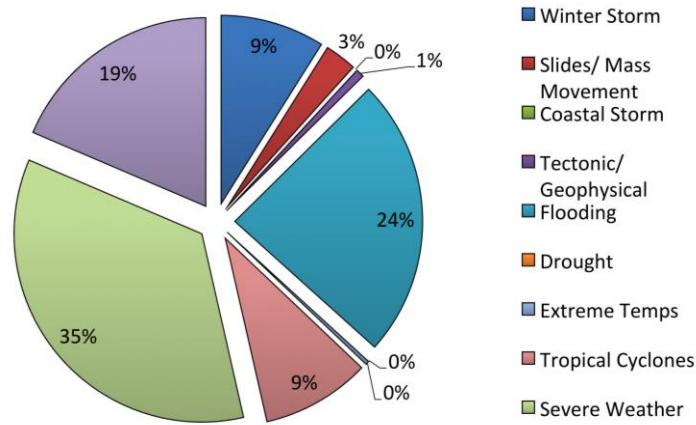


Figure 2-2 Disaster declarations by type; data from (FEMA n.d.)

The U.S. averaged 1,200 tornadoes yearly since 1950 (National Severe Storms Laboratory n.d.). However, the majority of these recorded tornadoes (90%) were considered “weak” tornadoes and rank as EF-0/1 (Livingston 2017) on the Enhanced Fujita Scale in Table 2-4. Often, the tornadoes that made the news as a disaster were EF-4/5 (or “violent tornado”) events and are considered rare events. Some recent disastrous tornado events of EF4 or higher ranking include the 2013 Moore, OK, 2011 Tuscaloosa AL, and 2011 Joplin, MO tornadoes. Each of these individual events resulted in at least \$2 billion (2015 USD) in damages (Storm Prediction Center 2015).

Table 2-4 The Enhanced Fujita Scale (McDonald 2002).

EF Scale	3-second Gust Wind Speed (knots)
0	56-74
1	75-96
2	97-117
3	118-143
4	144-174
5	>174

The tornado that struck Joplin, MO occurred on May 22, 2011 as a 1.6 km wide (1 mile) wide EF-5 tornado and resulted in approximately a cost of \$2 billion and the loss of 161 lives (Onstot 2016). This single event damaged nearly 7,500 residential structures along with 553 non-residential buildings (Kuligowski and Jorgensen 2014). In addition to many residential structures, severely damaged buildings included, but were not limited to, two fire stations, the Joplin High School, and a major Hospital (St. John's Regional Medical Center (SJRMC)) shown in Figure 2-3. The findings following the National Institute of Standards and Technology (NIST) technical investigation indicated that 135 of 161 fatalities were a result of building failures (Kuligowski and Jorgensen 2014; NIST 2011). This event remains the single costliest and deadliest tornado in U.S. history since records began in 1950. As a result, the 2011 Joplin Tornado will be further referenced within the research discussed in the following chapters.



Figure 2-3 Photograph of SJRMC damage following the 2011 Joplin Tornado, taken by Tiffany Kelley Photography (Kelley 2011).

2.1.2 METEOROLOGY OF SEVERE WEATHER

For modeling the impact of a hazard, it is best to first understand how the hazard occurs. The hazards to be specifically studied as part of this dissertation research are wind related. Windstorms occur as tornados, hurricanes, or what is termed “straight-line” winds. Straight-line

winds are often associated with a frontal boundary, flow off of a mountain, or a singular storm such as a derecho (the 2012 Ohio Valley/ Mid-Atlantic derecho caused power outages (Zubrick and National Weather Service 2012)). Specific fluid dynamic conditions govern how each event would occur.

In general, air typically moves as a result of a pressure differential, termed “pressure gradient force” (Ahrens 2008). This can be thought of similar to how water flows through terrain; steeper slopes have a “tighter” elevation gradient and water will flow faster, whereas a tighter pressure gradient (closely packed isobars) will result in stronger winds. Air masses of different pressure will also have different temperatures, which is why hot and sunny weather is typically associated with a high-pressure area. A front is merely the boundary between two air masses of different densities. There are a handful of different types of fronts, however, the one most commonly associated with more extreme winds is a cold front. This is due to the fact that cold, dry, and stable air is moving into a region of warm, moist, and conditionally unstable air (note that this air instability ties to the formation of storms). The cold front will lift the warm and moist air causing it to condense into clouds (Ahrens 2008). The more drastic the change in temperature, the stronger the front will be, resulting in potentially stronger systems with extreme winds.

Lift, instability, and moisture are necessary to form storms that will later bring strong winds and possibly tornados (with some other conditions). Because of these required elements, storms form on boundaries, such as cold fronts. Straight-line winds can come from thunderstorms, which include supercells, gust fronts, microbursts, squall lines, and derechos. A gust front (boundary between cold downdraft air and warm moist air feeding a storm) can cause a strong shift in winds, which may occasionally exceed 55 knots (63 mph) (Ahrens 2008). A microburst occurs when a storm’s downdraft hits the ground and spreads outward from the storm in a small area. These events can create damaging winds of up to 146 knots (168 mph) (Ahrens 2008). When a cluster of storms forms together, and the associated damaging winds

extend for hundreds of kilometers, this is what is termed a Multi-Scale Convection System (MCS) and could potentially form into a derecho. It is fairly common to see these storms in the shape of a bow on radar and therefore termed “bow echos”. These straight-line wind events can exceed wind speeds of 90 knots and are often associated with wide spread power outages and some structural damage (Ahrens 2008).

Straight-line winds and tornadic winds differ in how they may cause damage and how debris is transported during the event. Straight-line winds are just as they sound, strong winds moving along an approximately linear vector path. Tornadic winds are more tightly wrapped rotating winds, similar to how water appears when flowing down a drain. Radar examples for these events are shown in Figure 2-4, where (a) and (b) represent the convection and wind velocity of a straight-line wind event, and (c) and (d) represent the same for a tornadic type event. Tornadoes are much smaller in size than an MCS event and typically range from 100 to 600 meters wide and are ranked by damaging wind speeds through the Enhanced Fujita Scale, shown in Table 2-4 (National Weather Service n.d.). The same factors are needed to form a tornado as are needed for a storm/supercell: lift, instability, moisture, and additionally, shear to create a rotating column of air. However, the specifics to how exactly tornadoes form from a supercell remains unknown and is still being studied today. Because of the nature of the tightly rotating winds of a tornado, objects, sometimes as large as a railroad coach, can be lifted off the ground and subsequently dropped meters from its original location (Ahrens 2008). Essentially, these are violent fluid flow events that have the potential to severely impact a community.

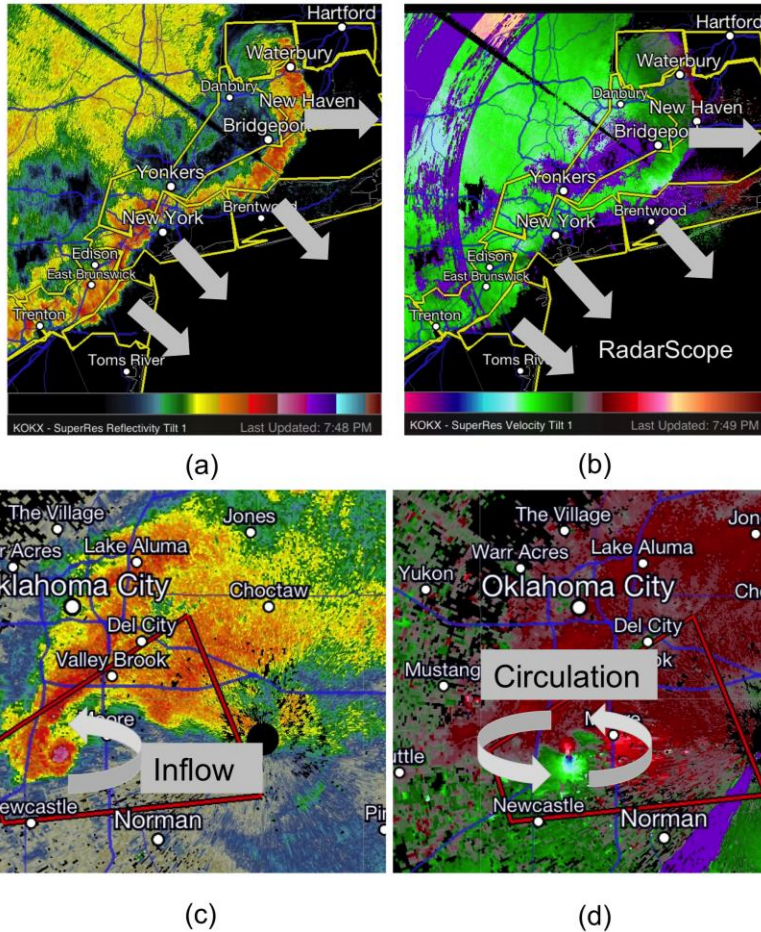


Figure 2-4 Radar images, taken using RadarScope™, of (a) convection structure of a straight-line wind event, (b) radar estimated wind velocity (green color represents motion towards radar tower, and red represents motion away from tower) of a straight-line wind event, (c) convection structure of a tornado-warned (red box) supercell, and (d) wind speed with rotation signature for a tornado warned supercell.

2.2 THE SOCIO-TECHNICAL ASPECT OF DISASTERS

The natural hazard, itself, is only a part of what contributes to a disaster. Arguably, the social, economic, and engineering aspects of *where* the hazard occurs are at the crux of a (un)natural *disaster*. Communities with certain population demographics have been found to be more vulnerable than others while certain building materials have been found to withstand wind pressure better than others. The resulting damage from a wind storm can sometimes force changes to building codes based on the observed structural failures. Such changes are applied

with the interest of reducing disaster-type outcomes in terms of economic damage and loss of life due to building failures.

2.2.1 ENGINEERING AND CONSTRUCTION PARAMETERS CONTRIBUTING TO DISASTERS

A natural hazard generally occurs through mechanisms that require no human interaction (exceptions could include fires and flooding due to failures of dams). For the research conducted herein, the engineering-based components that could turn a hazard into a disaster were primarily related to wind-building interaction, where wind would interact with a standard low-rise building as shown in Figure 2-5 below. The windward side of a structure would feel a positive pressure exerted on it, while the leeward side experiences a negative pressure force. In other words, there is a “suction-like” force being exerted on the leeward wall. The roof and sidewalls have a similar negative pressure on most of the respective surface areas. If windborne debris cause the building envelope to be breached, the wind interaction with the building will change to what is shown in Figure 2-6. This results in the development of internal pressure that will combine with the external pressure to increase damage to a structure (Yau et al. 2011).

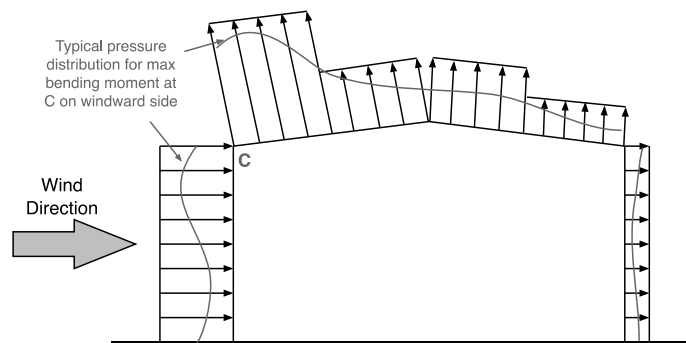


Figure 2-5 Instantaneous and simplified external pressure distribution on a low-rise building along with the static load distribution for a bending moment in association with the applied wind load (top corner C); after: (Holmes and Syme 1994).

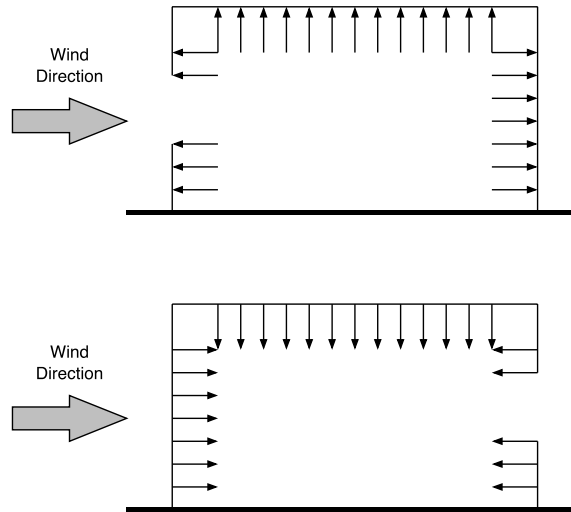


Figure 2-6 Internal pressure of building with a large/dominant opening and how this differs with location of the opening relative to wind direction.

Breaches to the building envelope cause internal pressure changes throughout the structure. Windows and doors are therefore considered critical areas as they are likely to break/open from resulting impacts. Even though windows and doors are most vulnerable to windborne debris, the damage, and possible loss, of a roof, can cause walls to become unstable due to a loss of lateral support. In damage surveys conducted after severe wind events resulting from hurricanes and/or tornados, one of the main building components inspected for damage is the roof and its connections. The failure of a roof can include the failure of multiple roof-wall connections and possibly the complete loss of a roof (Stenabaugh and Kopp 2012). Failure of these connections occur when the uplift force, created by the wind acting on the building, becomes greater than the roof's dead load or the connection's capacity. Stenabaugh and Kopp (2012) concluded that as more than one roof to wall connections fails, a temporary gap can form creating a change in the internal pressure and could lead to the roof "taking flight" or being ripped away from the structure.

In a study conducted by Christian Unanwa (2000), relative resistivity indices (RRIs) used in determining building damage decreased in higher story buildings, indicating that the ability of

a structure to resist wind damage decreased with height. This would seem logical since wind speed increases with height and are not impeded as much by friction in higher heights in straight-line (or hurricane) wind events (Unanwa and McDonald 2000). Unanwa used these RRI's to determine the degree of damage to a specific building by using damage bands, which bound the extreme degrees of damage a certain building class would sustain in a severe wind event. Building classes are commonly used in wind damage prediction, but can have broad definitions, the goal of these damage bands was to provide a more accurate damage estimation to a building or groups of buildings (Unanwa and McDonald 2000). The use of RRI's also touched on the effects other buildings have on each other. The RRI for a building was determined using many factors, one of which being the building's surrounding infrastructure (Unanwa and McDonald 2000). The factors used in creating these damage bands illustrated the importance of other features, such as the surrounding environment, in addition to construction type and height.

In another study, Yau (2011) evaluated the integration of similar various factors in wind damage to residential structures. This integrated model approach accounted for both the change in wind direction and speed as a storm passes as well as the effects of damage from buildings clustered together, similar to a residential neighborhood. As a hurricane or tornado moves along its track, the wind direction changes at a given location. It was theorized that the more wind directional shift involved, the more susceptible the structure is to wind-induced damage due to increasing the windward exposure areas. Areas downwind are also more exposed to windborne debris, similarly increasing the potential for structural damage (Yau et al. 2011).

The other component of Yau's research theorized that residential structures clustered together affect each other. This was supported by an example run of a 65 m/s and 45° angle wind field over a cluster of homes (4x4) identical in structure (Figure 2-7 illustrates this layout). The results showed that the homes at the corner where the winds first hit were less damaged

than the homes downwind in the cluster. The increased damage in the homes downwind was more obvious in an increased percent of window and door damage. This likely indicated that the debris from the first structures impacted the houses down wind. Once one home was damaged it created a chain like event of continuing damage downwind (Yau et al. 2011). Therefore, the denser the area of infrastructure, tree population, or other potential for debris, the more potential there would be for damage.

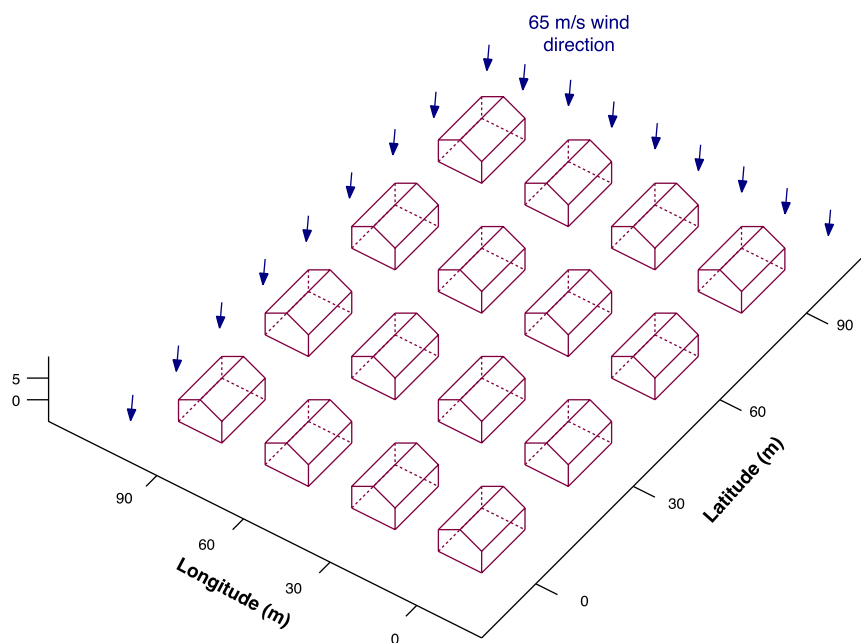


Figure 2-7 Neighborhood layout for assessing wind damage; after: Yau et. al. (2011).

Building type and quality has also been well established as a contributor to resulting level of damage. FEMA and URS have conducted investigations following extreme events and reported on observations and recommendations made by FEMA's Mitigation Assessment Team (MAT) that highlighted the differing impacts by building characteristics (Herseth and Ashley 2013). In addition to high infrastructure density leading to high damage, most high population areas also have buildings greater than 3 stories, which lowers resistivity to extreme winds. In correlation to building heights, most findings and recommendations made by FEMA tied to construction quality, year built, roof types, and construction faults and errors (Herseth and

Ashley 2013). The construction quality and year built are therefore considered significant factors in how a building will perform during a severe event. Older structures not up to recent building codes would typically be more vulnerable in extreme weather events. Essentially, the current research suggests that more populated, older locations would experience more damage for a set wind speed than smaller towns with new construction. When considering how these individual buildings inform functionality at the community level, “building clusters” assess building damage, and how it can be altered by age and infrastructure density, to specific building types (e.g. residential buildings, commercial buildings, manufacturing buildings, and so on) (McAllister 2018).

2.2.2 SOCIAL PARAMETERS CONTRIBUTING TO DISASTERS

While wind interacts with civil infrastructure, there are also people that use them and would therefore contribute to their maintenance and condition leading up to an extreme event. Demographics of an area’s population can relate the amount of resources available to invest in disaster mitigation and recovery following an event. For example, when evaluating economic damage and mortality, a large percentage of the world’s population lives near the coast, but the U.S. possesses a lower death toll and higher economic damage from coastal hazards due to being a more developed country (Nicholls and Small 2002), which would imply that higher income areas are more likely to afford safer housing as well as be more capable to react in a hazardous situation (Cutter et al. 2003; Simmons and Sutter 2005). However, in terms of economic damage, higher income areas are also linked to increase in damage costs by the increase in median home values (Hall and Ashley 2008). These relationships between income/resources and economic impacts are just one example of how social factors can contribute to apparent disastrous outcomes.

The combination of socioeconomic status and demographics data were used at the University of South Carolina (Cutter et al. 2003) in order to create the Social Vulnerability Index

(SoVI). The SoVI relates the two main components of location vulnerability: physical vulnerability (i.e. hurricane, tornado, and/or earthquake prone area), and the various characteristics of a population that determine how people are able to cope and recover from natural hazards (Cutter and Emrich 2006). The SoVI was designed based on the (modified) Hazards of Place Model shown in Figure 2-8 (Cutter 1996). The main factors of social vulnerability that are widely accepted include age, race, gender, and socioeconomic status. The SoVI used 11 factors (listed in Table 2-5), in an additive model in order to produce a SoVI score for each U.S. county. These 11 factors accounted for 76.4 percent of the variance in social vulnerability among U.S. counties. The SoVI county scores ranged from -9.6 (lowest) to 49.51 (highest) with a mean score of 1.54 and a standard deviation of 3.38. Corresponding to the demographics discussed, Manhattan Borough (New York City) was found to be the most vulnerable county in the U.S. Excluding Manhattan, the most vulnerable areas of the country appear to be in the southern half where there are more ethnic inequalities and higher population growth. The low vulnerability areas are less populated and generally homogeneous in nature (i.e. mainly white, suburban, and well-educated). These areas were found to be New England, eastern side of the Appalachian Mountains from Virginia to North Carolina, and the Great Lakes Region with Yellowstone National Park County topping the list. The results of the SoVI made it clear that variables such as unemployment, access to resources, homelessness, wealth, race, built environment, among others, play a key role in how prepared and susceptible a location is to a natural hazard.

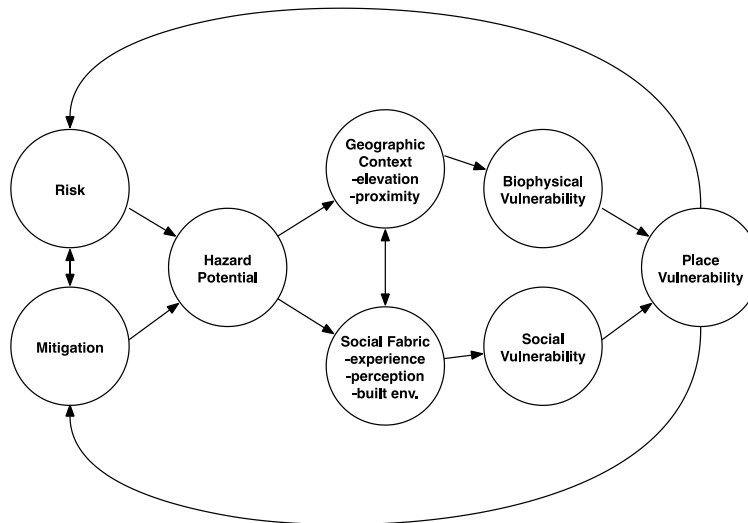


Figure 2-8 Hazards-of-Place Model of Vulnerability; after: (Cutter 1996)

Table 2-5 The 11 SoVI variables (Cutter et al. 2003).

Concept	Dominant Variable (Census data)	Correlation found in 2003 study
Personal Wealth	Per capita income	+0.87
Age	Median Age	-0.90
Density of built environment	No. of commercial establishments/mi ²	+0.98
Single sector economic dependence	% Employed in extractive industries	+0.80
Housing stock and tenancy	% Housing units that are mobile homes	-0.75
Race – African American	% African American	+0.80
Ethnicity – Hispanic	% Hispanic	+0.89
Ethnicity – Native American	% Native American	+0.75
Race – Asian	% Asian	+0.71
Occupation	% Employed in service occupations	+0.76
Infrastructure dependence	% Employed in transportation, communication, and public utilities	+0.77

Cutter, Boruff, and Shirley (2003) did not find any statistically significant results when comparing the SoVI to presidential declared natural disasters; however, incorporating SoVI into disaster modeling has gained attention in recent years. In a study performed by Burton (2010), the SoVI was used with FEMA hurricane damage assessments in specific areas where the 11 SoVI factors had an impact. Less extensive building damage (ex: Damage States 1 and 2) was

found to be mainly due to hurricane winds and storm surge, whereas societal aspects did not make a significant contribution until “extensive” damage (possibly Damage State 3) was reached. However, overall the meteorological impacts (storm surge) played a larger role than the societal factors. That being said, the social vulnerability factors that appeared to stand out more had to do with urban population, race, agriculture, and poverty level.

While the SoVI related a population’s vulnerability to disasters on the county level, other case studies have found additional social characteristics that may tie to the ability to recover from a natural hazard event. A review of such studies highlighted the importance of income and class to recovery times (Fothergill and Peek 2004). Lower income households took longer to recover more so as a result of resources and how quickly those were provided to different demographic groups. Another study, (Morrow 1999), that focused on the “neighborhood” level, instead of the county level as the SoVI did, proposed that at-risk groups involve concentrated areas of:

- Residents in group housing
- Elderly (high median age)
- Those on disability (physically or mentally disabled)
- Renters (housing tenure)
- Low-income households
- Women-headed households (Single female head of household with children)
- Ethnic minorities based on language spoken in the area
- Recent residents
- Larger households
- High concentrations of children/youths, homeless, and/or tourists and transients.

Ultimately, the conclusion of this study suggested that sustainable development programs, in the context of disasters, involve leadership at a more local level (Morrow 1999). In

other words, more “disaster-resistant communities” involve a level of “grassroots activism” (Geis 1997). While many of these “neighborhood” demographics overlapped with those on the county level from the SoVI, parameters such as group housing, disability, and women-headed households were not represented at the county level analysis. The Center for Disease Control (CDC) established another Social Vulnerability Index at the census tract level, which would be considered closer to the size of a “neighborhood”. This index included 15 census variables as outlined in Table 2-6.

Table 2-6 The 15 Social Vulnerability census variables (Flanagan et al. 2011).

Domain	Variable	Additional descriptions
Socioeconomic Status	% Individuals below poverty	Individuals who would be classified as below the federally defined poverty line
	% Civilian employed	
	Per capita income	
	% Persons with no high school diploma	
Household Composition/ Disability	% Persons 65 years of age or older	White Alone – (African American + Native American + Asian + Hispanic, Pacific Islander + two or more races + other)
	% Persons 17 years of age or younger	
	% Persons more than 5 years old with a disability	
	% Male or female head of household, no spouse present, with children under 18	
	% Minority	
	% Persons 5 years of age or older who speak English less than “well”	
Housing/ Transportation	% Multi-unit structure	> 10 units
	% Mobile homes	More people than rooms at household level.
	Crowding	
	No vehicle available	
	% Persons in group quarters	

Of these various studies, certain demographics continued to be discussed and highlighted a indicators of vulnerable populations. These demographics, therefore, link social vulnerability to natural hazard on various special levels and include:

- Income and Poverty
- Tenure (mobile homes, renting, group quarters)
- Age
- Education & employment
- Race & ethnicity
- Single female head of household (for 2 of the 3 studies)
- Disability (for 2 of the 3 studies)
- Access to transportation/ Infrastructure dependence (for 2 of the 3 studies)

These variables had some obvious ties with the engineering related contributors to disasters. Tenure, for example, could tie to the building size and height. Income/Poverty would relate the condition the structure may be in and if it is being maintained well. Also, these census demographics related a dependency on civil infrastructure through employment and access to transportation. These demographics were evaluated through various studies at county, census tract, and smaller levels to provide a comprehensive overview of the variables that may contribute to social vulnerability at different scales. The studies outlined above provided U.S. Census variables to consider within this research.

2.3 COMMUNITY RESILIENCE

2.3.1 CONCEPTUAL BACKGROUND

These social and engineering factors interact with a natural hazard to determine an overall impact to a community and how long it may take to recover. Community resilience has been generally thought of as the ability of a community to absorb and “bounce back”

from a hazard or impact event. The NIST definition of community resilience, with respect to natural hazards, stated that resilience is “the ability to prepare for anticipated hazards, adapt to changing conditions, and withstand and recover rapidly from disruptions” (Koliou et al. 2018; National Institute of Standards and Technology (NIST) 2017). A disturbance in the form of a natural hazard could cause a spike in population dislocation and/or economic loss while also negatively affecting building functionality, employment, and school attendance, among others. Typically, this has been represented by the graph shown in Figure 2-9 in that there is a standard level for a desired resilience metric (population dislocation, building functionality, employment rate, and so on), then the hazard strikes and there is a sharp decline. A community’s resilience goal would be to recover this metric back to its standard level, or trend, prior to the event over a period of time. This elemental curve relates the four R’s of resilience: robustness, redundancy, resourcefulness, and rapidity, which are also defined further in Figure 2-9 (Bruneau et al. 2003).

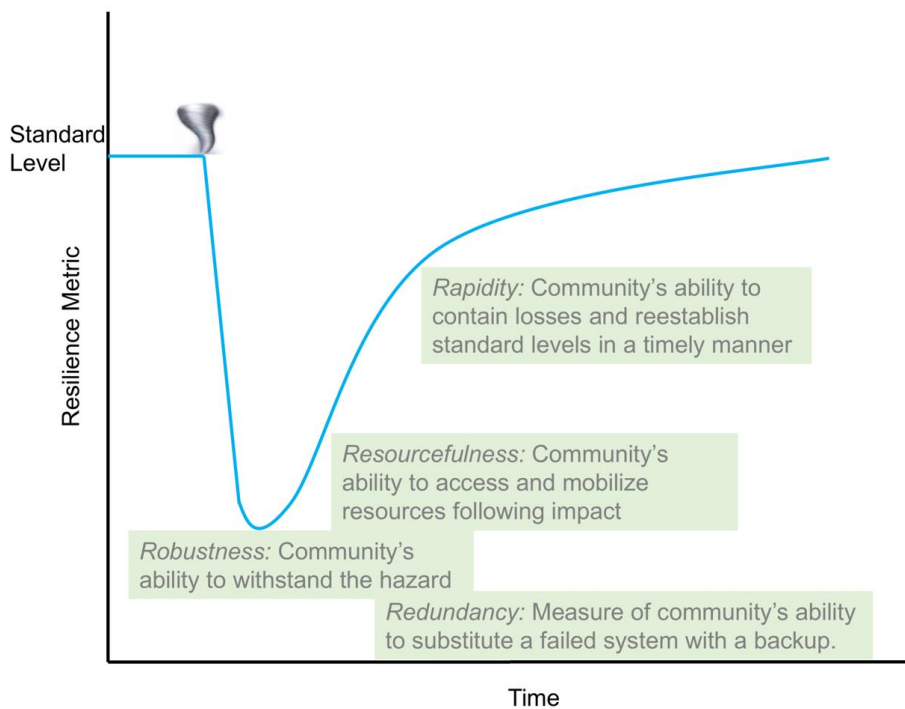


Figure 2-9 Typical resilience curve with its defined characteristics.

The concept of resilience as it relates to natural disasters conceptually began in the social science- and psychology-related fields with a focus on theory and frameworks (Cutter et al. 2008; Godschalk 2003; Gordon 1978; Holling 1973; Norris et al. 2008). These theories and frameworks/models, however, were what began to move this subject area forward. The SoVI provided a starting point in how community attributes relate to the potential for loss from a natural hazard (Cutter et al. 2003). The loss potential would then relate to the initial decline shown in Figure 2-9 immediately following the stressor event (hazard). The initial stage prior to the hazards consisted of “antecedent” conditions, or the locational characteristics, of the community and provides a basis for monitoring a community’s resilience, as was considered with the Disaster Resilience of Place (DROP) Model (Cutter et al. 2008). Such conditions include built, natural, economic, and social systems that were specific to one place over a (long) period of time, and could also be viewed as a network of physical and human systems (Godschalk 2003; Norris et al. 2008). These inter-organizational networked systems, with links, interactions, and overlap, have been thought of as one dimension of community capacity (Goodman et al. 1998). Visual representations of how vulnerability, resilience, and adaptive capacity could be related are shown in Figure 2-10.

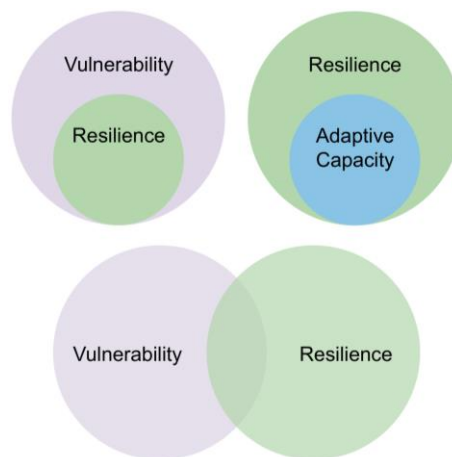


Figure 2-10 Conceptual relationships between vulnerability, resilience, and adaptive capacity within the concept of hazards, from (Cutter et al. 2008).

The concept of increasing community resilience has focused on the societal demographics (or capital) while also recognizing the importance that resources and damaged capital contribute (Cutter et al. 2003, 2008; Miles and Chang 2011; Norris et al. 2008). Therefore, in modeling community resilience, physical, economic, and social systems must interact simultaneously to influence each other.

2.3.2 CURRENT MODELING APPROACHES

Cutter (2003) introduced the initial SoVI and later the Disaster Resilience of Place (DROP) Model. Within the DROP model structure (shown in Figure 2-11), a community consists of established antecedent conditions, which interact with the hazard upon occurrence (Cutter et al. 2008). The hazard itself had characteristics as well. For example, a wind event would have a wind speed, areal extent, and a type of wind structure (tornadic, straight line, or possible hurricane). The impacts immediately following an event were improved or worsened by the community's coping ability and mitigation mechanisms (antecedent conditions). Therefore the impact was considered the sum of the antecedent conditions and the hazard. The impact was then evaluated for whether or not it exceeded the absorptive capacity of a community, in which the absorptive capacity would be related to the antecedent conditions. If this capacity was exceeded then the community can chose whether or not to adjust, or adapt, it's current conditions so that they may improve their resilience (Cutter et al. 2008). Figure 2-11 illustrates the DROP model framework.

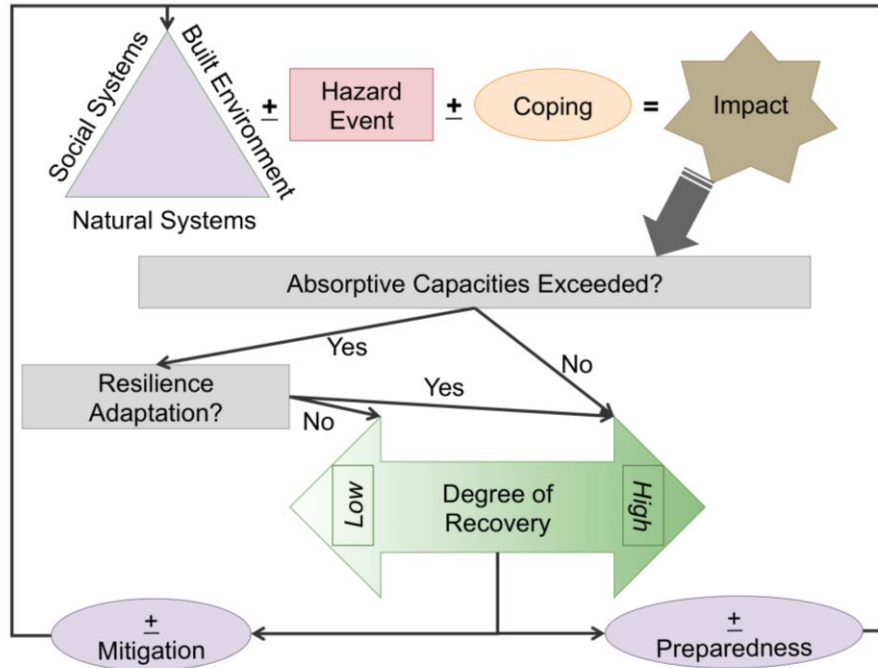


Figure 2-11 Disaster Resilience of Place Model layout, after (Cutter et al. 2008).

Other models and modeling frameworks have been introduced in recent years. Within these, Cimellaro (2010) outlined mathematical principles to reflect numerical assessment of structures similar to the DROP model and noted that resilience (R) can be computed as the area under the recovery curve shown in Figure 2-9. Within this structure, resourcefulness was considered the differential of the curve for the metric being evaluated with respect to time, rapidity was the ratio of loss to recovery time, robustness was considered the “capacity of keeping the variability of losses within a narrow band,” and redundancy was defined as possible options for resources contributing to loss or recovery (Cimellaro et al. 2010). Within engineering, economic losses would be described as repair/replacement costs dependent on a resulting building damage state. However, losses could also be calculated such that social characteristics are considered, such as social losses associated with population displacement. By this framework, the lower the initial impact drop in the resilience curve, or the less time it would take to recover, resulted in higher areas under the resilience curve, or higher R -values.

In 2011, the ResilUS model was introduced to represent damage and recovery over time of a community's capital (Miles and Chang 2011). The "capital" considered within this model were represented through three aspects: the built environment, economics, and social. Each of these were influenced by variables that not only included the hazard, but the building types, probabilistic availability of resources (materials and monetary), building occupant's loans and debt, time to file and receive resources (loans), and even injuries to building occupant/owner (Miles and Chang 2011). Within the modeling software itself (MATLAB), Markov chains were used to model recovery over time. However, this model did not include the use of GIS software for explicit spatial distribution. Overall this model was probabilistic in nature based on the occurrence likeliness of certain conditions, such as building damage state (Miles and Chang 2011).

Another recently published resilience model, Dynamic Finite Element Analysis of Resilience (FEAR), treated a community, as an area to be meshed similar to how finite element analysis is executed on structural components following the general dynamic equation of motion:

$$F(t) = M(t) \frac{d^2X}{dt^2} + C(t) \frac{dX}{dt} + K(t)X \quad (2-1)$$

where $F(t)$ is the load or hazard, $M(t)$ is the social vulnerabilities instead of mass, $C(t)$ represents the funds available for recovery instead of damping, and what is typically the stiffness, $K(t)$, is now the infrastructure robustness all of which are evaluated over time (t) (Mahmoud and Chulahwat 2018). Within this model the infrastructure robustness was considered as the effect various infrastructure systems have on others should these systems be disrupted. This study explored the use of finite element modeling concepts through the fictional city of Gotham by exposing it to a disturbance with consideration of health, housing, power, water, communication, and transportation lifelines. The use of the stiffness matrix allowed for visualization of how damage to one infrastructure system at a specific location may ripple

through the surrounding community and remaining systems (Mahmoud and Chulahwat 2018). However, the FEAR model is still in the theoretical stage of development and would require real-world community data to validate the model.

In addition to these proposed resilience models and model frameworks currently in use, a new platform named IN-CORE (van de Lindt et al. 2019) is currently being developed through the NIST Center of Excellence for Risk-Based Community Resilience Planning (NIST COE). This platform will allow for the ability to identify buildings by archetypes, spatially overlap a community with a specified hazard, model impact and recovery over time of a community's building stock, transportation systems, water network, and electrical power network (EPN), schools, hospitals, among others. Some of the probabilistic physics-based methods incorporated within this model are discussed within the following section.

2.4 PHYSICS-BASED APPLICATIONS IN IN-CORE FOR MODELING COMMUNITY IMPACT AND RECOVERY FROM NATURAL HAZARDS

2.4.1 MODELING BUILDING DAMAGE STATE

The engineering contributions to disasters, discussed above, are well established and can be modeled through mathematical concepts. The application of such mathematical concepts has been performed on the building system level for single or multiple hazards, as well as at building stock portfolio level (Lin and Wang 2016; Mehta et al. 1981; Memari et al. 2018). Since community resilience begins at the building level, advancements in building performance could help improve overall community resilience, specifically with respect to robustness and redundancy. As an example, in using finite element models to determine resistance, it has been found that, in areas subjected to both tornadoes and expansive soils, wood frame structures have deficient foundation connections, roof panels, and rafter-sill connections with respect to the tornado pressures exerted on the structures (Maloney et al. 2018; Wang et al. 2018).

Building stock portfolios (to include wood frame structures) were used in recent research and allowed for the illustration of how a whole community performs on the physical level (Lin and Wang 2016; Memari et al. 2018; Wang et al. 2018). The establishment of such portfolios involved engineering judgment on typical construction and the ability to assign all community buildings to such predetermined archetypes as shown in Table 2-7.

Table 2-7 Community building portfolio archetypes (Memari et al. 2018).

Archetype	Building Description
T1	Residential wood building – small rectangular plan, gable roof, 1 story.
T2	Residential wood building – small square plan, gable roof, 2 stories.
T3	Residential wood building – medium rectangular plan, gable roof, 1 story.
T4	Residential wood building – medium rectangular plan, hip roof, 2 stories.
T5	Residential wood building – large rectangular plan, gable roof, 2 stories.
T6	Business and retail building (strip mall)
T7	Light industrial building
T8	Heavy industrial building
T9	Elementary/middle school (unreinforced masonry)
T10	High school (reinforced masonry)
T11	Fire/police station
T12	Hospital
T13	Community center/church
T14	Government building
T15	Large big-box store
T16	Small big-box store
T17	Mobile home
T18	Shopping center
T19	Office building

Each of these archetypes consisted of an assumed construction, to include the material used for the main-wind force-resisting system (MWFRS) and the connection types for the components and cladding (C&C). For example, most homes (T1 through T5) were considered wood structures that would have wood walls as part of their MWFRS and nailed connections at the roof-wall interface, whereas a hospital was considered to be reinforced concrete in which the roof was a concrete slab that was connected to the walls through the use of rebar (Memari et al. 2018). These structural components were evaluated through an assessment of whether a specific number of failures occurred due to the wind loading exceeding the resistance capacity

of the materials and types of connections. The loading and resistance capacity were described by a fragility defined by a lognormal distribution with a known mean and coefficient of variation, which were gathered from a literature review of experimental data. Monte Carlo Simulation (MCS) was used to establish a range of varying resistance values based on the experimental data that would subsequently be compared to loading values for various wind speeds. The fragilities consisted of four (4) possible damage states. The relationship between demand and capacity was described by the limit state function, $g(\mathbf{X})$:

$$g(\mathbf{X}) = \mathbf{R} - (\mathbf{W} - \mathbf{D}) \quad (2-2)$$

where \mathbf{X} is the variable uncertainty that explains the limit state condition, \mathbf{W} is the wind load, \mathbf{R} is the resistance, and \mathbf{D} represents the dead load that contributes to wind resistance. The fragility functions were developed to describe the probability of exceeding a specified limit state (in this case the building damage state) for various levels of hazard intensity (in this case the wind speed). Fragilities were expressed as a lognormal cumulative distribution functions such as:

$$F_r(x) = \Phi \left[\frac{\ln(x) - \lambda}{\zeta} \right] \quad (2-3)$$

where x is the wind intensity measured as the 3-second gust, $\Phi[.]$ is the normal cumulative distribution function, λ is the capacity's logarithmic mean, and ζ is the capacity's logarithmic standard deviation. Each building system component therefore has a distribution of its capacity, which was then compared to the wind load (which also consisted of uncertainties) acting on both the MWFRS and C&C. The calculation of the wind velocity pressure for straight-line winds at height z , q_z (in N/m²), was given by ASCE 7-10 as (American Society of Civil Engineers 2010; van de Lindt et al. 2013):

$$q_z = 0.613K_zK_{zt}K_dV^2 \quad (2-4)$$

where K_z is the exposure factor, K_{zt} the topographic factor, K_d the wind directionality factor, and V is the wind speed in m/s. The wind pressure loads acting on the MWFRS and the C&C were then given by:

$$p_{MWFRS} = qGC_p - q_i(GC_{pi}) \quad (2-5)$$

$$p_{C\&C} = q_z[GC_p - (GC_{pi})] \quad (2-6)$$

where q and q_i are the velocity pressures at height z , G is the gust-effect factor, C_p is the pressure coefficient, and GC_{pi} is the internal pressure coefficient, which is based on open areas allowing wind into the structure. These calculations were performed on the individual component level and aggregated up to the building system by evaluating potential failure paths. Example resulting fragility curves from this research referencing ASCE 7-10 are shown in Figure 2-12. Related research has also been conducted in the interest of determining the mean and standard deviations for various building materials' resistance capacity and the pressure factors in the above equations (Ellingwood and Tekie 1999; Federal Emergency Management Agency (FEMA) 2009; Lee and Rosowsky 2005; National Association of Home Builders (NAHB) 2003; National Institute of Standards and Technology (NIST) 2006) as well as in developing fragility functions for specific archetypical buildings under wind hazards (Ellingwood et al. 2004; Memari et al. 2018; Standohar-Alfano et al. 2017)

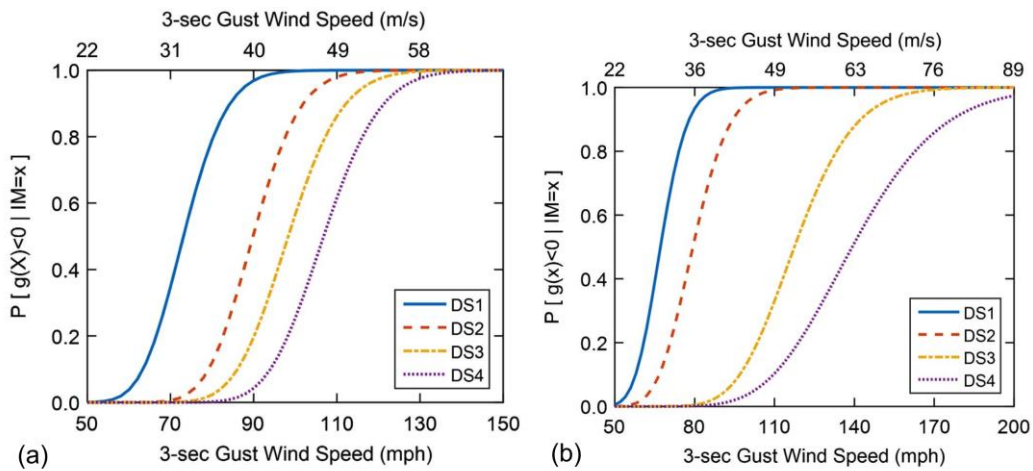


Figure 2-12 Building damage state fragilities for (a) light industrial buildings (T7) and (b) heavy industrial building (T8) from Memari et. al. 2018.

2.4.2 MODELING BUILDING RECOVERY

A building's damage state would subsequently result in an economic loss and the lowering of overall building functionality. The functionality of a building describes the level to which the building can be utilized for its normal purposes. The time required to reestablish a building as "Fully Functional" (rebuilt and reoccupied) has been considered the "recovery time" in relevant modeling research. The recovery time begins with the initial damage state and is tracked until a "fully functional" status is reached.

Following an extreme event, buildings have been previously considered "tagged" by the categories listed in Table 2-8. These "tagged" categories were then associated with an *approximated* equivalent damage states used in establishing fragilities (Almufti and Willford 2013; Lin and Wang 2017a; Memari et al. 2018). In evaluating the recovery time of a building stock, each building was evaluated by Lin and Wang (2017a) for how long it would take to reach the "Fully Functional" state.

Table 2-8 REDiTM (Almufti and Willford 2013) Placards following a disaster an approximate corresponding damage state (Memari et al. 2018)

Functionality State	ATC Placard	Damage Description	Damage State
5	Fully Functional (FF)	None	0
4	Baseline Functionality (BF)	Minor damage. Primarily cosmetic (siding and shingles) damage.	1
3	Re-Occupancy (RO)	Minor to moderate nonstructural damage.	2
2	Restricted Use (RU)	Moderate structural damage that is not considered life threatening.	3
1	Restricted Entry (RE)	Complete destruction or life threatening damage.	4

According to Lin and Wang (2017a), there are two phases considered in determining a recovery time: (1) delay time, which includes inspection and permitting, and (2) rebuilding. In modeling such recovery time, Lin and Wang utilized Markov Chain analysis to include the

uncertainties in the post-disaster functionality state and decisions owners may make that influence the delay time (Lin and Wang 2017a). This delay time included time to inspect the building, time to secure funding for repair, and time to commission architects. The delay time contributes to the overall wait time, which was considered highly variable since it is dependent on many socio-economic factors in addition to the construction market. In essence, each functionality state inherently included the wait time of the previous functionality state, such that only BF would not include a permitting time. The delay time was also considered to be longer for worse-off functionality/damage states.

In application, factors considered for recovery time modeling included the building construction and occupancy class, income, and housing density for residential zones (Lin and Wang 2017b). The building's functionality state, in application using a hypothetical community, Centerville (Ellingwood et al. 2016) was determined similar to MCS methods for creating building damage state fragilities, in which empirical data of these factors consisted of a mean and coefficient of variation. From this data, the mean recovery time by functionality state is redrawn in Figure 2-13. Following this step, delay times, construction times, and ability to obtain financing for repairs and rebuilding were combined. The socio-economic characteristics were important when considering the ability of each residential zone to obtain financing resources (Lin and Wang 2017b). Ultimately, this work considered recovery time to be a culmination of financing, construction mobilization, permitting (where applicable), and construction time based on the damage state of the structure. Such recovery times are also a function of social vulnerability and recovery policies (Sutley and Hamideh 2017).

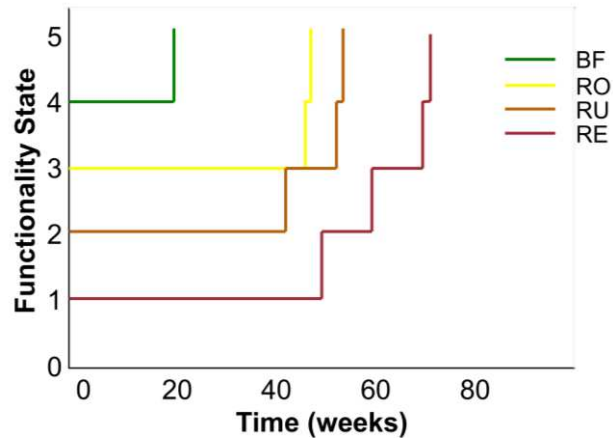


Figure 2-13 Mean conditional building level restoration process from Lin and Wang (2017b).

While the use of 19 archetype fragilities was hindcasted and verified through the 2011 Joplin tornado (Attary et al. 2018), this recovery research has been primarily modeled within the hypothetical town of Centerville (Lin and Wang 2017a; b). Therefore, the research work discussed herein will further provide a comparison of the physics-based methods, outlined above, and machine learning methods, outlined in the following section, for modeling damage state only.

2.5 MACHINE LEARNING APPLICATION

The previous sections provided an overview on natural hazards, social vulnerability, engineering practices, and the basis for resilience. This section (and the following section) will instead cover a background and current applications for the methods to be explored within this dissertation research. Machine learning is a data analysis modeling approach that has gained popularity recently due to data availability and the ability to store large data sets. Graph theory, which will be discussed in Section 2.6, is a means by which to analyze a complex network and infer meaningful observations of the network behavior. Both will be used herein for modeling and evaluating community build stock damage (impact) and recovery.

2.5.1 CONCEPTUAL OVERVIEW

Machine learning falls within the purview of Artificial Intelligence (AI) by attempting to mimic how the human brain learns through data analysis and pattern recognition. In essence, this is accomplished through various forms of regression analysis given a historical data set. This historical data set would consist of multiple input variables that could be tied to a specific desired output or outcome. Within AI, this data set can either include data with known outputs and inputs to establish a “supervised” network, or only include inputs and adjust as new outputs become available real-time, in the form of an “unsupervised” network. However, as the technology currently stands, any form will require data to be gathered, analyzed, and understood by the AI.

One type of machine learning approach is the use of Artificial Neural Networks (ANNs), which consist of nodes, representative of neurons, and connections between those nodes, representative of synapses, that relate the data through the network. ANNs consist of layers of neurons: an input layer, hidden layer(s), and an output layer as illustrated in Figure 2-14. An ANN can have one hidden layer or multiple hidden layers (ℓ). As in Figure 2-14, each of the example four input neurons connects to each of the example four hidden neurons in the neighboring layer. These connections can either be activated (excited) or deactivated and can vary in strength through a calculated weight value. Within the brain, it is not necessary that every single neuron connect to every other neuron, but connections within will establish paths taking input stimulus information to other neurons that eventually excite an action within a person. How this is accomplished mathematically for ANNs, through various training algorithms, is outlined as part of the Methods Section 3.1. In building an ANN, training establishes the connection patterns (weights) between neurons in order to produce a lowest possible error in relating the input variables to a desired outcome.

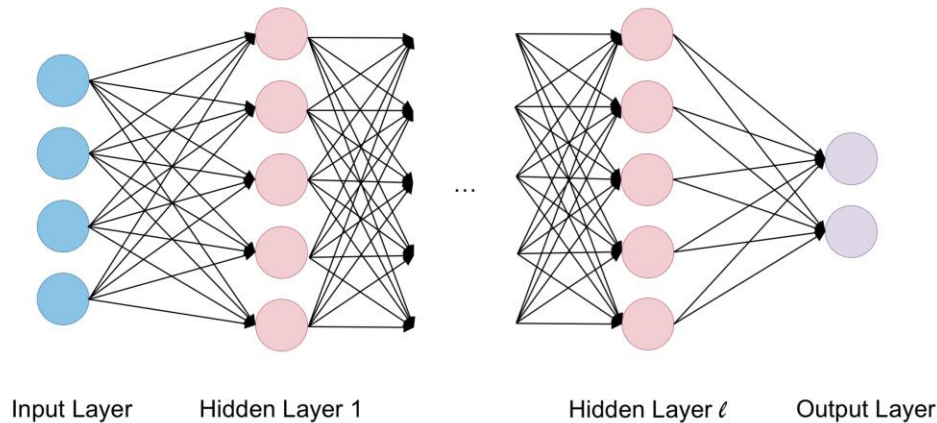


Figure 2-14 Typical multi-layer feed-forward neural network structure with up to ℓ hidden layers.

2.5.2 CURRENT APPLICATIONS

Once an ANN is trained and constructed so that it has clear data pathways, it can then be used to illustrate statistical relationships for practical purposes in pattern recognition, prediction modeling, and forecasting. Uses of ANNs include many applications; from handwriting recognition to self-driving vehicles. This is also one way a computer or website could “know” to suggest certain parameters or other websites to a user. ANNs have been developed for use in various fields, from business and finance to water resources to medicine. The use of neural networks in medicine appeared to be the most widely used application of ANNs, so much so that MATLAB even has an example batch of patient data in order to hypothetically diagnose cancer. The prominent medical fields using these models seem to be clinical and diagnostic medicine. This application dates back to 1989 with the first use of ANNs to diagnose the risk level of chest pains (Baxt 1995).

In a field more relevant to civil engineering, hydrologic and rainfall runoff modeling are other popular applications of ANNs. Most of these networks were multilayer with backpropagation training (Dawson and Wilby 2001). Typically ANNs designed to model hydrologic flow computed either the discharge or model stage from a rainfall event. The variance occurs in the inputs and the method of approach, which depend on the hydrologic

model classification. In general, ANNs for hydrologic modeling were considered parametric functions that relate meteorological variables to runoff using transfer functions (Dawson and Wilby 2001). The models were either lumped, where the catchment basin is treated as a single unit, or distributed with the use of a catchment system containing subsystems (Dawson and Wilby 2001). The inputs can be as simple as past rainfall records to more complex. More complex and incorporative models could account for seasonal variations, which incorporated the relative rainfall and discharge perturbations, and time step segments (Shamseldin 1997). The designer defined input data and method can have an effect on the outputs and accuracy of the model for certain event characteristics, which results in some models becoming more useful than others in specific situations (Shamseldin 1997). Even with that, the ANNs for hydrologic modeling seem to have produced relevant enough results in comparison with other types of hydrologic modeling.

ANNs are applicable to many more problems including credit card fraud protection, airline seating allocation, loan approval, real estate analysis, missile guidance and detonation, and continuous-casting control during steel production (Widrow et al. 1994). Those applications are only the multilayer nonlinear problems, as are the above examples. Most applications of ANNs use a nonlinear system, since the priority benefit of using ANNs is to relate complicated data. Linear ANNs would be similar to best-fit analysis. The ANN type is dependent on the type of problem the designer is trying to solve and leads to a versatile application of ANNs while still proving an accurate modeling tool. The use of this modeling tool has also been applied to predicting storm surge and broadly forecasting hurricane impacts (Lee 2006; Pilkington and Mahmoud 2016, 2017a; b). The forecasting of hurricane impacts was conducted with multi-hazard and locational inputs that were related to an overall economic damage output categorization (Pilkington and Mahmoud 2016, 2017a; b). The research work herein seeks to expand upon such work on a more discrete level by looking at the impact to an individual building by a singular hazard.

2.6 COMPLEX NETWORKS

2.6.1 CONCEPTUAL OVERVIEW

Within network theory, graphs consist of objects connected to one another through a structural framework. A network can range from a lattice structure, to a random graph, to a small-world graph, as demonstrated in Figure 2-15. A lattice structure and random graph are considered networks in which topological features are random, or trivial, whereas a small-world graph consists of non-trivial topological features. This is to say that a random graph may look at the probability of objects (or nodes) connecting and small-world graph considers that these connections are determined values with corresponding implications, and are therefore not random.

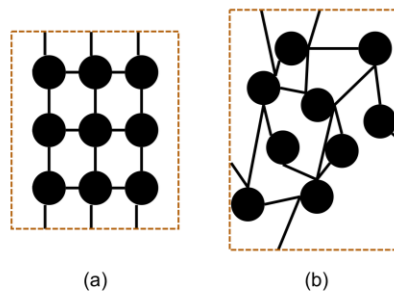


Figure 2-15 Visual differences between a (a) lattice structure and (b) a graph (either random or small-world).

Networks are essentially visual mathematical graphs to represent relationships among data. Small-world graphs consider each node's potential to be reached by another through a series of steps (or paths) even if these nodes do not necessarily neighbor each other. These graphs are commonly used in modeling social networks, the architecture of the Internet, or infrastructure, with the connection of buildings through roadways as an example. In each of these networks, there is a justification for established connections between multiple nodes. For a simple example, there was a joke in the 1990s that one person would only be "7 degrees from Kevin Bacon" (an actor). This implied that if one person traced links between people they knew

(family or friends or professional) to another person's connections (family, friends, or professional), eventually there would be a set of people (nodes) that connected any one person to Kevin Bacon. This example solely serves the purpose to illustrate that those connections were not random but specific and that, eventually, two nodes would connect. A physical example would be how two buildings connect by a series of roads. If a person is traveling from home to their office, there may be multiple roadway options and if construction is occurring, the person may be rerouted through other potential roadways but still, ultimately, be able to make it to work just with a longer travel time.

The research conducted herein will focus on those small-world graphs with distinct connections. In order to analyze such networks/graphs, graph theory is often used. Graph Theory requires an established set of nodes and edges (connections), by which information would flow between nodes. Such analyses focus on measuring attributes such as: the degree of connections entering and exiting a node, the possible paths (of connections) between two nodes, and/or if there are certain nodes that "cluster" together through strong connections.

An incredibly complex network that has been of significant interest to many is the brain. The brain has been well known to constitute a complicated structural network consisting of nodes, or neurons/cells, that connect through synapses (Cajal 1995; Swanson 2003). Neurons within a certain portion of the brain are also thought to connect to other portions of the brain based on spatial proximity (Bullmore and Sporns 2009). The topological structure and synapse lengths have been evaluated as a potential factor in many cerebral type diseases. More recently, studies have been conducted using graph theory to analyze differences in the brain by age, the presence of Alzheimer's, and the diagnosis of schizophrenia, which were able to identify structural network difference between patients with the disease and those without, such as weakened connections between specific sections of the brain (Achard and Bullmore 2007; Bullmore and Sporns 2009; Fair and et. al. 2007; He et al. 2008; Micheloyannis and et. al. 2006; Rubinov and et. al. 2007; Sporns 2002; Supekar et al. 2008). Being able to apply graphical

analysis to a brain network involved being able to obtain a reasonably fine resolution of the brain's structure and/or function from a Magnetic Resonance Images (MRIs) or Functional Magnetic Resonance Images (or (f)MRIs) and electroencephalograms (EEGs), which would then be used to construct a networked graph, as procedurally outlined in Figure 2-16. These studies then evaluated the resulting graphs using shortest path and centrality analyses.

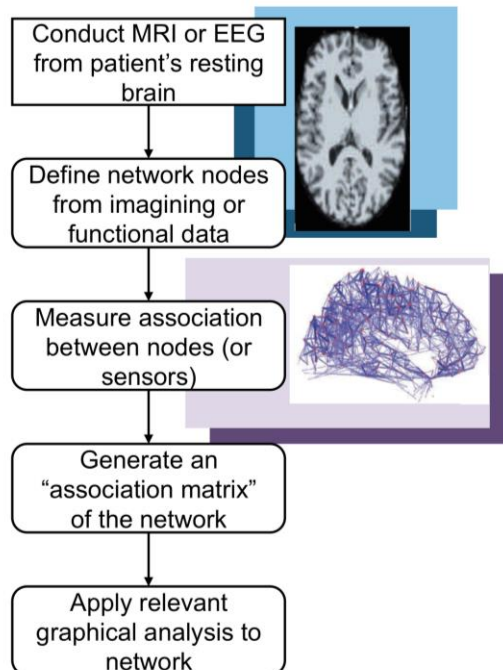


Figure 2-16 Process for creating a network from human brain data (Bullmore and Sporns 2009).

These recent studies provide a basis for using graphical analysis (Graph Theory) to understand the patterns formed in artificial neural networks, since these are primarily based on how the human brain learns. Similar concepts in graphical analysis (path length, clustering, closeness, and hubs) will be discussed further in the methods chapter of this dissertation. Essentially, combining these two methods (ANNs and graph theory) provides an opportunity to explore the variances between different network types in order to draw conclusions on how variables (neurons) contribute to an outcome (actions).

2.7 SUMMARY

Current approaches to modeling community resilience as it pertains to natural hazards are typically separated by discipline. Sociologists, engineers, and economists tend to have individual models with consideration to a specific hazard. Additionally, modeling debris flow in a wind event and its effect on the building envelope in a real world scenario is incredibly complex as it involves changes to building fragilities as debris breaches the envelope based upon the fluid dynamics of the surrounding atmosphere. Combining these multidiscipline models in a cohesive manner is of interest within the field of natural hazards but has proven challenging to accomplish, which is likely why most models currently treat each discipline separately and then attempt to combine. The use of ANNs could assist in solving this predictive modeling problem by providing a means of interconnecting multiple disciplines in a single cohesive model.

Within an ANN designed with the predictive goal of building damage or recovery time from extreme wind events, each input neuron can represent engineering, debris potential, and socio-economic factors in relation to the locational hazard severity. The use of hidden layers within the ANN structure allows these variables to integrate in a nonlinear manner before producing an output damage or recovery time. The research discussed within the following chapters seeks to address whether or not this modeling approach would be applicable for modeling building damage and recovery time for a community subjected to a wind hazard.

While applicability of ANNs has become popular across multiple fields, it also raises concerns due to its inherent “black-box” nature. Most ANN modeling results are typically explainable but not necessarily interpretable. As was done with human brain network connections, graph theory could provide a way forward in interpreting ANN structures. By attempting to open up this “black-box”, it may be possible to further evaluate how exactly socio-technical variables interact, with respect to a wind hazard scenario, to result in building specific damage states and time to rebuild following the event. The use of graph theory will therefore

provide not only a means of interpreting the resulting ANNs and assessing their applicability, but also a means forward in understand how we may be able to combine multidiscipline models in the future.

CHAPTER 3 MEANS AND METHODS

3.1 ARTIFICIAL NEURAL NETWORKS

Within this research, ANNs were used to create models that could predict a building's damage state and recovery time from a wind-related hazard event. Building an ANN requires complete data sets with inputs and known corresponding results, or "targets". The term "building" herein refers to the processes of multiple iterations (or epochs) of analysis through a data set to reach a lowest possible error. Therefore, one build consists of multiple iterations and results in the lowest possible error achieved during the iterative analyses. The purpose of these multiple iterations, and how the error is calculated, will be discussed in detail within the following subsections.

An ANN's structure consists of multiple layers, each with multiple neurons (or nodes): an input layer, hidden layer(s), and an output layer. The input layer has a neuron for each input parameter and the output layer has a neuron representative of each potential outcome (in this case either a damage state or recovery time). The hidden layer(s), which receive data from input neurons to be carried to the output neurons, can vary from a few neurons to millions, which would require a significant computational power. In other natural hazard impact modeling problems, it has previously been found that an ANN should have at least 10 hidden neurons and that a significantly higher number of neurons can slow down computations in building the ANN without significantly lowering the resulting error (Pilkington and Mahmoud 2016).

Supervised feed-forward networks, as was used for this research, involve programmer-controlled data provided to the ANN, where such data only flows "forward" from input to hidden to output layers. A graphical representation of this layout and the above-defined terminology was shown previously in Figure 2-14. Determining the structural layout was the first step in building an ANN, and within this research, a 10-hidden neuron structure was used as a starting

base, with 5 output neurons, and a varying number of input neurons across multiple models. In this structure, each input connected to each hidden neuron, which then connected to each output neuron.

The building process typically consists of training, validation, and testing phases. In the training phase, the bulk of the data (70% of the data points) was used to initialize neuron biases and connection weights. In the validation phase, a smaller sample of the data (15%) was used to check the error between what the network produced as an output and what the target was. In the testing phase, the remainder of the data was used to check the network error. However, there were cases where a build would only consist of training and testing phases, which primarily occurred in using Bayesian Regulation training methods (Beale et al. 2018). In such cases, the testing phase was then used to check the output error as the validation phase would have, with the data from the validation phase moved to the training phase.

Each connection within the network has an adjustable weight value that would dictate if a connection is activated, and if so, how “strong” of a connection. The hidden and output neurons also have bias values acting on the neurons themselves, which shift the intercept of the transfer function as will be shown in the following sections. Within each network build, the weights and biases were adjusted during each iteration. At least six iterations were conducted, and if the first of the six proved to produce the lowest possible error, then that is the resulting end network that moved on to the testing phase and was subsequently applied. If not, then the weights and bias adjustments continued until a lowest possible error was reached. Because of this strategy, having too few of iterations to check results could lead to ANNs with high error, while having too many could cause the build process to continue indefinitely. Therefore, six iterations were used to check for the minimum error.

Section 3.1.1 will cover the mathematical principles, process (as summarized in Figure 3-1), and variations to be addressed within this research to build ANNs. The best performing builds, those with the lowest percent error for the whole data set, will then be applied in real

scenarios and validated through hindcasting. The data collection methods will also be discussed, in detail, as this is a critical part of the ANN build and hindcasting process.

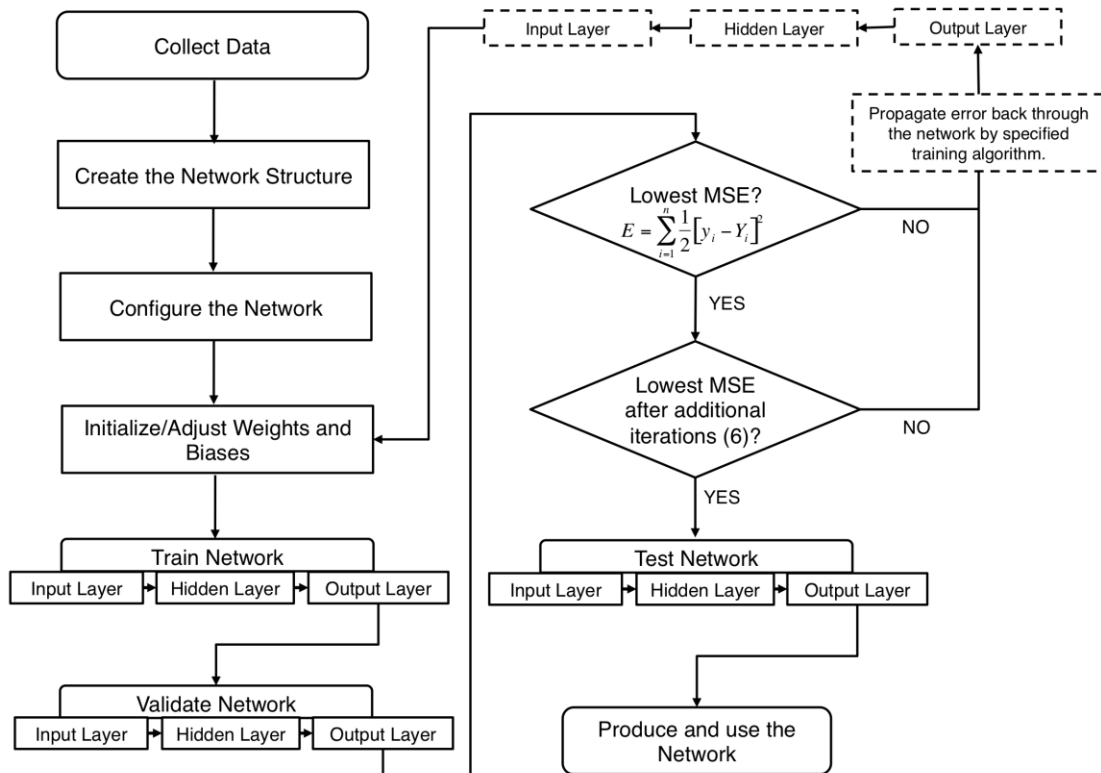


Figure 3-1 Overall process to build an Artificial Neural Network (MSE stands for Mean Square Error, and is discussed in detail in the following sections).

3.1.1 USING MATHEMATICAL PRINCIPLES TO TEACH MACHINES

Through the use of a data set with known outcomes (targets) associated with input variables, ANNs were built to establish patterns for how the inputs relate to the targets through adjustments to the weights and biases. The principals used in creating these patterns may vary, but were essentially types of regression analyses. These relationships between neurons of different layers consisted of a neuron value (x), connection weights (W), node biases (b), and transfer functions (s-curves), as shown in Figure 3-2. The relationships and algorithms discussed within this section began to be introduced before computing power was even available to accomplish such data intensive modeling and have been utilized and built upon in

subsequent years. However, these foundational concepts are still relevant to within recent ANN applications.

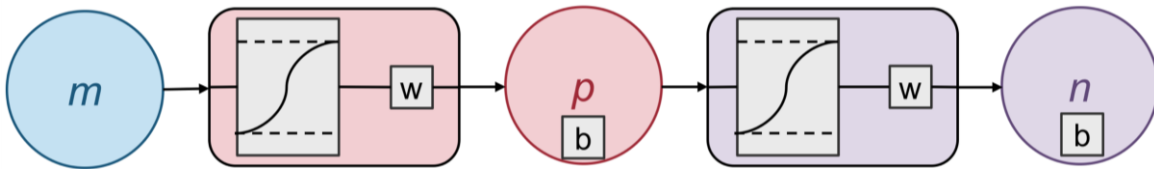


Figure 3-2 Parameters contributing to the relationships between neurons and where those “act” within the network structure (m is the number of inputs, p the number of hidden neurons, and n the number of outputs).

The data set (D) used to build the ANNs consisted of inputs and outputs. However, within this data set the scales for each input variable differ. For example, wind speed ranged from 0 to 175 knots, while the median year built (year of building construction) ranged from 1800 to 2018. The transfer function served as a mean to normalize data before entering the next layer, such that each input had the same bounds. In keeping with this concept, there was a transfer function associated with the inputs before entering the hidden layer, and the hidden neurons before entering the output layer. The use of a transfer function, which has an s-curve shape, introduced the non-linear attribute of ANNs.

When the weights on the connections between each of these inputs to a hidden neuron were updated, as will be described further in this section, it was typically proportional to the change in the input vector. If, for example, all the input vectors were positive, then all the weight updates feeding into the neuron would be the same sign. This would result in weights that can only increase or decrease together, which would be undesirable (LeCun et al. 2012). Therefore, the goal was to normalize each input data set such that the average would be near zero with a covariance of one. The most common forms of transfer functions are the log-sigmoid, tan-sigmoid, and pure linear function. The pure linear function was not utilized, as the desirability of using an ANN is its nonlinear nature. The log-sigmoid and tan-sigmoid functions are bound by $[0,1]$ and $[-1,1]$, respectively, as outlined by the following equations:

$$f(s_i) = \frac{1}{(1+e^{-s_i})} \quad (3-1)$$

$$f(s_i) = \frac{2}{(1-e^{-2s_i})} - 1 \quad (3-2)$$

where s_i is each neurons' activation (or voltage to excite), ranging from infinity to negative infinity, such that

$$s_i = b_i + \sum_{j=1}^{i-1} W_{ij}x_j \quad (3-3)$$

where W represents the weight from the j th to the i th neuron, b is the bias on the i th neuron, and x relates to the neuron values being “fed” into the following layer (Svozil et al. 1997; Werbos 1990), as shown graphically in Figure 3-3.

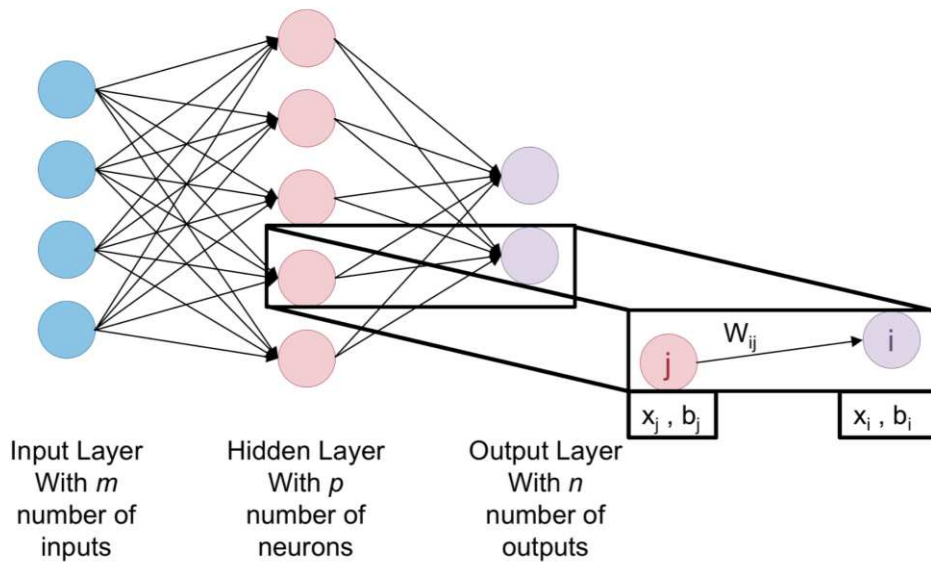


Figure 3-3 Relationships of weights and biases between a network's neurons.

This research, along with most other classification type problems, used target values that are binary. This may seem to suggest that a log-sigmoid transfer function would be ideal as it bounds the asymptotes to zero and one. However, choosing this function would cause weights to become “stuck”. The training process would attempt to fit the output data as close as possible to the target values (causing over-fitting), which would only be achieved asymptotically, causing large weight values that would eventually result in a gradient that produces weight update

values to be close to zero (LeCun et al. 2012). Therefore, the tan-sigmoid function was used from as the transfer function in building these ANNs.

The weights and biases were updated, as previously mentioned, as part of the process to minimize error between the output and target values using standard backpropagation in a multi-layer network. Backpropagation refers to the fact that the error value was transmitted backwards through the network from output to hidden to the input layer. Within this research, ANNs were trained by minimizing the mean square error (MSE) or sum square error (SSE), E , between the network output value, y , and the actual target value (known from data set), Y , as computed by:

$$E(w_{ij}) = \frac{1}{z} \sum_{i=1}^n [y_i - Y_i]^2 \quad (3-4)$$

for n number of output neurons (for example, damage states 0-4) with $z=n$ for MSE and $z=2$ for SSE approaches.

Subsequently, the target value, Y , was a function of the data set $D(x,y)$ and the activation function, s . The error determined in Equation (3-4) was propagated back through the network to adjust the weights and biases as well as change the neuron activations by means of a myriad of training algorithm approaches. Most of these approaches predicate on first determining the gradient of the Cost (Error) Function (3-4) with respect to the weights ($-\delta w_{ij}$), such that

$$\frac{\partial E}{\partial w_{ij}} = \frac{\partial E}{\partial y_i} \times \frac{\partial y_i}{\partial w_{ij}} = -(Y_i - y_i)x_i = -\delta w_{ij} \quad (3-5)$$

The $-\delta w_{ij}$ parameter would eventually update to a zero value in over-fitting cases if the log-sigmoid activation function was used in first normalizing the data. Table 3-1 outlines some of the method variations used in achieving this step. Changing how the network learns, through each of these algorithmic methods, was one of the proposed variations to the ANNs in determining the best performing network for the problem types to be addressed herein.

Table 3-1 Learning Algorithm Variations for updating weights and biases.

Acronym	Name	Brief Description
LM	Levenberg-Marquardt	Least-squares curve fitting function (Marquardt 1963).
RP	Resilient Backpropagation	Function fitting depending on the gradient of the transfer function with respect to the weights (Riedmiller 1994).
BFG	BFGS Quasi-Newton	Function fitting with respect to the transfer function gradient (Gill et al. 1981).
SCG	Scaled Conjugate Gradient	Gradient descent with line search techniques to adjust “steps” to fit a function (Møller 1993).
CGB	Conjugate Gradient with Powell/Beale Restarts	Function fitting with respect to the transfer function gradient. Update for each iteration is a factor of the previous gradient and the previous direction used to find the minimum point of the function (Powell 1977).
CGF	Fletcher-Powell Conjugate Gradient	Function fitting with respect to the transfer function gradient. Update for each iteration is a factor of the square of the previous gradient and the square of the current gradient (Scales 1985).
CGP	Polak-Ribiere Conjugate Gradient	Function fitting with respect to the transfer function gradient. Update for each iteration is a factor of the square of the previous gradient and current gradient (Scales 1985).
OSS	One Step Secant	Function fitting with the goal of determining where the gradient is zero (Constantinescu et al. 2008).
GDX	Variable Learning Rate Backpropagation	Function fitting similar to gradient descent with the incorporation of momentum training (Mathworks n.d.).
BR	Bayesian Regulation	Probabilistic approach using Bayes Theory (Buntine and Weigend, Andreas 1991; Neal 1992).

3.1.2 PROPOSED VARIATIONS

An ANN can be altered by many different characteristics, including but not limited to: the training algorithm, the performance function, the number of checks performed during validation, the number of hidden neurons, the transfer function, and even how the data was divided for

each stage. For the research discussed herein, the number of checks was six (6), number of hidden neurons was ten (10), the transfer function was the tan-sigmoid function, and the data was divided as a 70/15/15 among training/validation/testing phases. The training function was a mathematical approach used to track the provided data through the network and adjust connection weights and neuron biases as outlined in Equations 3-1 through 3-5. For pattern recognition, multi-layer, feed-forward networks, only certain performance functions were used: MSE and SSE. These two ANN characteristics (training algorithm and performance function) were the initial ANN structural variants to be adjusted, as they may prove more useful for exploring different problem types.

Within this research, the training algorithms and performance functions were first assessed for an initial model containing all the data gathered (Model 1) before moving on to evaluating model variations. The training algorithms examined for Model 1, for both damage and recovery modeling, were shown in Table 3-1. In evaluating the various training algorithms, the same performance function (MSE) was used followed by the SSE performance function. The mathematical differences between training functions are outlined as follows:

LM is a least-squares curve fitting function that began its first training iteration with an initial guess of s (the activation function) to be adjusted by δ (Marquardt 1963). As one of the first algorithms created for machine learning purposes, LM uses the Jacobian Matrix, \mathbf{J} , and identity matrix, \mathbf{I} , in order to adjust s by

$$(\mathbf{J}_i^T \mathbf{J}_i + \lambda \mathbf{I}) \delta_{ij} = \mathbf{J}_i^T [y_i - f(s_i)] \quad (3-6)$$

where λ was considered a kind of “damping” variable that can change size for each iteration. Similarly, RP uses a weight related update value, Δ , that ties to the weight value change, Δw , as follows (Riedmiller 1994):

$$\Delta w_{ij}^{(t)} = \begin{cases} -\Delta_{ij}^{(t)}, & \text{if } \frac{\partial s}{\partial w} > 0 \\ +\Delta_{ij}^{(t)}, & \text{if } \frac{\partial s}{\partial w} < 0 \\ 0, & \text{else} \end{cases} \quad (3-7)$$

with update-values following each iteration (t), as follows:

$$\Delta_{ij}^{(t)} = \begin{cases} \eta^+ * \Delta_{ij}^{(t-1)} , & \text{if } \frac{\partial s^{(t-1)}}{\partial w} * \frac{\partial s^{(t)}}{\partial w} > 0 \\ \eta^- * \Delta_{ij}^{(t-1)} , & \text{if } \frac{\partial s^{(t-1)}}{\partial w} * \frac{\partial s^{(t)}}{\partial w} < 0 \\ \Delta_{ij}^{(t-1)} , & \text{else} \end{cases} \quad \text{where } 0 < \eta^- < 1 < \eta^+ \quad (3-8)$$

These equations were executed for neuron bias values (b) much in the same way the weights were adjusted. Additionally, these procedures were performed for every possible neuron connection. In other words, \mathbf{w} is a matrix containing all weights from the input to hidden layers and the hidden and output layers.

Similar to LM and RP, a significant portion of training algorithms were based in optimization using conjugate gradient where initial weight values were assumed and adjusted. This is to say that these algorithms were function-fitting problems that used a function gradient scale and direction to update weight (and bias) values. Simply put, this would describe weight updates such that:

$$w_{ij}^{(t)} = w_{ij}^{(t-1)} + a \times \delta w_{ij} \quad (3-9)$$

where a is the step to be minimized along the search direction δw_{ij} . Starting with a simpler version of how δw_{ij} was determined, gives the conjugate gradient method in the form of the BFGS Quasi-Newton Learning Algorithm, which defines:

$$\delta w_{ij} = -H/gw_{ij} \quad (3-10)$$

where gw_{ij} is the gradient at a specific point on the function and \mathbf{H} is the Hessian matrix. This value was initiated as the steepest point then adjusted per the calculated network error. For the remaining algorithms, with the exception of BR, the determination of δw_{ij} is outlined in Table 3-2 (Beale et al. 2016; Møller 1993).

Table 3-2 Conjugate Gradient Based Training Algorithms

Algorithm	$\delta w_{ij} =$	where	Equation
CGB	$-gw_{ij} + \delta w_{ij}^{(t-1)}$		(3-11)
CGF	$-gw_{ij} + \delta w_{ij}^{(t-1)} \times \frac{r^{(t)}}{r^{(t-1)}}$	r is the normal square of the gradient	(3-12)
CGP	$-gw_{ij} + \delta w_{ij}^{(t-1)} \times \frac{(gw_{ij}^{(t)} - gw_{ij}^{(t-1)}) \times gw_{ij}^{(t)}}{r^{(t-1)}}$		(3-13)
OSS	$-gw_{ij}^{(t)} + 0.001 \times \delta w_{ij}^{(t-1)} + 0.1 \times gw_{ij}^{(t-1)}$	The values 0.001 and 0.1 are used in this study but can be altered.	(3-14)
GDX	$MC \times \delta w_{ij}^{(t-1)} + LR \times MC \times \delta P / \delta w$	MC is the momentum constant (=0.9), LR is the learning rate (0.01), and P is the performance of that iteration	(3-15)

The majority of previously established learning algorithmic methods evaluated ANNs as a function-fitting problem. BR, however, is probabilistic focused in Bayes Theory such that,

$$p(w_{ij} | D_i) = \frac{P(w_{ij})P(D_i | w_{ij})}{\int P(w_{ij})P(D_i | w_{ij})} \quad (3-16)$$

In other words, BR evaluates the probability of the weights, w_{ij} , on the connections between neurons given the data set, D (Buntine and Weigend, Andreas 1991; Neal 1992).

Within this research, the various training methods and square error types were explored for their impact on the resulting network built to address the problems of modeling building damage state and recovery from severe weather events. Following the network training method variations, different possible input arrangements were considered with the ultimate goal of evaluating what potential parameters should be used in determining impact and recovery of a community's building stock.

To determine the best performing network algorithmic methods and input variations, the percent error (number of parameters misclassified through all phases), training performance (how well the network was able to minimize error through backpropagation), false positive rate (FPR), false negative rate (FNR), true positive rate (TPR), and true negative rate (TNR) were tracked. The FPR, FNR, TPR, and TNR are associated with the receiver operating characteristics (ROC) of the network, which was why they were deemed valuable parameters to judge the network. The percent error is essentially an overall result of these rates. As an example, the FPR is known as the number of false positives associated with the produced network. For example, a false positive is similar to the “crying wolf” outcome where it is said a “worse” result will occur, but it does not and can be given by the equation:

$$FPR = \frac{\text{false positives}}{\text{all output positives}} \quad (3-17)$$

The remaining rates are given by the following equations

$$FNR = \frac{\text{false negatives}}{\text{all output negatives}} \quad (3-18)$$

$$TPR = \frac{\text{True positives}}{\text{all output positives}} \quad (3-19)$$












$$TNR = \frac{\text{True negatives}}{\text{all output negatives}} \quad (3-20)$$

The “true” rates were desired to be closer to one (or 100%), while the “false” rates were desired to be closer to zero. Model 1 was initially built a minimum of 50 times for each training algorithm outlined above. The data from these builds was then assimilated in order to determine the mean, mode, maximum, minimum, and standard deviation for each performance characterizing parameter (PCI). FPR, FNR, TPR, and TNR were originally calculated for each “class”, for example the damage state classification neuron, but the mean of all the five classes was used in the evaluation of the PCIs in the interest of assessing the accuracy across the whole network. In order to ensure this was an adequate representation of each algorithm, the PCI data from multiple builds was evaluated for a coefficient of variation of less than 0.5 with

95% of the data falling within +/- 2SD (two standard deviations). In other words, majority of builds did not vary by more than 50% of the mean, making the sample size representative of the most likely PCI outcomes. If 50 builds did not result in meeting these requirements, then additional builds were created until the PCI data fell within these requirements, resulting in builds for certain algorithms counting in the hundreds. The “best performing” Model 1 builds were determined to be those with lower percent errors (typically associated with a lower mean square error), FPR, and FNR, but higher TPR and TNRs. From this point, those best performing ANN methods (training algorithms and performance functions) were used in the subsequent step of altering the input parameters.

Two ANN model types were created within this research: one type to determine building damage state and one to determine recovery time. The inputs to the neural network were altered multiple times with the desired goal of determining which factors best contributed to a resulting damage state and/or recovery time. Model variations for the inputs contributing to damage state are outlined in Table 3-3, in which certain variables were lumped together, such as race (e.g. either all race categories were included in the model or none were). The 10 damage models were designed so that subsequent evaluation could determine if an ANN was able to capture debris potential and how some socioeconomic factors may influence the resulting damage states. The primary form of evaluating this was through the PCIs and how each model compared to the other models. The model with the most desirable PCIs was then chosen as the final ANN for application. However, in application, an ensemble consisting of multiple ANNs of the same structure (different weights and biases), for the best build performance across training algorithms and model input variations, was used for graphical analysis and hindcasting the Joplin, MO tornado event.

Table 3-3 List of variables and associated models that contain each. (Blue shading indicates current factors considered and green indicates new factors to combine. Key images are various forms of clipart (CanStockPhoto n.d.; ClipartXtras n.d.; Emojipedia n.d.; GalleryYoPriceVille n.d.))

Input Variable	Models Associated	Key
Hazard (wind type, speed, and event size)	1 2 3 4 5 6 7 8 9 10	
Structural (year built, occupancy, roof & wall materials, roof shape, footprint)	1 2 3 4 5 6 7 8 9 10	
Surface Roughness	1 2 3 4 5 6 7 8 9 10	
Estimated Percent Forested (and Impervious Surfaces)	1 7 8 9 10	
Tenure (% own, % rent)	1 2 5 8 9	
Housing & Population Density	1 7 8	
Total Population	1 2 4 5 6 7 8 9 10	
Age	1 2 6	
Race (% Asian, African American, Native American & Hispanic)	1 2 6	
Industry Employment (extractive and service)	1 2 4	
Income (per capita & income: poverty)	1 2 4 9 10	

3.1.3 DATA COLLECTION

Building an ANN hinges on the availability of reliable data with known matching inputs and targets. In order to build an ANN that could be used to ultimately forecast the damage and subsequent recovery from a wind hazard scenario, historical events must be evaluated for relevant information based on what is available. Within this study, the NWS Damage Survey viewer was used to analyze damage photos for the structural characteristics and their respective damage states following a wind-related weather event (National Weather Service 2018). This site also listed a wind speed associated with each geo-tagged damage photo.

These photos and satellite images provided the structural and hazard related inputs, respectively, introduced in the blue sections of Table 3-3. The remaining data was extracted from the 2015 U.S. Census American Community Surveys (ACS). This data was available by census block, block group, tract, and county. NWS survey photos from January 1, 2011 to December 31, 2015 were used in order to match data availability of ACS block group demographics. However, it is worth noting that ACS data does have significant error distributions and will therefore impact the resulting ANNs built. For this research it was determined that an individual building would be located within a census block group and would assume the characteristics of that group. The U.S. Census block groups were chosen for the social parameters because while it is the second smallest size, it is not too fine as to create issues in processing large data sets. Census block groups, like blocks, are bounded by roads, water, and governmental defined boundaries and are therefore different shapes and sizes. The relevant demographic data of a block group assigned to a building spatially residing within its boundaries, were chosen based on the SoVI (Cutter et al. 2003) and other peer reviewed vulnerability indices (Burton 2010; Flanagan et al. 2011; Fothergill and Peek 2004; Morrow 1999; Sherrieb et al. 2010). This data was considered as the building's surrounding conditions potentially affecting the structure itself.

With an ANN, all data must be in numeric form; therefore, a key was created to denote structural component type designation (such as roofing material), hazard type (such as tornadic versus straight-line winds), and locational characteristics (such as surface roughness). This full key can be found in Appendix A. While Census data represents a numerical range, the structural data is mostly categorical. However, in reconciling this discrepancy, the categories were established with some sense of order. For example, the materials were "ranked" by their modulus of elasticity such that a lower ID value of "1" would indicate a material with a lower modulus of elasticity than the other materials available.

The output damage states were defined based on commonly accepted and previously applied definitions (Memari et al. 2018; The Federal Emergency Management Agency 2016) as outlined in Table 3-4. These damage states were also chosen over the “Degree of Damage” (DoD) scale so that they may be compared to the previous work conducted by Memari et al. (2018), which included 19 different archetype fragilities. In essence, each survey photo of a structure was assigned multiple attributes to illustrate its structural characteristics, surrounding demographics, hazard, and its ultimate damage state. These input data were extracted from multiple sources and are detailed in Table 3-5.

Table 3-4 Windstorm Damage States for Buildings and EPN

Damage State	Range of damage ratio (%)	Description	Equivalent FEMA Assessment Description	Additional Descriptions	Ex. NWS Wording or Image descriptions
0	0	No damage	No damage		
1	> 0-10	Slight damage	Affected. Some missing shingles. Cosmetic damage such as siding.	One or two damaged/down EPN wires.	"Threshold of visible damage" (typically)
2	> 10 - 20	Moderate damage	Minor. Nonstructural damage. Blown out windows.	Most wires off EPN pole. Poles tilted as if being lifted out of ground.	"Loss of roof covering <20%"
3	> 25-50	Substantial to heavy damage	Major. Failure or partial failure of structural elements. Missing roof but walls still intact. Water line 18" above floor.	EPN pole cracked/ all wires down. Manufactured home shifted off piers (HUD)	"Large sections of roof structure removed." "Most walls remain." "Uplift of roof deck"
4	> 50	Very heavy damage (destroyed)	Destroyed. Complete failure of at least two structural components. Imminent threat of collapse.	EPN pole completely down	Exterior wall collapse, but some of roof might remain.

Table 3-5 Potential Input Variables

Input Category	Input Sub-Category	Description	Source	Additional collection method notes
Hazard	Hazard Type	Designation of wind or flooding hazard	(National Weather Service 2018)	See Appendix A Designation
	Intensity 1	Primary descriptive data such as wind speed		
	Intensity 2	Secondary descriptive data such as tornadic versus straight-line winds		
Locational	Surface Roughness	ASCE designations based on surrounding landscape.	(American Society of Civil Engineers 2010)	Visual estimation based on satellite view of area surrounding the parameter in question.
	% Impervious Surfaces	Approximately how much of the surrounding area consists of roads, buildings, or other non-natural surfaces.	Satellite (Google 2018)	
	% Forested	Of the remaining pervious surfaces, approximated amount of trees (area).		
	Housing Density			
	Median Age			
	Per Capita Income			
	% African American			
% Hispanic			Calculation to retrieve as fraction of total population	
% Native American				
% Asian			(U.S. Census Bureau 2018)	
	Tenancy	Percent owning their own property (over renting)		Calculation based on total housing units
	Unemployment Rate	Poverty to income ratio		

Table 3-5 Potential Input Variables Continued.

Input Category	Input Sub-Category	Description	Source	Additional collection method notes
Buildings	Year Built	Median year built for census block	(IBC 2007)	See Appendix A
	Year Retrofitted	Any upgrades in structural performance (if none value of zero entered)		
	Occupancy	IBC Occupancy Class		
	Wall Material	The actual MWRFS and the façade. Connections were assumed to be based on the materials.		
	Roofing Materials	The actual MWRFS and the cover. Connections were assumed to be based on the materials.		
	Roof type/shape	Standard roof designations		
	Extra Measures Height	If a note of structural measures such as hurricane straps/ties. The equivalent number of stories.		
Footprint Area	Estimated as very small (trailer) to extra-large (shopping mall).			

The variables listed in Table 3-5 were chosen based on factors used to create structural fragilities, common structural concerns found in case studies, social vulnerability related to natural hazards, and any other attributes of the hazard that would ultimately affect the structure. Some of these parameters, such as percent area forested and the size of the hazard event, are intended as options in communicating potential debris impacts of a building, to an ANN learning system. In other words, increased number of trees nearby indicates a potential for branches to

become projectiles, while a larger tornado event would encompass more debris to be transported across the path. Similar logic was used in deciding to incorporate the housing density, since Yau et al. (2011) showed that neighboring buildings do have an effect on structural damage.

The building data points used to build the ANNs discussed herein were all taken from various severe wind events across the state of Missouri, due to the idea that the Joplin tornado would later be used to validate the models. The focus on one state allowed for inherent similarities among the population and building codes, however if other states were included in the data set, then an identifier variable could be added to alert the ANN to changes in the data's inherent location characteristics. All data points (buildings) from the NWS Damage Survey Viewer, within the state of Missouri (minus the Joplin tornado), were exported as a shapefile and the census block group data shapefile (specifically, the ACS 2015) was obtained from U.S. Census. Both were analyzed within ArcGIS and each data point was associated with the census characteristics of the block group it resides in, with examples shown in Figure 3-4. The values for the percent area forested and percent impervious surfaces were estimated through satellite views of the area. The resulting data set contained 117 features, each with 31 attributes to be assessed as possible ANN inputs and 5 additional attributes to denote damage state. The recovery ANN models included similar inputs that followed the same concept of a building residing in a census block group. However, the 5 outputs became 6-month, 1-year, 1.5 years, 2 years, and over 2 years (abandoned) time to rebuild and reoccupy (recover).

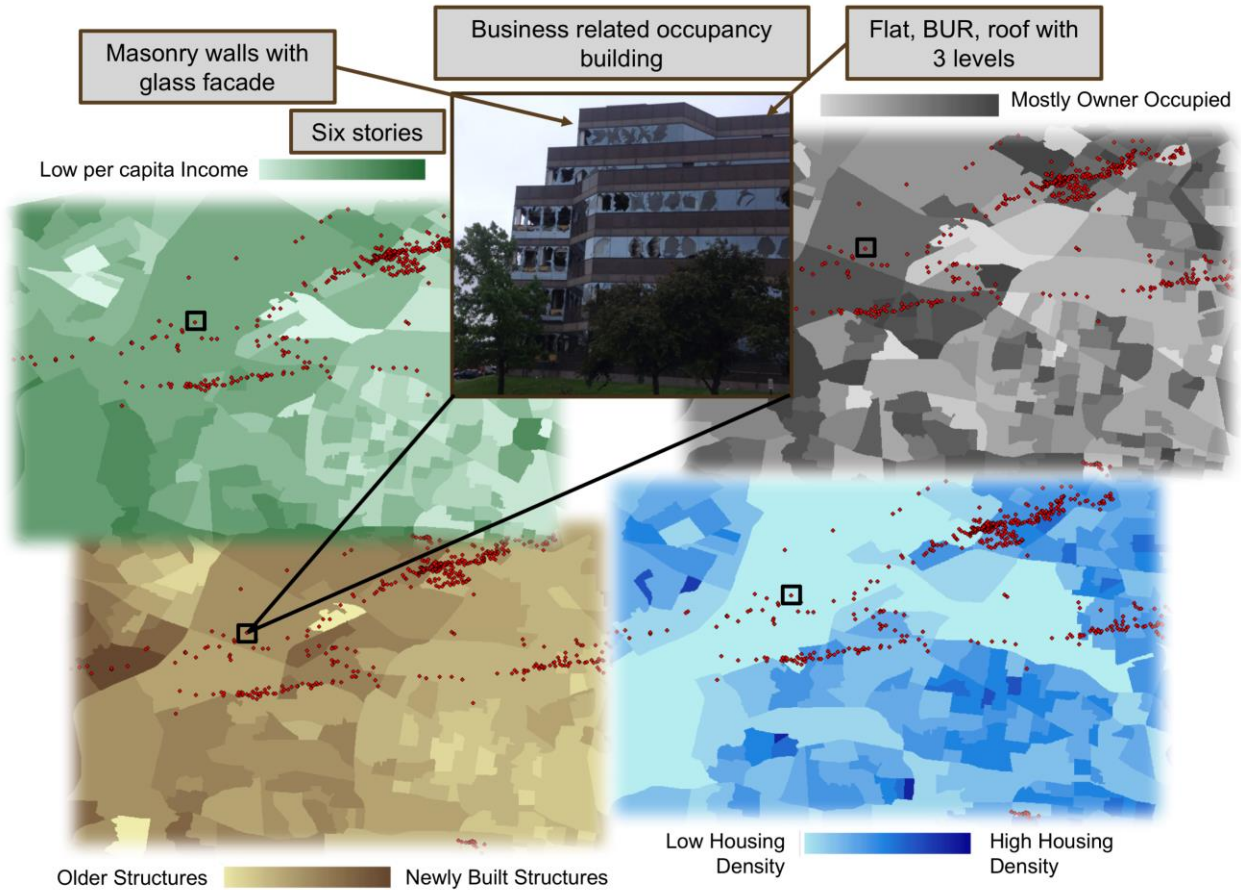


Figure 3-4 Example structure feature and the U.S. block group data of where it is located.

In gathering this data, the most subjective, or difficult, portion was evaluating the photos found through the NWS Damage Survey Viewer. Only NWS damage points with photos could be used, but even those posed difficulties in deciphering the original structure shape and materials if the building was completely destroyed. If a photo showed a house (or even roof) completely gone, then the materials and roof shape were taken from context of nearby debris, neighboring homes, standard construction for the building type described, and prior satellite imagery where possible. Mixed materials, especially in the building façade, were taken into account through the use of decimal numbers and are further detailed in Appendix A. The occupancy type was typically noted in the damage survey, and if not, educated judgment was used based on structural appearance and the surrounding buildings. The ASCE surface

roughness was typically assigned as either B or C depending on if the structure was in an urban or forested area, or in the plains. For example, farmlands were treated as surface roughness C. Examples of each of the damage states and some of the associated characteristics from photos throughout the state of Missouri for various extreme wind events are shown in Figure 3-5 through Figure 3-8.


Damage State 1	Item	Value/Category	Designation
	Median Year Built (BG)	1971	N/A
	Occupancy	Business	304.1
	Walls	Reinforced Masonry & Glass	7.9
	Roofing	Concrete Slabs & BUR	7.4
	Roof Type	Flat with 3 levels	1.3
	Height (stories)	6	N/A
	Footprint Area	Large	4
	Owner Occupied (BG)	73%	N/A
	Per Capita Income (BG)	\$30,332	N/A
	Housing per sq. meter (BG)	1.27e-5	N/A
	Population per sq. meter (BG)	2.01e-5	N/A

Figure 3-5 Damage State 1 structure with example ANN input values.

Damage State 2	Item	Value/Category	Designation
	Median Year Built (BG)	1975	N/A
	Occupancy	Farmhouse/shed	312.1
	Walls	Wood & Plastic	5.3
	Roofing	Wood and Aluminum	5.8
	Roof Type	Two intersecting gables	10.12
	Height (stories)	2	N/A
	Footprint Area	Medium	3
	Owner Occupied (BG)	74%	N/A
	Per Capita Income (BG)	\$24,174	N/A
	Housing per sq. meter (BG)	1.00e-5	N/A
	Population per sq. meter (BG)	2.38e-5	N/A

Figure 3-6 Damage State 2 structure with example ANN input values.

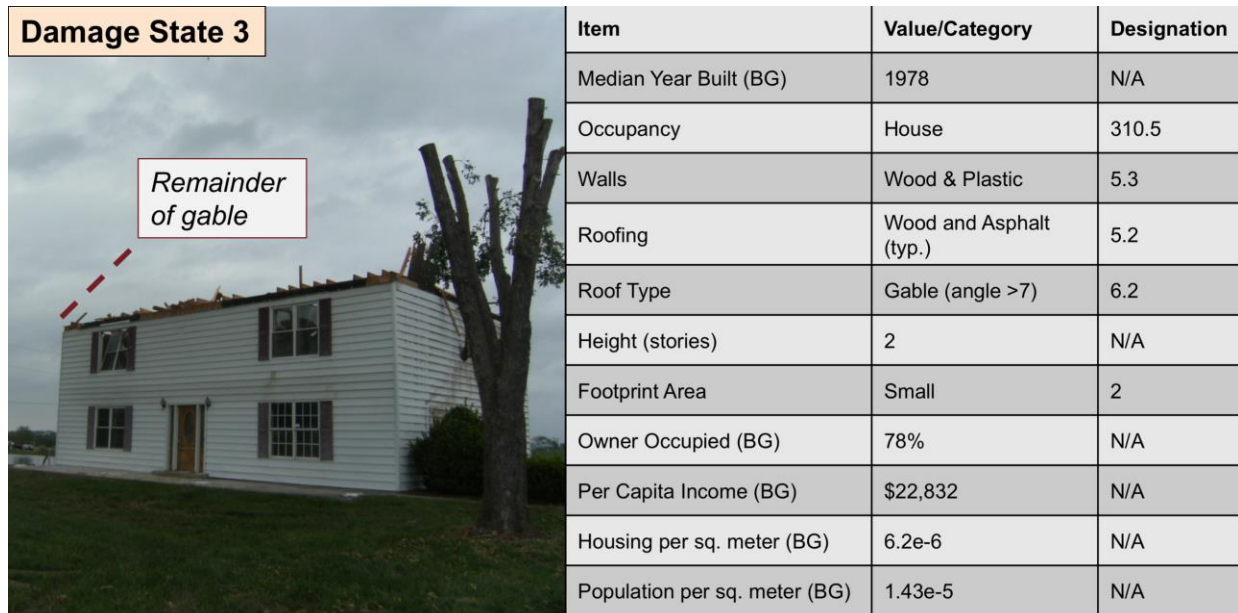


Figure 3-7 Damage State 3 structure with example ANN input values.

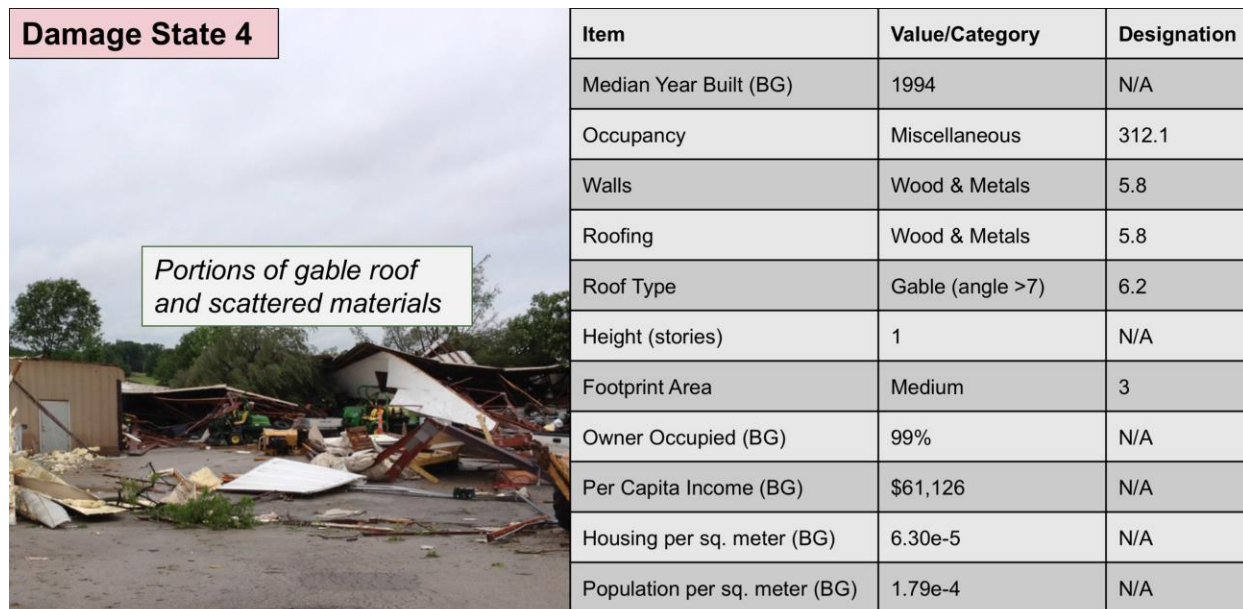


Figure 3-8 Damage State 4 structure with example ANN input values.

These same 117 data points, which cover an array of wind events, locations, structures, and damage states, were then used in creating the recovery model ANNs. Each photo was geotagged and then located within Google Earth, which possesses an ability to step back through satellite images over time. Once a structure was geographically located within Google Earth

based on the NWS geo-tagged photos, a visual assessment was made of the structure prior to the hazard event up to 3 years following the event, which would bring us to present day, if possible. Each structure’s condition was assessed for whether it was rebuilt and reoccupied by 6 months, 1 year, 1.5 years, 2 years, or not yet recovered by 2 years. Each structure (feature) was given a recovery score at each time step as shown in Table 3-6. A building was considered “good as new” when it reached a recovery state four. The output data for the ANNs was coded as whether it had recovered by each of the time designations listed. Furthermore, in addition to the input parameters listed in Table 3-5 social factors outlined in other studies (Flanagan et al. 2011; Morrow 1999) (in addition to the SoVI) were introduced. This was conducted based on a previously established concept that recovery has a stronger social component than damage theoretically would due to contributions of social vulnerability to permitting and construction delay time. These new parameters are shown in Table 3-7.

Table 3-6 Recovery States defined by (Curtis and Fagan 2013)

Recovery State	Description	Sub-Category	Elaboration
1	Uninhabited	2	Liveable: unoccupied
		5	Blighted
		10	Non-livable: extreme
2	Cleared		Lot empty due to destroyed home or clear for reconstruction
3	Rebuilding	1	Frame skeleton is up. This would only appear for homes needing a complete rebuild.
		2	Walls are enclosed
		3	Non-structural components have been added. Likely that DS 2&3 would not require more than this
		4	Cosmetic finishes
4	Rebuilt and Occupied		“Good as new”
5	No rebuild/new structure		Abandoned lot

Table 3-7 Additional Input Variables for Recovery ANNs

Input Category	Input Sub-Category	Description	Source	Additional notes
Locational	% Population over 65 yrs	Total number of males and females over 65 years of age divided by the total population.	(U.S. Census Bureau 2018)	
	% Population without vehicle	Number of persons without access to a vehicle divided by the total population.		
	% One year residence	Number of persons living in a metropolitan statistical area for at least one year, divided by the total population		One year residence variable chosen with goal of communicating ties to community
	% Single female head of household	Number of female heads of households, no spouse, with own children under 18 years, divided by total population		
	% Group quarters	Number of people in group quarters divided by the total population		
	% Disability	Number of people claiming disability divided by total population		

As with analyzing the original damage state photos, there were some complications in evaluating satellite images. The main issues were with concern to where a photo was geo-located and what building was the focus associated with the photo. In these cases, neighboring features present in both the photo and satellite imagery were compared to determine which structure was being evaluated. There were instances where a structure could not be either located or evaluated from the satellite imagery. These cases were classified as “ND” or “no data” and were removed from the data set, resulting in a final tally of 93 data points for the recovery models. Other instances causing an ND classification included: satellite images with a large time span gap (example: image availability in 2012 and 2015) with no way to ascertain when the structure was repaired, and images that may still show a structure damaged or being

repaired but there are no more recent satellite images to determine when repairs were completed. A damaged structure, as it appears through Google Earth at various points in time, is shown in Figure 3-9. Figure (a) shows a standard progression in rebuild, while Figure (b) shows how occupancy was used in determining recovery for buildings with damage states that were less obvious from a satellite view.

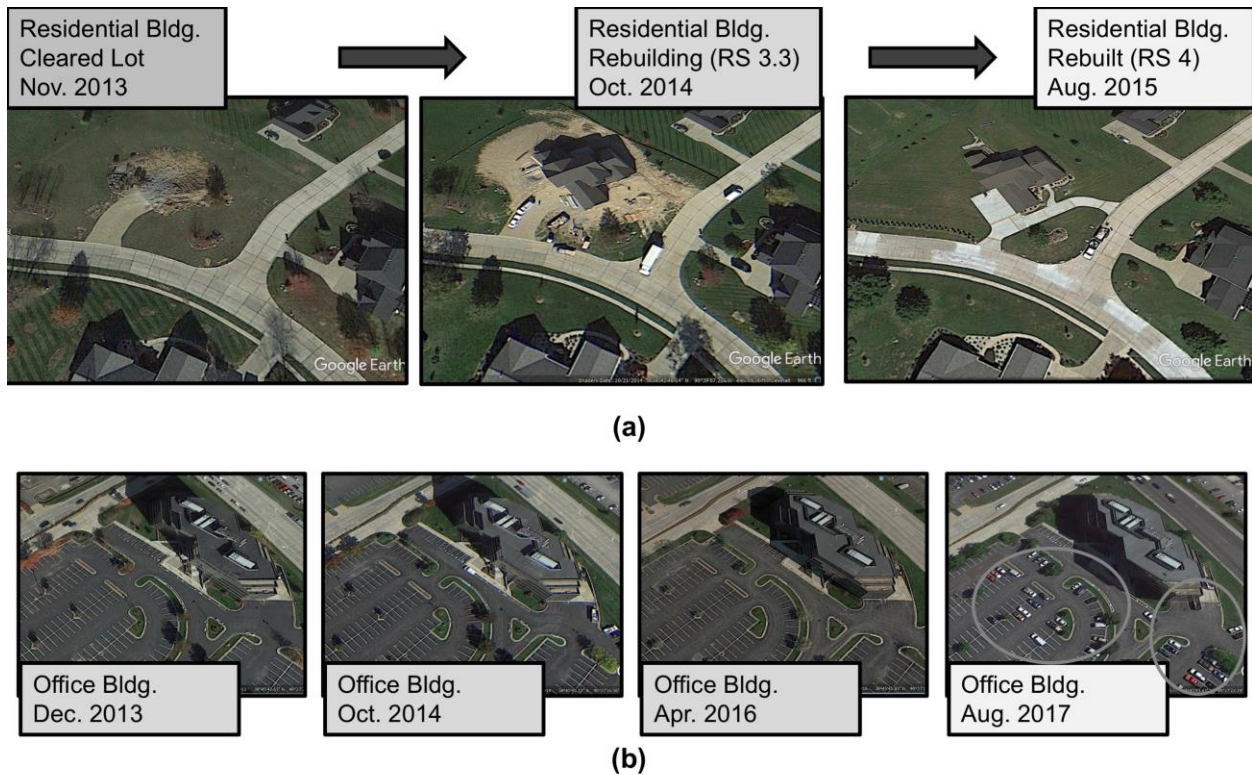


Figure 3-9 Example Google Earth images and corresponding recovery states over time for (a) DS2 residential building that decided to rebuild from June 1, 2013 tornado event and (b) DS1 office building (windows were blown out) that wasn't reoccupied until August 2017 following June 1, 2013 tornado event (circles show indications of building in use).

The ultimate goal of creating any model is to validate it with a real-world event. Within this research, the 2011 Joplin tornado was used as a hindcasting validation event. Therefore, all the above-mentioned data points fall within the state of Missouri in the interest of data consistency and the time it would take to review every image over multiple years. The resulting building damage state and recovery from the Joplin tornado also needed to be post-processed and analyzed. This is discussed in detail in Section 3.3.

3.1.4 CONCLUSION

Of the data collected, as described above, the inputs variables relate to input neurons within the ANNs, while each damage state or recovery time, relate to the output neurons. The inputs were then connected to the outputs through a hidden layer of 10 hidden neurons, where each input was assumed to connected to each hidden neuron and each hidden to each output neuron, with initialized network weights and biases. The data was then normalized through the use of a transfer function and processed through the network structure, resulting in an output damage state or recovery time. This output was compared to the known damage state (gathered from NWS survey photos) or the known recovery time (determined from Google Earth) to determine a MSE or SSE for a specific training algorithm. This error was then propagated back through the network to adjust the weights and biases. Once a minimum MSE or SSE was reached, a built ANN was produced and it's PCIs were tallied. This process was repeated multiple times for each training algorithm, performance function, and model (varied inputs) to gather statistics on how well each network structure established patterns. The best training algorithm and performance function were chosen prior to varying the model inputs. Then the best performing model was chosen, resulting in the final ANN structure, in which multiple networks were then built to create an ensemble. The networks within this ensemble fell within the best 50% of each PCI range. These final networks were then further analyzed using graph theory in order to determine more detail on what patterns were established.

3.2 GRAPH THEORY

Graph Theory (or graphical analysis) is another mathematical concept that relates nodes (neurons) through edges (connections) and provides a way to analyze a networked graph structure. Within this research, Graph Theory was used as a mean to interpret the final ANNs as

to how the input variables, both engineering and social, relate to each other and to the final outputs (damage states and recovery times), similarly to how work has been conducted in interpreting human brain fMRIs and/or EEGs. Instead of measured brain activity, though, the ANN and its final weights (connections) made up the graph to be evaluated.

3.2.1 OVERVIEW

One of the main goals within this study was to identify connectivity between socioeconomic and engineering parameters as it pertains to the problem of wind hazard impact and recovery of a community. Graph theory models connectivity through a networked set of vertices (\mathbf{V}) and edges (\mathbf{E}) such that the graph (\mathbf{G}) follows the function

$$\mathbf{G} = \mathbf{G}(\mathbf{V}, \mathbf{E}) \quad (3-21)$$

This is the traditional base equation in establishing a graph. Since in this study graph theory was used in conjunction with ANNs, the vertices were instead thought of as neurons (\mathbf{X}), which encompassed m input nodes, p hidden nodes, and n output nodes for to total amount of nodes (or neurons) Q ($m+p+n = Q$). The edges were then considered similar to the neuron connections and the associated weights (\mathbf{W}), such that

$$\mathbf{G} = \mathbf{G}(\mathbf{X}, \mathbf{W}) \quad (3-22)$$

Note that bolded variables denote a matrix, whereas subscripts (for example, w_{ij}) were used to trace equations between individual neurons within the ANN structure outlined previously. An individual weight (w_{ij}) within the set \mathbf{W} was considered the value associated with a connection (uv) between two vertices within the set \mathbf{X} . Some graphs may consist of connections, e , where the directionality is not the same across the graph while some may be considered “undirected” such that uv is considered the same as vu (Jungnickel 2005).

$$e = uv \quad (3-23)$$

In using graph theory to evaluate feedforward ANNs, the graph was considered a directed graph, such that connections flowed from input to hidden to output neurons. In other

words, only weights of positive values were used in constructing a graph from a feedforward ANN, as negative weights denoted the “deactivation” of a connection. Not all neurons were connected, however, some had multiple “walks” for how to go from one neuron to another using a different sequence of connections (Jungnickel 2005).

There are three commonly used measures to identify importance: *degree*, which is the number of a neuron’s neighbors, *closeness*, which is the shortest distance of neuron x_i to every other neuron, and *betweenness*, which is considered as a ratio of the number of shortest paths that pass through x_i from two distinct neurons to the total number of shortest paths between the same two neurons (Freeman 1979; Jungnickel 2005). Previous studies in evaluating fMRIs and EEGs used mainly degree and shortest path (closeness). These analytical measures were the focus of similarly analyzing ANN graphs that consist of neurons and connection weights.

3.2.2 ANALYTICAL CONCEPTS

The ANN structure has already been previously defined within Section 3.1. Based on this already given network structure, the following graph analyses were used to evaluate social and engineering connectivity to resulting wind hazard impact and recovery:

Shortest Path:

The shortest path problem considers the minimum “length” to travel from neuron j to neuron i . A common example of this concept would be to consider two buildings with multiple road routes from building A to building B. Each road had a travel time associated with it, which would be equivalent to a weight value. The shortest path problem assesses the shortest travel time between A and B (Bellman 1958). With an ANN, the travel time was considered equivalent to the weights, such that the shortest path (P) is defined as

$$P = \text{Min} \left[w_{ij}^{\text{input-hidden}} + w_{ij}^{\text{hidden-output}} \right] \quad (3-24)$$

where the possible path summations were simply the possible routes information can flow from input to hidden and then hidden to output layers. Higher value weights were considered stronger

connections between neurons; therefore, the results of this analysis allowed for an evaluation of how strongly an input correlated to the desired output.

Degree:

The degree of a neuron was considered as the number of connections associated with said neuron (Diestel 2017). This was further subdivided into how many of those connections were “entering” the neuron, or the “in-degree” (D_{in}), and how many were exiting the neuron, or the “out-degree” (D_{out}), such that

$$D_{in} = \sum e_{ij}^{(p \text{ or } n)} \tag{3-25}$$

$$D_{out} = \sum e_{ij}^{(m \text{ or } p)} \tag{3-26}$$

where in-degree could only be calculated for on the connection (e) a hidden (p) or output (n) neuron, and out-degree can only be calculated for an input (m) or hidden neuron (p) in a feedforward network. By using graphical analysis, a single neuron was isolated for its contribution to the network (inputs) or its reliance on data translated through the network (outputs).

Closeness:

Closeness is another way to measure a neuron’s importance within the network. This form of centrality measures the inverse sum of the weights from one neuron to all other neurons such that

$$C = \left(\frac{A_x}{Q-1} \right)^2 \frac{1}{\sum w_{ij}^x} \tag{3-27}$$

where A_x is the total number of reachable nodes, Q is the total nodes within the network, squared then divided by the sum of all reachable connection lengths (weights) from node x . For in-closeness, the focus of this analysis was on the output neurons, as these are the factors with data feeding “in” to them. Conversely for out-closeness, the focus was on the input neurons.

Betweenness is often considered a measure of centrality. In early definitions, centrality was considered the sum of the minimum distances from one node, x_i , to all other nodes in the

graph (Bavelas 1950; Beauchamp 1965; Sabidussi 1966). However, for feedforward ANNs this would primarily provide information of the hidden neurons. In this research, the focus was on the inputs and outputs. Therefore, betweenness was not included herein.

3.2.3 CONCLUSIONS

Based on the applicability of the above-mentioned graphical analysis procedures, and those used to analyze fMRIs and EEG, shortest path, degree, and closeness centrality were used to further analyze the constructed ANNs. The shortest path analysis was used to determine which inputs were strongly, or weakly, connected to which outputs. Degree and closeness centrality were used conjunctly to determine how influential an input was to the entire network or how widely influenced an output was by the numerous inputs. Additionally, as was similarly performed with human analyses, two different network models (of various inputs) were assessed for how these graphical results changed when new information was incorporated to the network. The results of this analysis provided additional insight into the socio-technical aspect of community damage and recovery due to wind hazards.

3.3 VALIDATING MODEL RESULTS THROUGH HINDCASTING

A hindcast requires model results compared to actual observed results of an event in order to ascertain a level of error from the modeling approach(es). Therefore, data comparable to model outputs must be recorded and available. Currently, the most extreme events have such detailed data on more refined scales. The hindcasting event used herein was the 2011 Joplin, MO EF5 tornado. Damage states of buildings immediately following the tornado were documented by Jasper Co., USACE, and NIST. Additionally, researchers at Kent State University periodically visited Joplin for years following the event, to record video data of the recovery process (Curtis and Fagan 2013). These then were the sources used in the validation through hindcasting portion of this research.

3.3.1 ASSIGNING BUILDING DATA TO JOPLIN COMMUNITY

Before any model can be further validated, the Joplin Community's building stock was first categorized in the same manner as the model inputs. The primary models being validated through hindcasting herein are the ANN models; however, there must be consistency in the building categorization so that the results may be considered comparable to a physics-based approach. Therefore, the buildings within Joplin were assigned the 19 archetypes proposed by Memari et al. (2018) and each archetype was given corresponding ANN input values as outlined in Table 3-8.

Table 3-8 Cross-Identification of 19 Building Archetypes and ANN Descriptors

Archetype	Description (Memari et al. 2018)	Walls	Roofing	Roof Shape	Size & Height	Occupancy
T1	Residential wood bldg., gable roof	5.3	5.2	10.22		310.5
T2	Res. wood bldg., gable roof	5.3	5.2	10.22		310.5
T3	Res. wood bldg., gable roof	5.3	5.2	10.22		310.5
T4	Res. wood bldg., hip roof	5.3	5.2	7		310.5
T5	Res.l wood bldg., gable roof	5.3	5.2	10.22		310.5
T6	Strip-mall, reinforced masonry, gable roofs, metal sheathing	7.1	10.8	10.12		309.1
T7	Light industrial, aluminum siding	8	10.8	1		311.2
T8	Heavy industrial, reinforced masonry, flat roof	7	10.4	1		306.3
T9	Elementary/middle school, unreinforced masonry, flat roof	6.1	6.4	1	Data taken from provided geo-tagged building information	305.1
T10	High school, reinforced masonry, flat roof	7.1	7.4	1		305.1
T11	Fire station, brick exterior walls, gable metal roof	1	5.8	6.2		304.1
T12	Hospital, glass walls with unreinforced masonry, concrete frame, flat roof	7.9	7.4	1.2		308.4
T13	Community Center, unreinforced masonry	6.1	7.4	6.2		303.4
T14	Government building, reinforced masonry	7.1	7.4	1		304.1
T15	Large big-box	6	10.8	1		309.1
T16	Small big-box	6	10.8	1		309.1
T17	Mobile home	0.5	0.5	6.1		310.4
T18	Shopping center, reinforced masonry, partially glass flat roof.	7	10.4	1		309.1
T19	Office building, masonry bldg., asphalt shingles and wood rafters	7.1	5.2	6.2		304.1

The remaining ANN input values were extracted from the U.S. Census data of the block group within which a building was located, with a surface roughness of B throughout the city of Joplin and a percent forested area ranging from 2-50% depending on building location. Each building was also located within a certain EF-Scale based on the historic wind swath of the Joplin tornado and randomly assigned a wind speed value (in mph) within that scale's range. The Joplin tornado was also considered a large tornadic wind type event.

3.3.2 DATA ASSIMILATION OF KNOWN RESULTS FROM THE JOPLIN TORNADO

Researchers at Kent State University were able to travel periodically to Joplin, MO for the five years following this disastrous tornado event. They were able to take geo-tagged video data representing some of the buildings within the tornado path and the current state these were in (Curtis and Fagan 2013). The video was then post-processed by assessing which recovery state a single building would be categorized in by Table 3-6 and expanded upon for specifics of the rebuilding process by Table 3-9, in which Recovery State 3 was expanded upon and a Recovery State 6 was added. The same buildings were visited over equal intervals over this 5-year period and a date of rebuilt and occupied (Recovery State 4) status was ascertained. Post-processing of this data involved visually reviewing video data to ascertain the Recovery State of each building. Once that was determined, the latitude and longitude were used to match it to a building polygon within the ArcGIS data shapefile to add the Recovery State as an attribute.

Table 3-9 Cross-Identification of 19 Building Archetypes and ANN Descriptors

Recovery State	Sub-State	Description
3	1	<u>Frame Skeleton</u> : Foundation laid (typically remains following a wind event) and building frame is going up.
	2	<u>Enclosure</u> : Installation of roofing structure and exterior walls.
	3	<u>Non-structural</u> : Completion of roof sheathing and installation of doors and windows. This will also include laying utility piping and conduit.
	4	<u>Non-Structural/Cosmetics</u> : Installation of interior sheetrock (as applicable) and exterior finishes (e.g., brick stucco). This will also include completion of finishes such as interior cabinets and painting
6		A new structure built on land that is not the same archetype as the original.

The data currently provided by Dr. Andrew Curtis’s research group covered the rebuilding process through year 2, which was considered comparable for the design of the recovery ANNs. Dr. Curtis’s group gathered video data for over 3,000 buildings within the tornado track. For hindcasting using the models created herein, only these data points were used even though the number of structures within the tornado path was over 8,000.

The video data also provided a mean by which to categorize each building’s initial damage state as Curtis et al. (2013) also documented these. However, the research discussed herein refers to building Damage States (DS) instead of the Tornado Injury Scale (TIS) previously defined by Curtis (2013). The necessary conversions from TIS to DS by structure types are described in Table 3-10 & Table 3-11.

Table 3-10 Converting TIS ranking to DS for wood and steel buildings (Curtis and Fagan 2013; Memari et al. 2018).

<i>TIS Descriptions</i>	TIS	DS	<i>DS Descriptions</i>
No visible damage	1	0	<i>No damage</i>
Minor visible damage (usually loss of roof tiles, gutters, and other facades.)	2	1	Slight damage to doors and winds/roof covering-able to be occupied and repaired
More substantial roof loss and/or boarded windows, and doors	3		
Large sections of roof material are lost, as are less rigid sections of the house such as the collapse of carports	4	2	Moderate damage to windows and or doors/roof covering - not able to be occupied but repairable
The building has shifted on its foundation or sizable holes have been knocked through walls or the roof	5	3	Not able to be occupied but repairable
The roof has been removed	6		
Exterior walls have collapsed	7		
All exterior walls have collapsed, leaving just a few inner walls standing	8		
The entire structure has been reduced to rubble	9	4	Not able to be occupied and not repairable
Even the debris has blown away, leaving just dirt or concrete slab	10		

Table 3-11 Converting TIS ranking to DS for masonry and concrete buildings (Curtis and Fagan 2013; Memari et al. 2018).

<i>TIS Descriptions</i>	TIS	DS	<i>DS Descriptions</i>
No visible damage	1	0	<i>No damage</i>
Minor visible damage (usually loss of roof tiles, guttering, and other facades)	2	1	Slight damage to doors and winds/roof covering-able to be occupied and repaired
More substantial roof loss and/or boarded windows, and doors	3	2	Moderate damage to windows and or doors/roof covering - not able to be occupied but repairable
Large sections of roof material are lost, as are less rigid sections of the house such as the collapse of carports	4	3	Not able to be occupied but repairable
The building has shifted on its foundation or sizable holes have been knocked through walls or the roof	5		
The roof has been removed	6		
Exterior walls have collapsed	7		
All exterior walls have collapsed, leaving just a few inner walls standing	8	4	Not able to be occupied and not repairable
The entire structure has been reduced to rubble	9		
Even the debris has blown away, leaving just dirt or concrete slab	10		

Once the building damage states were converted from their already identified TIS, the video data were then evaluated for the same building's condition over time. At each time interval the buildings were given a recovery state designation, outlined in Table 3-6 and Table 3-7. These recovery states (RS) are intended to progress towards a full recovery, with RS4 indicating the building is completely rebuilt and reoccupied. RSs5 & 6 were added to illustrate when a lot has either been abandoned or rezoned for a different usage. Additionally, RS3 was expanded upon to document where in the construction (rebuilding) process a structure was. An example of one of these rebuilding states is shown in Figure 3-10 with graphics from the video player used to analyze the data.

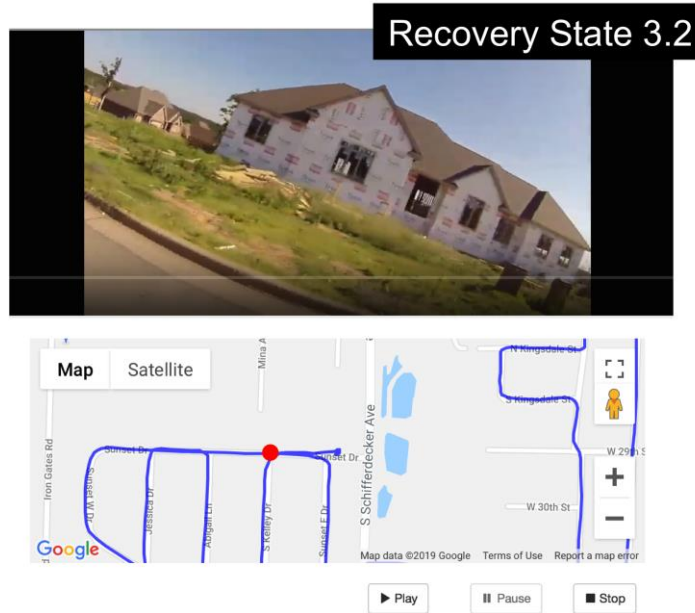


Figure 3-10 Example image of a RS 3.2 building as seen when using video player to review recovery data. Red dot indicates location within Google Maps.

Once the building recovery states were identified for each feature (building), the time to recover that feature was determined by evaluating when RS4 was reached. Following this process, the number of buildings in each DS and each recovery time were summed and subsequently evaluated for how many of those buildings in a specified DS recovered in 1 year, 1.5 years, 2 years, or greater than two years. For example, what percentage of buildings that were classified as DS4 recovered by 1 year? Recovery time of each archetype was then summarized for evaluation as well.

Following this generalized analysis were specific spatial analyses. The first spatial analysis was to see if buildings within a neighborhood recovered at the same times. These neighborhoods were first considered to be parcels of land that contained multiple building and were bounded by roads. To evaluate each neighborhood, individual layers were created from the RS data shapefile such that all buildings of 1-year recovery time were on one layer, all buildings of 1.5-year recovery time were on another layer, and so on. Each of these layers was then spatially joined with the neighborhood parcels, so that the parcel itself would take on a RS

for the buildings residing within it. This neighborhood analysis was meant to investigate whether a building recovered at the same pace as its neighbor.

The next analysis was conducted to determine whether or not certain Census Block Group neighborhoods recovered the same or consisted of a variety of recovery time patterns. This analysis was conducted in the interest of comparing the overall pattern of damage state distribution and relative recovery times, as described above for the whole data set, at the block group level. These block groups were also associated with specific demographic data from the 2010 U.S. Census American Community Survey (U.S. Census Bureau 2018). Select demographic options were evaluated based on results from building damage state and recovery ANNs, the availability in the 2010 ACS, and their relevance to Joplin. For example, Joplin is not racially or ethnically diverse in comparison to the rest of the state. Therefore, demographics related to race and ethnicity were not analyzed for the Joplin dataset. This data analysis allowed for potential explanation as to why one block group may have recovered its DS4 buildings faster than another block group, while also providing additional context to the results from analyzing the designed ANNs.

CHAPTER 4 RESULTS AND MAIN OBSERVATIONS

4.1 SYNOPSIS

The research conducted herein involved the creation of two different models, one for predicting damage state and one for recovery time. There are three evaluation steps for each of the two. The first step was to build the best possible ANNs through evaluating the training algorithms and various model input variables. For both damage state and recovery, the final models utilized Bayes Theory (BR) as a means to train the data. Additionally, in this step found it was found that the final models must include both social and structural (engineering) factors. The second step involved the use of graph theory to further examine how patterns were made within the network using the shortest path, degree, and closeness centrality calculations. The results of this step showed varying importance among the input variables. For example, the use of a building occupancy type and tenure were shown to be critical variables in determining damage state. The third, and final, step was to validate both models against video recorded data following the 2011 Joplin tornado. The results showed 40-50% damage state match and 20-40% recovery time match at the individual building level. This chapter outlines these results in more detail.

4.2 IMPACT MODELING

The first ANN types built were designed with the intent of predicting a building's damage state resulting from wind hazards. The general structure is shown in Figure 4-1, with 10 hidden neurons and 5 output neurons representing damage states (DS) 0 through 4. The inputs varied for each of the 10 models outlined in Table 3-3 and generally consisted of hazard-related inputs, structural, and social characteristics. Section 4.2 covers the results from alternating training theory algorithms, variations in model inputs, a graphical analysis of the final ensemble of ANNs

used to predict damage state, and final model validation through hindcasting the 2011 Joplin tornado. The final ensemble of ANNs has the same inputs and training algorithm, but different connection weights and neuron biases as a result of the build process. These ensemble ANNs therefore process data independently to provide output values from each network and are averaged when used in application for hindcasting the 2011 Joplin tornado.

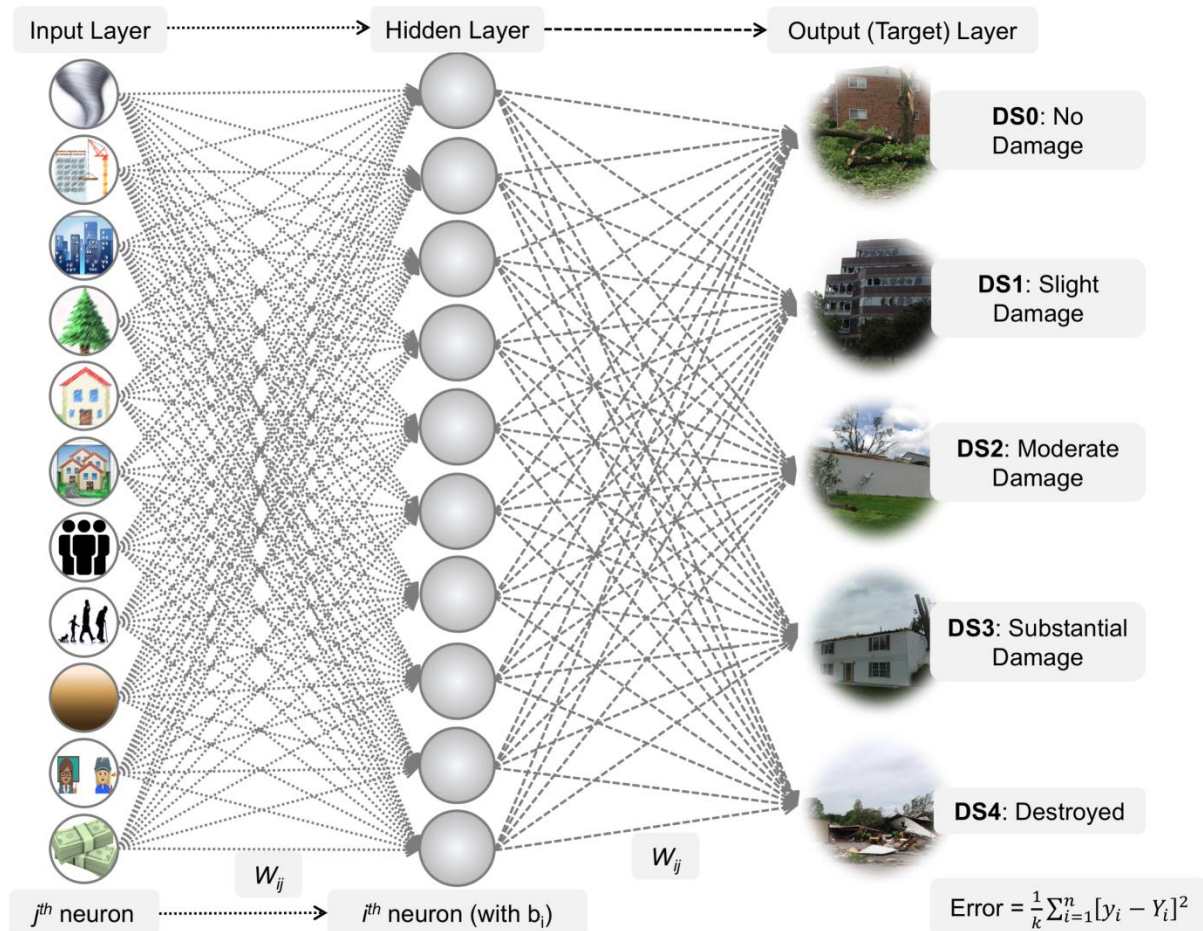


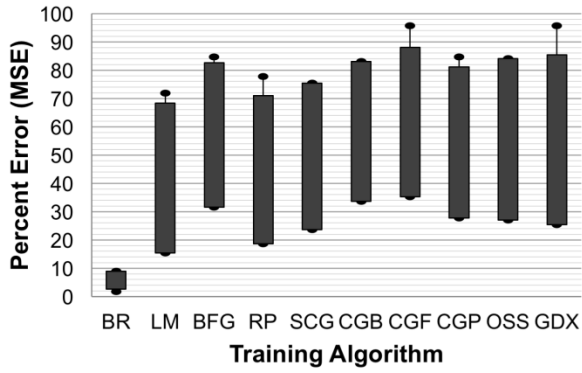
Figure 4-1 ANN structure for relating hazard, structural, and sociological inputs to building damage state. (Photos are from NWS damage surveys (National Weather Service 2018). Input images are various forms of clipart(CanStockPhoto n.d.; ClipartXtras n.d.; Emojipedia n.d.; GalleryYoPriceVille n.d.))

4.2.1 TRAINING ALGORITHM VARIATIONS

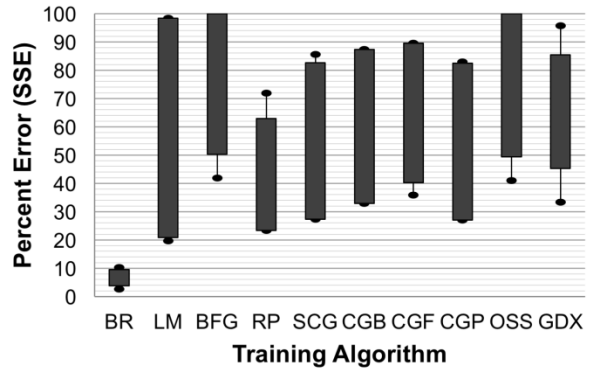
The training algorithms outlined in Table 3-1 represent the core of current theories in neural network training. These theories utilize variations on gradient descent methods or Bayes Theory. The merit to applying a specific theory can change depending on the problem being

modeled. Each ANN was “built” once the lowest possible error (MSE or SSE) had been reached through multiple iterations. Each ANN model herein was built a minimum of 50 times (with multiple iterations within each build) to determine a range and subsequent mean for each PCI for training algorithm capability comparisons.

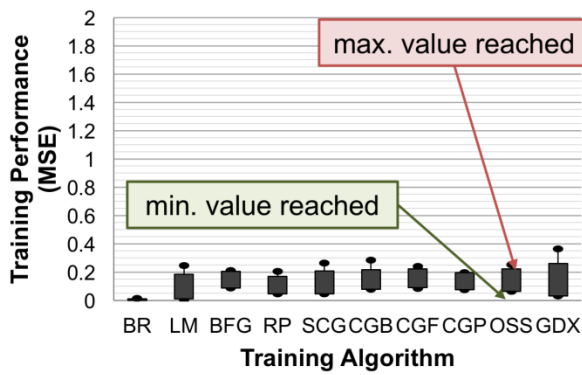
In modeling building damage state, across most algorithms, the PCI’s were more desirable with the MSE performance function than the SSE function as shown in Figure 4-2, Figure 4-3, and Figure 4-4. These figures show the majority of builds that were within the +/- 2SD by the thick bars and the maximum and minimums reached by the extended lines/nodes from those bars. The BR training algorithm (with a percent error mode of 4.3%) clearly best fits the desired PCIs out of all the training algorithm options with 100% of the builds bounded by the maximum and minimum values reached. The LM and RP training algorithms (percent error modes of 54.7% and 34.2%, respectively, for the MSE performance function) were the next best performing algorithms. While LM had better false negative rates, the percent error mode for RP was lower than LM. LM’s PCIs were also highly varied with a change from MSE to SSE performance along with the OSS algorithm approach. RP is the only algorithm that actually showed improved results when switched from the MSE to SSE performance. Note that when evaluating the performance functions, training performance is desired to be close to zero, which indicates that the ANN outputs are closely matching the targets.



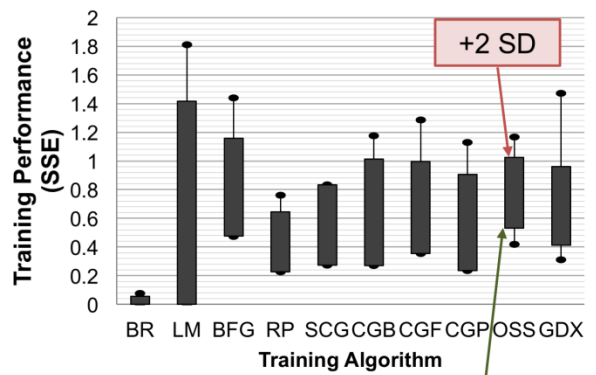
(a)



(b)

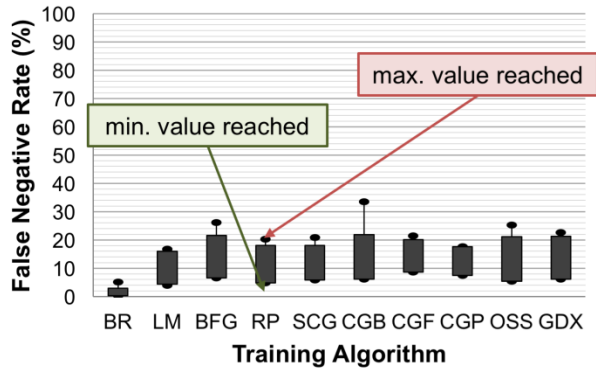


(c)

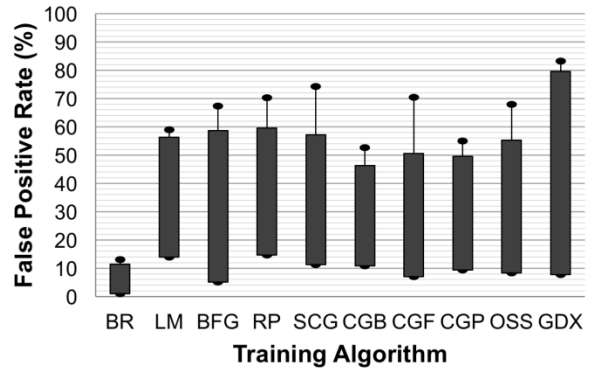


(d)

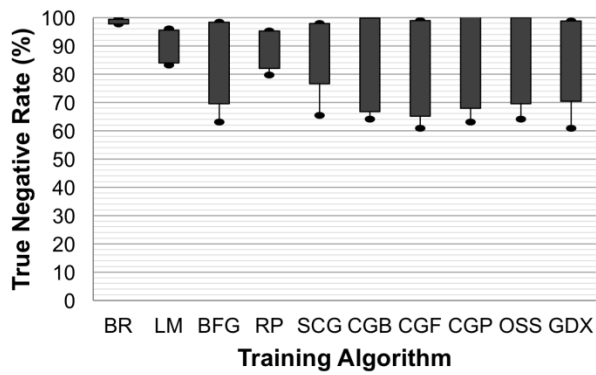
Figure 4-2 (a) Percent error for MSE performance, (b) Percent error for SSE performance, (c) training performance for MSE performance and (d) training performance for SSE performance for the explored training algorithms.



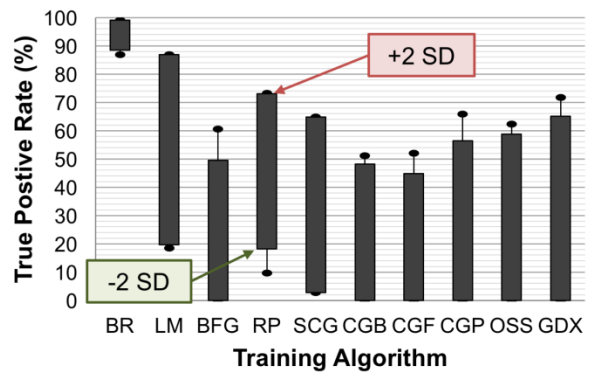
(a)



(b)

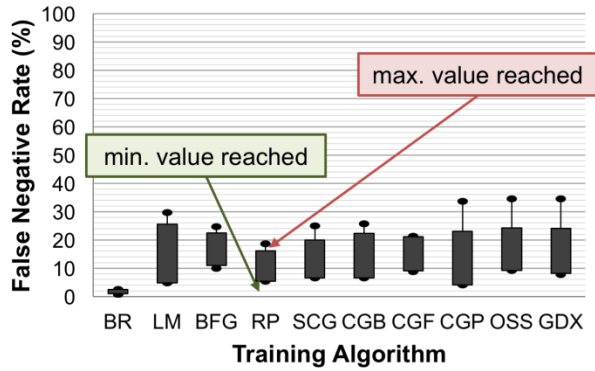


(c)

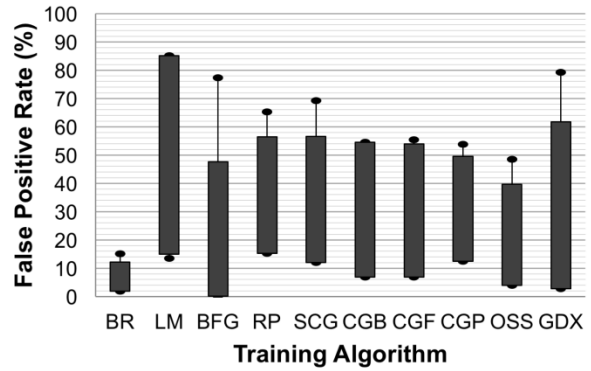


(d)

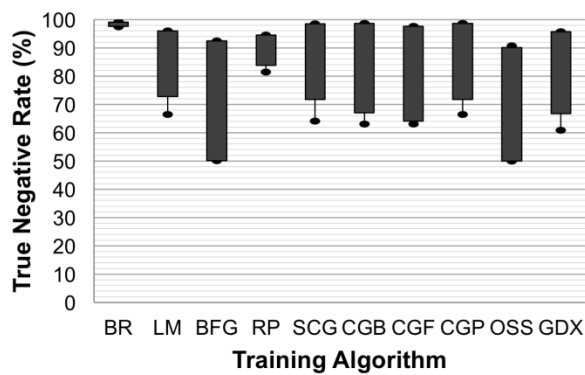
Figure 4-3 Explored algorithms' (a) FNR, (b) FPR, (c) TNR, and (d) TPR for MSE performance.



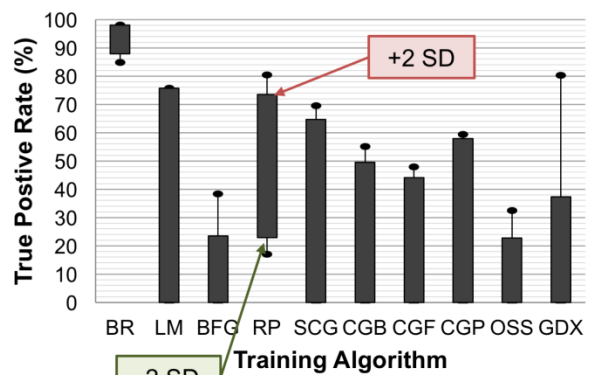
(a)



(b)



(c)



(d)

Figure 4-4 Explored algorithms' (a) FNR, (b) FPR, (c) TNR, and (d) TPR for SSE performance.

Based on the above results, BR with MSE performance, LM with MSE performance, and RP with SSE performance were chosen for the next step in evaluating model input variations to evaluate the effect of combining sociological and engineering related variables in determining damage state. While BR clearly produces the lowest percent errors in training, the LM and RP algorithms were also used in the following step as a check that the conclusions being drawn were consistent across each training theory and not a result of over-fitting, which can occur in using BR methods.

4.2.2 INPUT VARIABLE VARIATIONS

The multi-variant aspect of this research occurred in the evaluation of multiple models of varying data inputs for modeling the same predictive outputs. These were created in order to evaluate how structural and sociological characteristics relate to determine impact from wind related hazards. It was noted above that, among the PCIs, if the percent error was low, so were the false rates, while the true rates were higher (as desired). The percent error associated with an ANN is equivalent to how many data points fell within a network-produced output that did not match their target (known) output. In order to evaluate this, 10 ANNs of varying inputs were built as outlined in Table 3-3 with Figure 4-1 relating how those variables fit in the ANN mathematical structure.

The 10 models were designed with the intent to learn what sociological factors interact best with hazard and structural related factors causally linking to impact, in the form of building damage state, from wind related events. It may also be possible that none of the subject factors interact well and this remains simply an engineering-related problem (Model 3). The results of building these 10 different models are shown in Figure 4-5. As can be seen, the best performing models include certain sociological factors such as housing tenure and per capita income. Additionally, the models with variables that relay debris potential to the ANN, such as percent area forested and housing density, performed very well. *What was also noticeable across each learning algorithm was that Model 3, solely hazard and engineering related inputs, was one of the poorer performing models, indicating that determining impact from wind hazards, in terms of physical damage state, is not solely a structural engineering-related problem.*

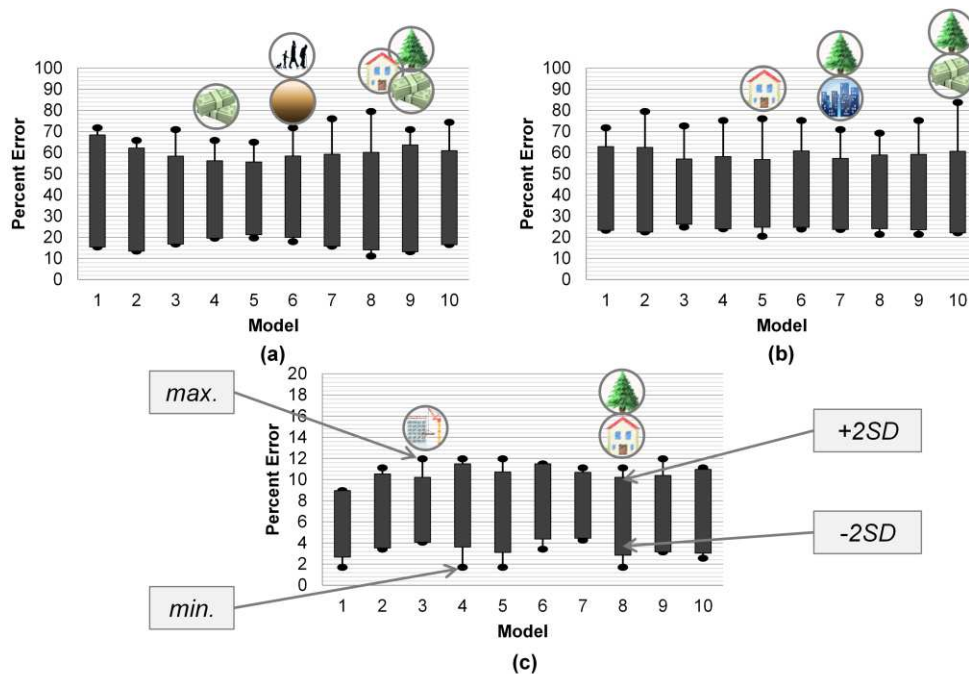


Figure 4-5 Resulting percent error data ranges from 80+ ANN builds for (a) LM, (b) RP, and (c) BR training algorithms (Key images are various forms of clipart(CanStockPhoto n.d.; ClipartXtras n.d.; Emojipedia n.d.; GalleryYoPriceVille n.d.)).

The results from model variations with BR, LM, and RP algorithms, showed Model 3 as one of the worst performing options and Model 8 as one of the better performing options, indicating that the BR results showed a similar pattern in model comparison to that of the LM and RP results. Therefore, BR will be used for the following assessments and for creating the final model ensemble consisting of multiple (designated A through F) ANNs.

As previously stated, Damage Model (DM) 3 served as a control comparison of how damage states have been historically modeled in considering the hazard and engineering characteristics (structural, surface roughness, wind speed). Damage Model (DM) 8 was built as a mix of DM5 and DM7 in consisting of the housing tenure (percent owners and percent renters) and the potential for debris impacts (percent forested area and the housing density) based on the relatively improved performance of these models across the three algorithm types. Both DM3 and DM8 had final model ensembles built for comparative evaluations in the following sections. Figure 4-6 shows the percent error of the ensemble ANNs A through F for both DMs,

as well as the confusion matrices for the lowest percent error ANNs of each model. The percent error of each ANN build is defined as the percent of data points incorrectly matched to their known target outcome during the training, validation, and testing phases. Within a confusion matrix, ANN outputs were compared to the desired targets. If the outputs matched the targets for a data point it was tallied along the diagonal of the matrix. The confusion matrices illustrated that many data points were correctly placed to their resulting output damage state during training and testing. The matrices shown in Figure 4-6 are examples; it is possible to reach the same percent error with differing misplaced data points. These final ensemble ANNs all fall within the 50% lowest possible error from the build analysis, shown in Figure 4-5, and with ROCs clustered primarily in the “true positive” region as shown in Figure 4-7.

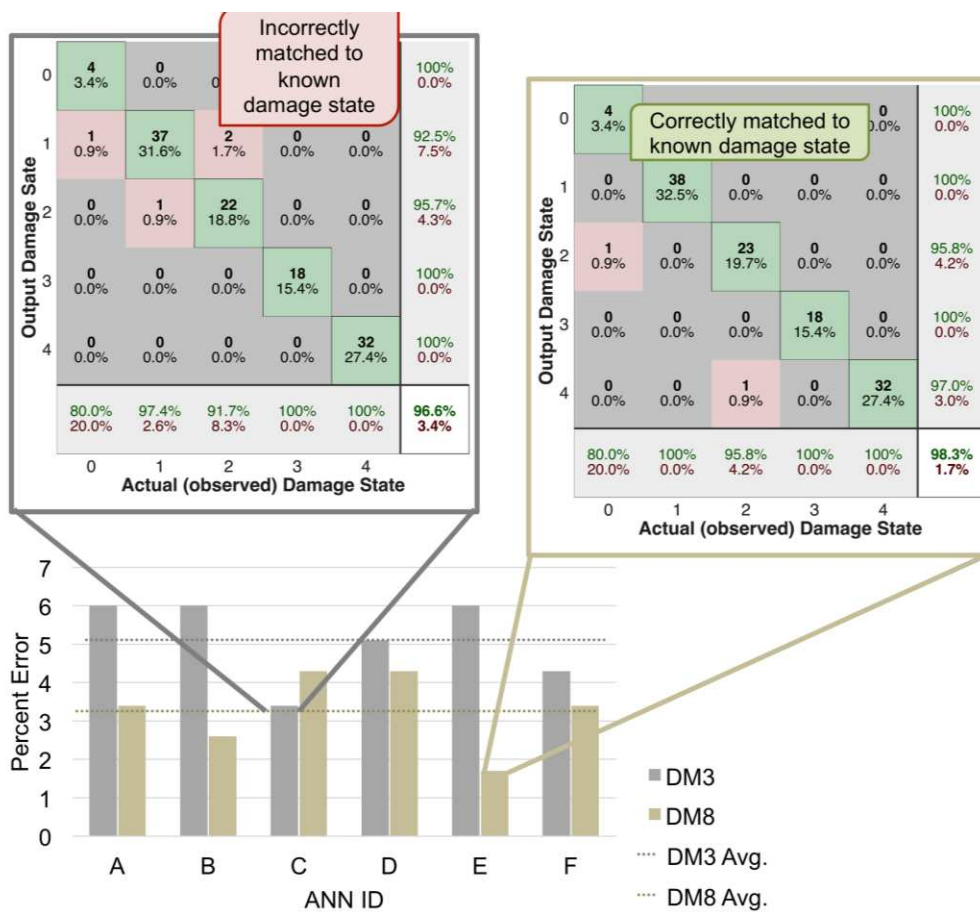


Figure 4-6 Final Ensemble ANNs' build percent error and how that error occurred through the training process as shown by respective confusion matrices.

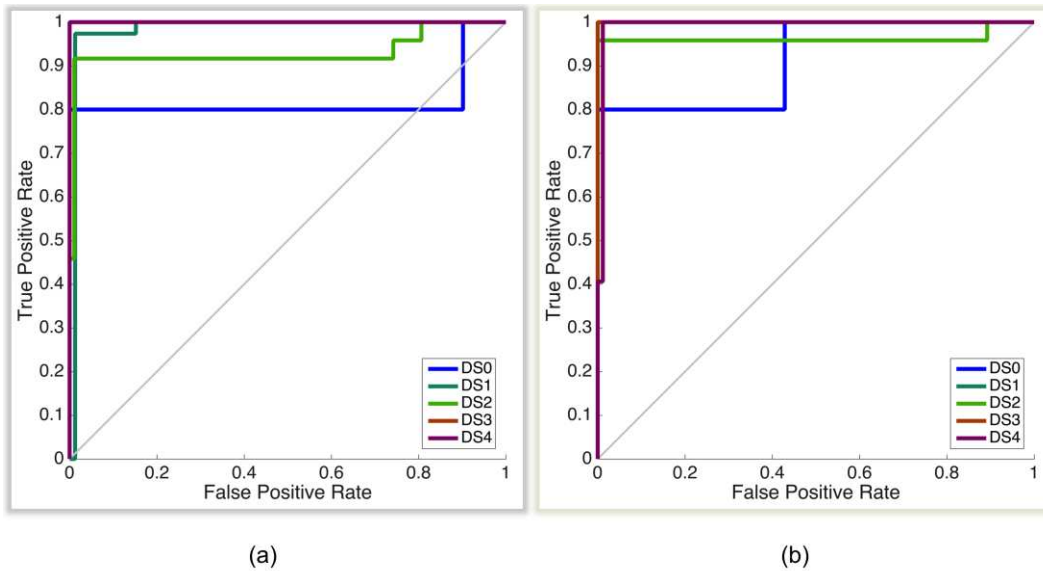


Figure 4-7 ROCs for ensemble ANNs (a) DM3-C and (b) DM8-E.

Having a perfectly performing ANN is rather unrealistic, but a desirable ANN will have a lower number of incorrectly placed data points and primarily high true positive rates. DM3's percent error was higher for all algorithm types with some having data points output as far off as three damage states. However, DM8 showed a focus in error in the DS3 and DS4 regions for those it did misplace. A 1.7% error (BR) was the lowest percent error reached across all algorithms and model builds.

From the above results and analysis, BR was considered the best performing training algorithm with DM8 being the best structure. The final machine learning model for predicting impact to a community's building stock, therefore, consisted of an ensemble of 6 ANNs requiring DM8 inputs, with 10 hidden neurons, and 5 output damage states, trained using BR to reach a lowest possible MSE. These final 6 ANNs for DM3 and DM8 were used for the following graphical analysis and hindcasting individual building damage from the 2011 Joplin Tornado.

4.2.3 GRAPHICAL NETWORK ANALYSIS

Once the ANN model structure was established, graph theory concepts were then used to analyze the relationships between the various inputs and the resulting building damage state.

This analysis was designed to mirror work previously performed in analyzing brain fMRIs and EEGs by specifically looking at the shortest path problem and centrality of neurons within a network (degree and closeness). For this analysis only the combined network (Approach A from the shortest path analysis) was used. This was performed so that the influence of each parameter to an overall model result could be evaluated.

The shortest path analysis allowed for observations in what inputs may be strongly connected to specific damage states. For this analysis within an ANN, the interest focused on higher connection weights. Therefore, if the shortest possible path from one neuron to another was a relatively high value, then any other path options within the network would be equally, or more, strongly connected. However, in this evaluation, two approaches were taken: (a) combining all the ANNs into one overall network to determine the shortest path within the resulting combined network, and (b) evaluating the shortest path from each input to each output within each of the six individual ANNs and averaging the results. This allowed for a way to validate conclusions to be drawn from the results of each approach. If a relatively strong connection (high weight values) was found in both approaches, then that was considered a finding of this analysis. Similarly, the weaker connections were also evaluated. It is worth noting that a strong/weak connection between a specific input and specific output did not necessarily indicate that this input was/ was not valuable to other outputs; only that this input had an increased contribution to a specific output.

Figure 4-8 and Figure 4-9 show the relative results in calculating the shortest path for DM3, primarily engineering-related inputs, and DM8, the final suggested predictive model. By analyzing both DM3 and DM8, the effect of including social factors could be assessed. In DM3, the roof material and building height showed a strong connection to DS0. This was considered reasonable due to the fact that the wind pressure increases with height and wind damage tends to first appear at the roof level. The wind speed was also found to be strongly tied to DS4, which was to be expected given that at a certain wind speed, the rest of the factors would become less

vital in determining the resulting damage state. Additionally, weaker connections were found between the event size and DS0 and DS2, as well as the connection between surface roughness and DS1, suggesting a relationship between areal extent and lower damage states. Once tenure and density factors were introduced to the network for DM8, a shift occurred from strong connections between structural aspects to *how* the structure was used. While a strong connection still remains between building height and DS0, building occupancy and tenure have now become strong contributors to DS2 and DS3, respectively. These connections indicate a potential criticality of how the structure is used and maintained to whether or not the resulting building damage becomes an insurance write-off (DS3) or not (DS2). Housing density has taken the place of surface roughness in being weakly connected to DS1, and event size has shifted from being weakly connected to DS0 and DS2 to being weakly connected to DS4. These shifts could indicate that the event's size contributes more to lower damage states and housing density, or debris potential, takes its place at higher damage states, which would illustrate a criticality of density over size for worsening damage.

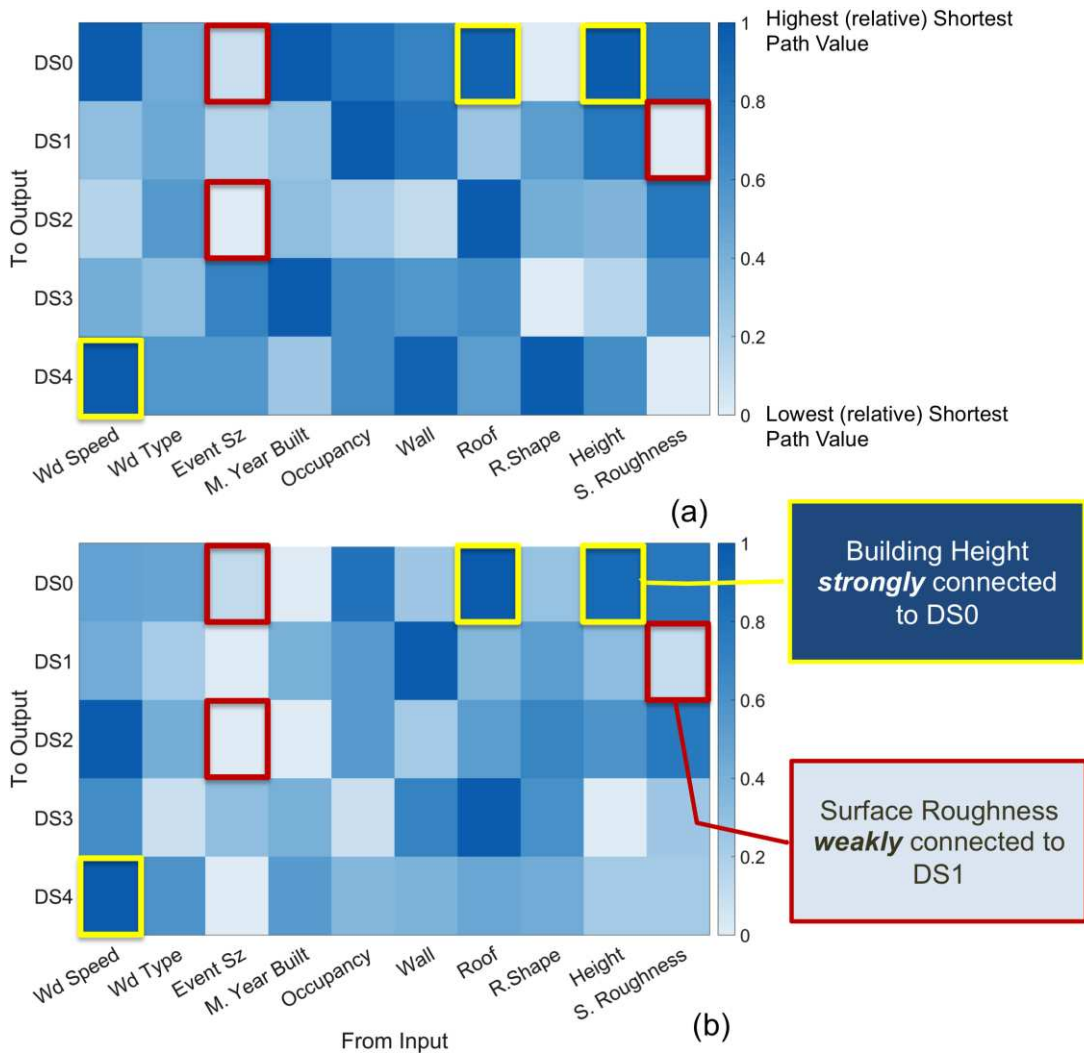


Figure 4-8 Shortest path relative values for DM3 (a) combined ANNs and (b) averaged results from each ANN.

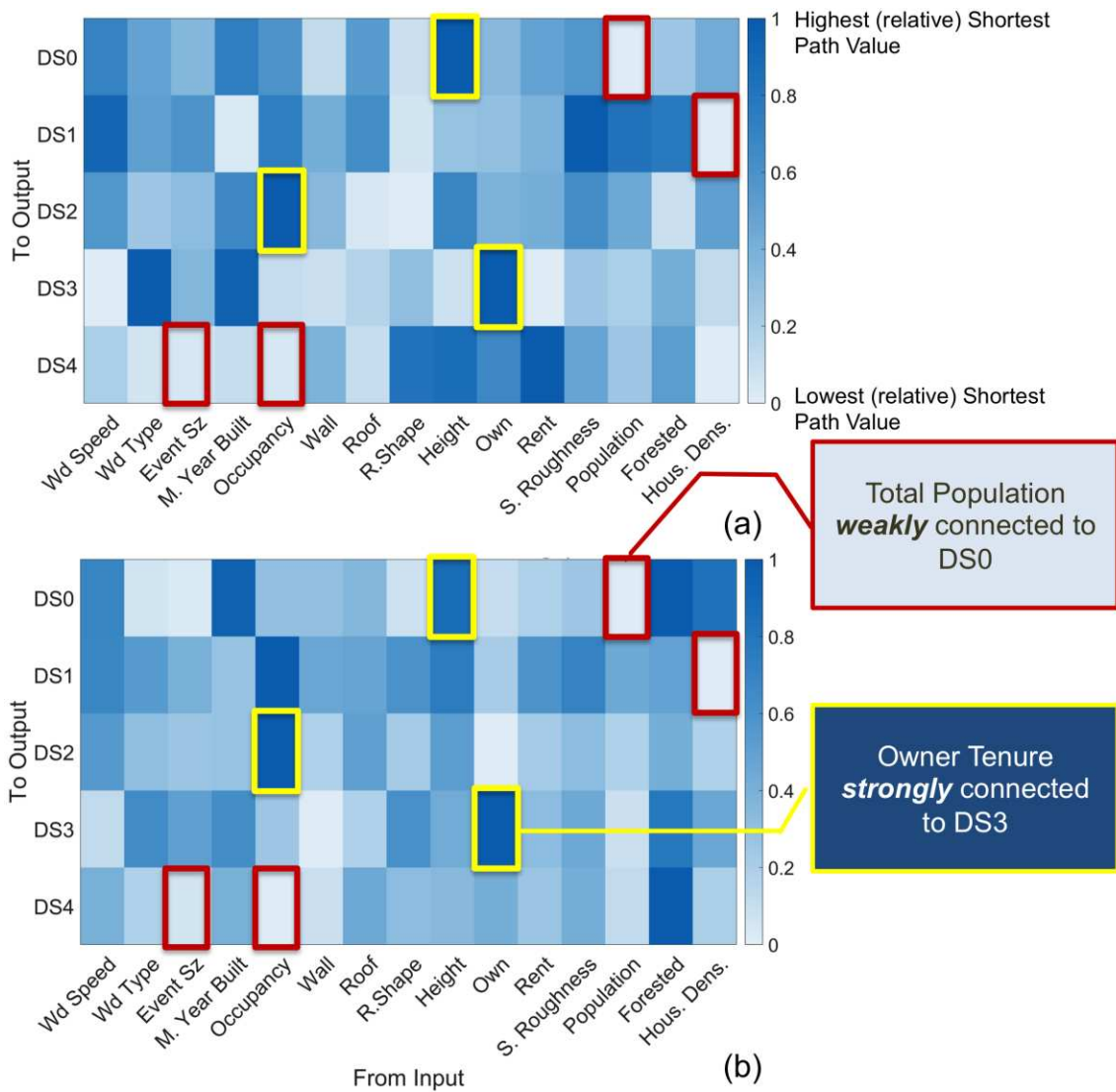


Figure 4-9 Shortest path relative values for DM8 (a) combined ANNs and (b) averaged results from each ANN.

The shortest path results revealed how each input connects to each output. The centrality analysis, through the concepts of closeness and degree, related how connected a neuron is within the network as a whole. In other words, a high shortest path result indicated that a specific input is strongly influencing a specific output, while a high centrality score indicated that a specific input has wide-spread influence to the network or that a specific output is influenced by many variables. Both in- or out-degree and in- or out-closeness scores (“in”

being for output/DS neurons and “out” being for input neurons) were evaluated for analysis and validation that if one neuron had a high degree, it also had a relatively high closeness.

Figure 4-10 shows the centrality scores, plotted as closeness versus degree, for DM3. Plotting both scores together allowed for an assessment of how closely degree rank matched closeness. It is interesting to note that the association between the two centrality scores for DM8 more closely match a linear relationship, than those for DM3. Specifically, the output (DS) neurons did not share similar centrality scores for DM3 and appeared to be less consistent and therefore less organized. DM3, as shown in Figure 4-10, resulted in a combined network where the wind event size, building height, and surface roughness contribute widely to the overall network. In combination with the shortest path results, this would suggest that building height is a significant factor in determining damage state, for the current engineering-factor-based modeling approach, as it is widely connected within the network as well as strongly connected to DS0.

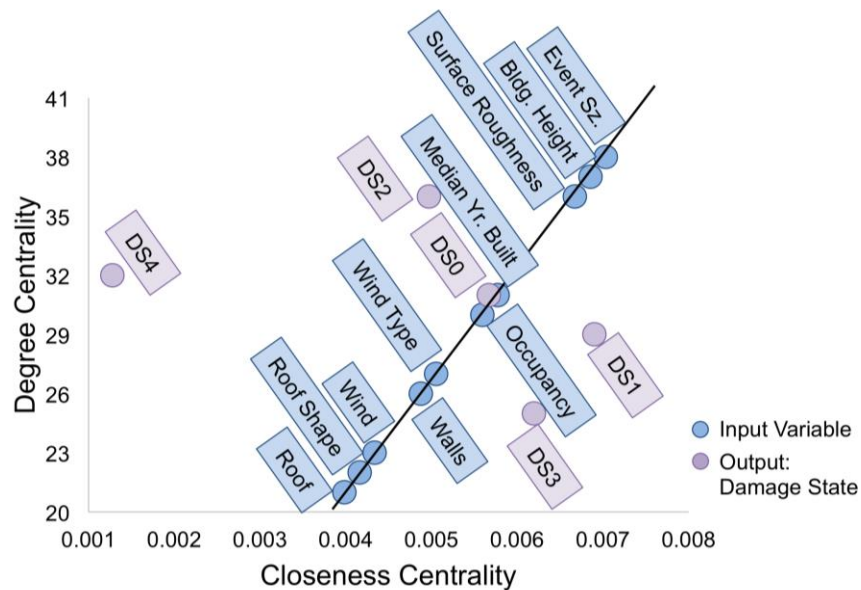


Figure 4-10 DM3 (combined ANN structure) centrality scores as closeness versus degree.

While DM3 represented current modeling variables, DM8 introduced some social and debris potential variables. The centrality scores that resulted from adding in these new factors

are shown in Figure 4-11. Wind speed, population, housing density, roof shape, and wind event type and size were all inputs that connected widely to the possible outputs within this network. DS4 and DS0 were also widely influenced by the inputs. The output DSs were also more aligned than in the centrality analysis of DM3, suggesting more organizational structure within the network. Conversely to widely-connected parameters, surface roughness and building height showed lower centrality scores, which indicated that these were not widely influential parameters with the model. *This does not indicate that these are not important parameters for modeling building damage state from wind hazards, more so that these parameters may have been focused more towards specific damage states instead of having a breadth of influence to the network.* Building height, for example, showed higher connectivity to the lower damage states through the shortest path analysis in Figure 4-9. The variable order along the linear path ultimately changes between DM3 and DM8 as the variables are altered and the ANN compensates.

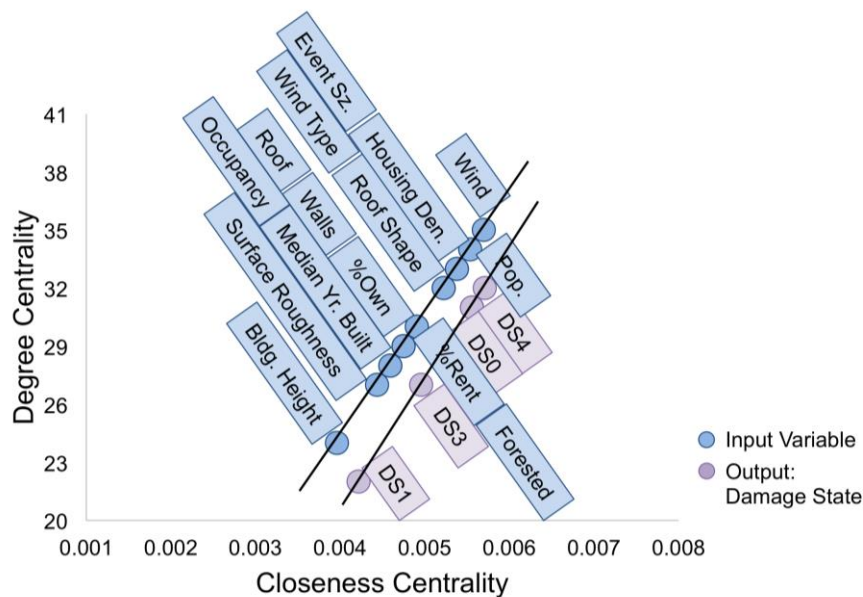


Figure 4-11 DM8 (combined ANN structure) centrality scores as closeness versus degree.

The results from the centrality analysis showed more organization among the output damage states within the DM8 structure than within the DM3 structure. Additionally, the shortest

path analysis results illustrated a shift in stronger connections from structural factors to building usage related factors. However, across both model types, the size of the wind event was shown to have a high connectivity within the network, indicating that the areal extent (tornado path) contributes well to all possible damage states. Similarly the building height presented a strong connection to DS0 independent of the incorporation of social factors.

4.2.4 HINDCASTING DAMAGE FROM THE 2011 JOPLIN TORNADO

In order to validate the applicability of this approach for predicting the damage states of buildings, the 2011 Joplin, MO Tornado was simulated using DM3 and DM8, then compared to actual damage statistics and the results from using physics-based fragilities. The tornado path and intensity was overlaid with the community building stock within ArcGIS. The tornado path gave the EF scale zones, which required random wind speed values within each range to be assigned to the buildings based on location within the path. Next, the buildings were coded so that the ANN could interoperate the engineering characteristics along with the corresponding Census data. To do this, the near 8,000 buildings were assigned by archetype as outlined in Memari et al (2018). These archetypes were then given ANN variable designations as outlined in Table 3-8.

The results from modeling using the ANNs were compared to that of the physics-based fragilities originally modeled by Memari et al (2018) and Attary et al (2018). Within the physics-based analysis, the probabilistic value for damage states 1 through 4 based on 3-sec gust wind speeds were calculated through Monte-Carlo analysis as discussed by Attary et al (2018). These probabilities are mutually exclusive and collectively exhaustive. The most likely damage state provided by these probabilities was used for comparison against the ANN outputs in the interest of comparing predictions for a specific damage state.

The overall results shown in Figure 4-12 and Table 4-1 demonstrate an initial validation of this overall modeling approach using ANNs. The building damage spatially followed the

tornado intensity and actual damage satellite image track (Missouri Spatial Data Information Service n.d.) as well as resulting in an *overall* 10-13% error when tallying building damage states. This overall error was simply the sum of all buildings within a DS designation and was determined from the combination of DS's 1 & 2 and DS's 3 & 4 largely due to the fact that determining damage state is a qualitative analysis, which introduces a degree of error within the actual observed results as well. Following an event, DS's 3 and 4 are considered total losses, monetarily speaking, and as this is an arguably more critical component in determining impact, the errors shown in Table 4-1 were considered acceptable.

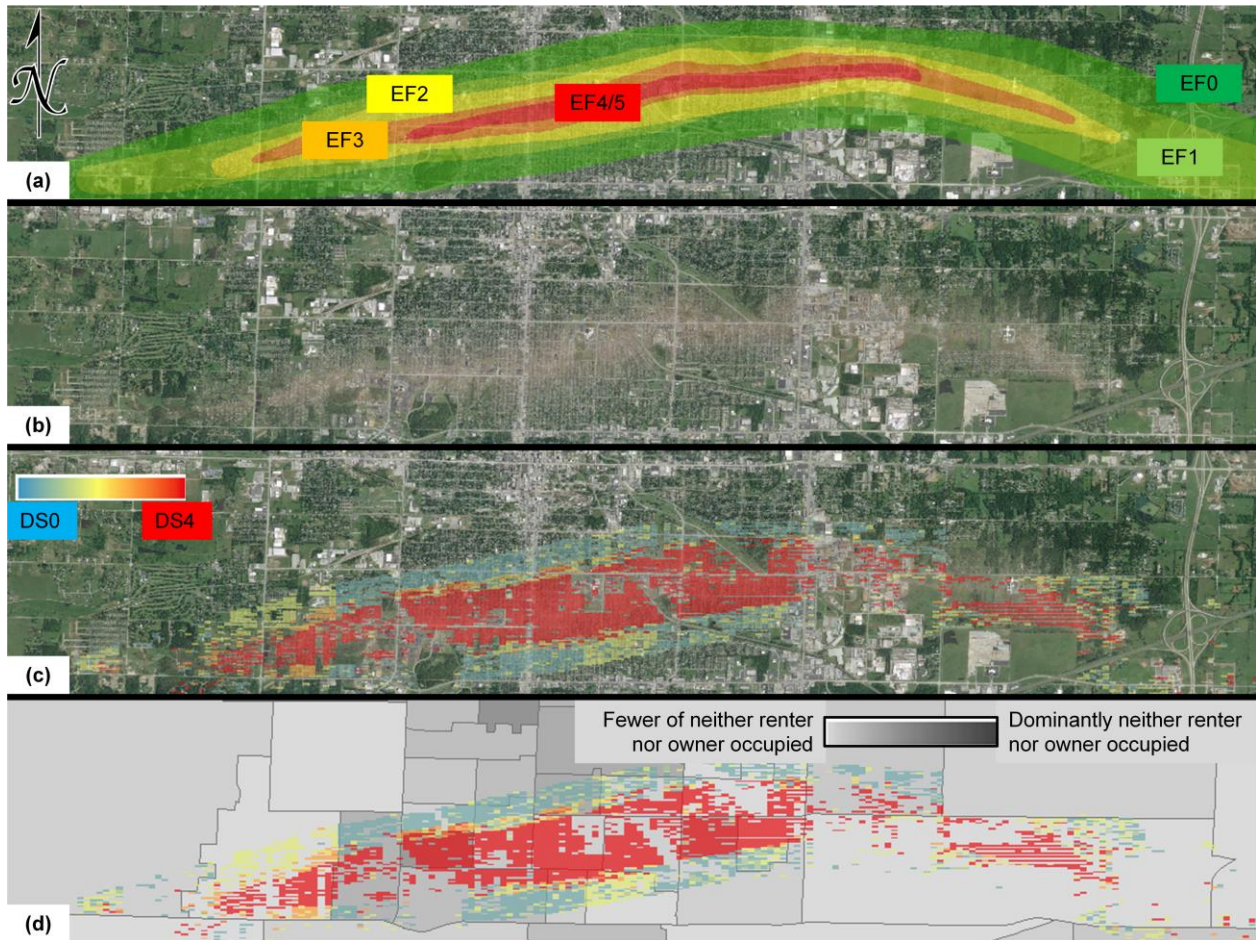


Figure 4-12 (a) May 22, 2011 Joplin tornado track, (b) resulting damage path(Missouri Spatial Data Information Service n.d.), (c) Model 8 ANN determined damage path over actual satellite image, and (d) Model 8 ANN damage path over local tenure demographics(U.S. Census Bureau 2018).

Table 4-1 Total buildings damaged as recorded by Jasper County, MO and the United States Army Corps of Engineers (USACE) with comparison to physics-based fragilities and DM8 ANN results.

	Light DS1	Moderate DS2	Combine DS1 & DS2	Totalled/ Extensive DS3	Demolished/ Catastrophic DS4	Combine DS3 & DS4	Total Buildings with Damage
Jasper County	3,865	736	4,601	1,238	2,520	3,758	8,359
USACE	2,013	1,641	3,654	1,632	2,322	3,954	7,608
Avg.			4,127			3,856	7,983
ANN DM8 Results	2,519	1,074	3,593 (13% error)	268	3,974	4,242 (10% error)	7,835 (2% diff)
Physics Based Results	1,290	1,193	2,483 (40% error)	293	4,727	5,020 (30% error)	7,503 (6% diff)

Following this initial assessment, an exact building-to-building match was evaluated using video data from Kent State University immediately following the event. When each individual building's predictive damage state was analyzed against its matched observed damage state from video cataloged images, it was found that the physics-based and ANN approaches produced overall similar results, that were of higher error than the generalized results above. However, both the physics-based approach and ANN DM8 have a match percentage of roughly 40-45%, indicating similar modeling accuracy when categorizing a community's building stock by 19 archetypes. The ANN DM8 did categorize 187 buildings, of the 3,283 buildings recorded in the video data, to the observed damage state that the physics-based model missed (Figure 4-13). Similarly, the physics-based approach matched 70 buildings that the ANN DM8 failed to correctly categorize.

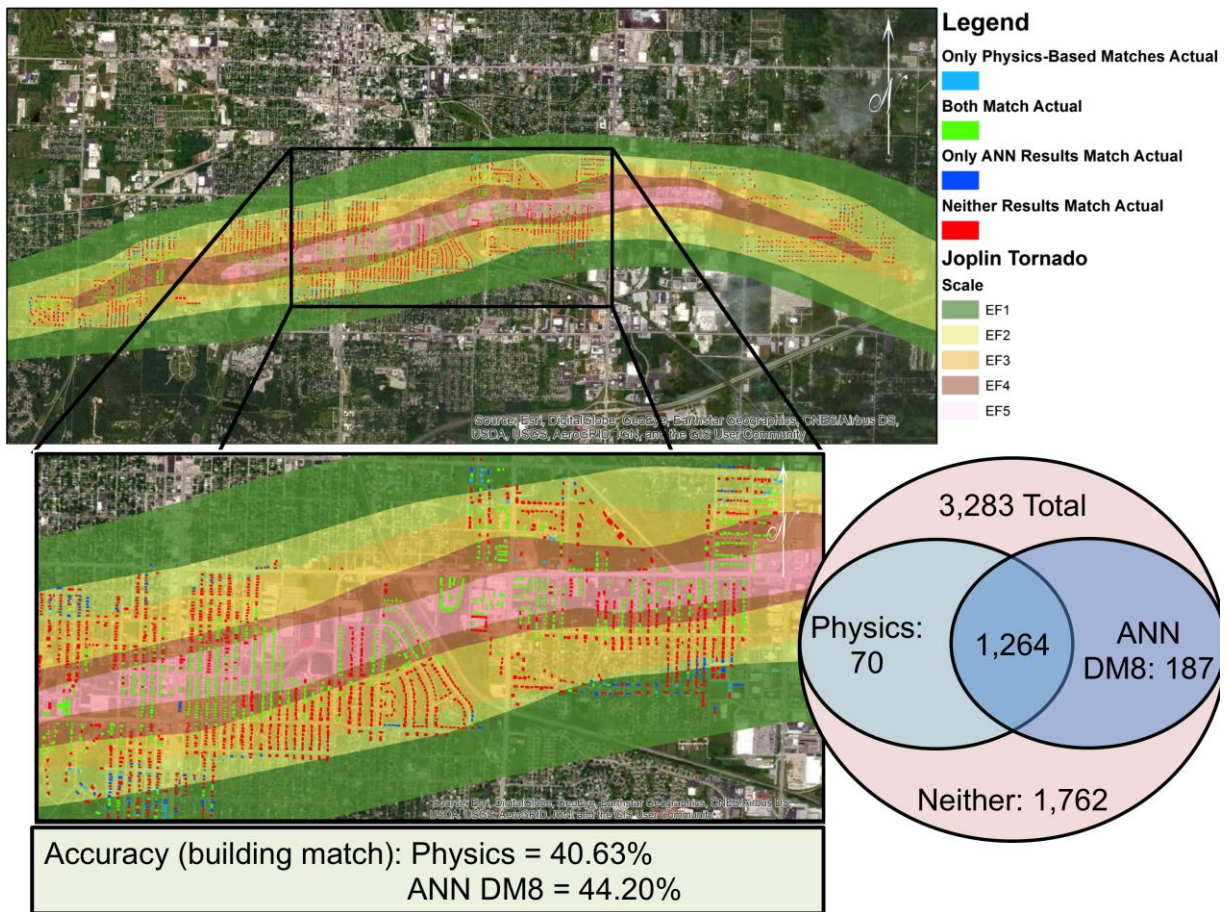


Figure 4-13 Results in matching individual buildings damage state to that modeled from physics-based and ANN methods.

The results above were subsequently separated by building archetype as best as possible. Building descriptions provided in the shapefile data linked to video observations were matched to the 19 archetypes outlined for the modeling discussed herein. The majority of these buildings were residential archetype 1, as summarized in Table 4-2. These buildings also showed a higher error for both physics-based and ANN models. However, this may be attributed to the much larger number of buildings categorized under this archetype than any other. Marginally lower errors occur in matching the damage state of T6, strip mall, archetypes. A difference in relative error did occur for the T19 archetype, office buildings, in which the physics-based model results matched more accurately than the ANN results.

Table 4-2 Summation by Building Archetype

Archetype	Physics Matching Video Observations	ANN DM8 Matching Video Observations	Total Number of Building Captured by Video	Percent Error: Physics	Percent Error: ANN
1	1253	1361	3197	60.8%	57.4%
2					
3					
4					
5	11	11	22	50%	50%
6	15	14	28	46.4%	50%
7					
8					
9					
10					
11					
12					
13					
14					
15					
16					
17					
18					
19	21	17	36	41.7%	52.8%

An additional comparative analysis was conducted between ANN DM3 and DM8. DM3 would be considered closer to the physics-based approach, based on the input variables used. The results of the analysis shown in Figure 4-14, therefore, appear similar to the results in Figure 4-13. DM3's percent error almost exactly matched that of the physics-based error on the building level. However, while the percent errors match, the number of buildings matched only by DM3 was 184, which was greater than the 70 matched only by physics when compared to DM8. The number of buildings only matched by DM8 to the observed damage state is greater when compared to DM3 than the physics model, suggesting a greater overlap between DM8 and physics-based modeling even though the variables used to create each model differ.

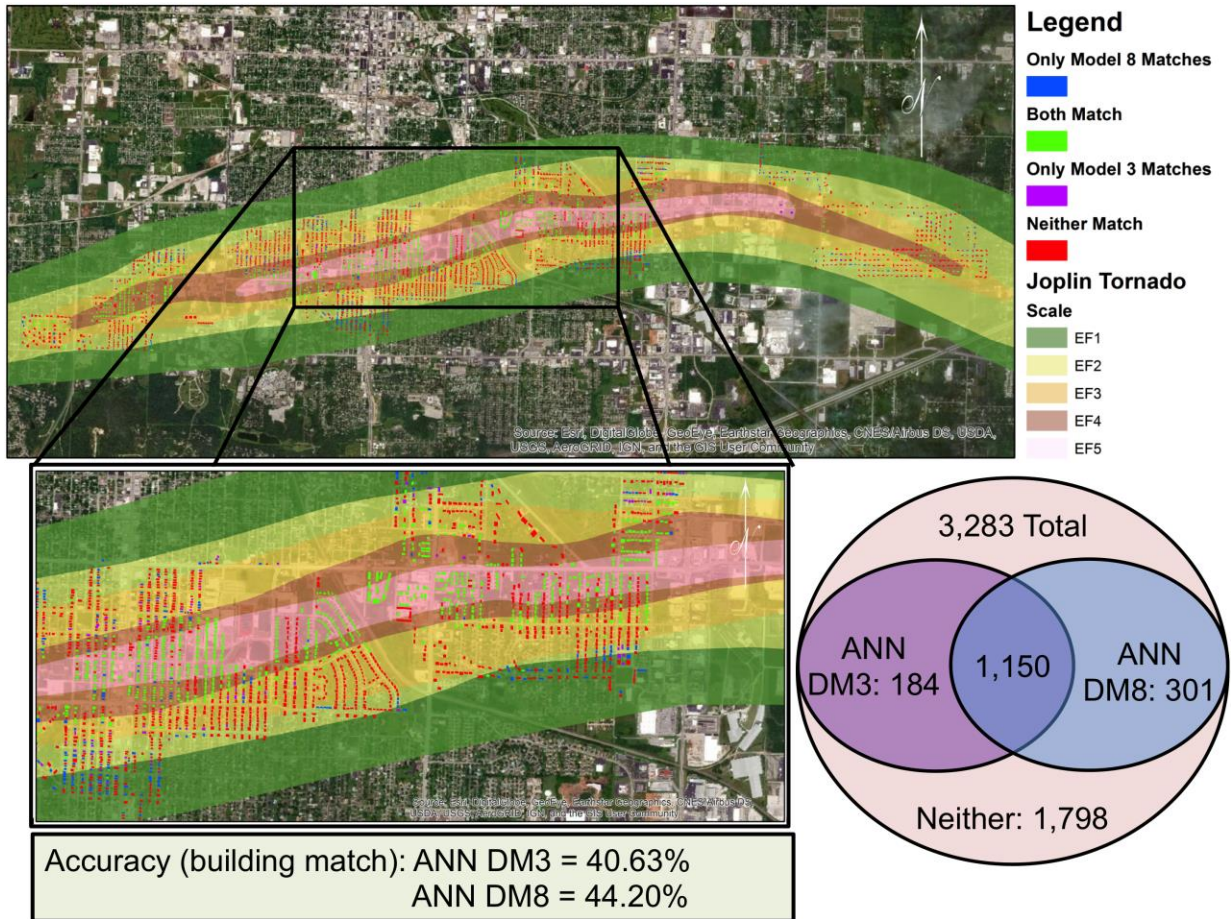


Figure 4-14 Results in matching individual buildings damage state to that modeled from DM3 and DM8.

Overall, the application of ANN modeling proved only slightly, if at all, more accurate than physics-based modeling. The differences in individual building matching accuracy were considered essentially negligible. However, it is noted that the ANN models were fitted to the originally identified 19 archetypes, which constrained the modeling approach. In future applications, the community building stock could be refined further per the structural characteristic designation codes outlined in Chapter 3 and Appendix A. It is theorized that if these designations were applied, the resulting match percentages would increase.

4.3 RECOVERY

Following the construction and analysis of the damage state ANN models, similar build evaluations and network analyses were executed in the interest of modeling recovery time. For this work, the term “recovery” refers to when a building was rebuilt and reoccupied. The general structure for the recovery model was similar to that of Figure 4-1, with 10 hidden neurons and 5 output neurons representing recovery times of 6 months, 1 year, 1.5 years, 2 years, and greater than 2 years (or abandoned). The inputs vary for each of the 15 models, as outlined in Table 4-3, for how they may differ from the damage models, and generally consist of hazard-related inputs, structural, and social characteristics. Some social characteristics for recovery were added based on the literature review, as well as a “1 year residence” factor, which was added in attempt to further communicate individual ties to a community. Recovery Model (RM) 1 consisted of all possible variables, RM2 utilized primarily social parameters, and RM15 was designed to be a “bare minimum” model in terms of inputs. The remaining models were based on how previous models performed during the build process and involved the removal of different select variables. Section 4.3 covers the results from alternating training theory algorithms, variations in model inputs, a graphical analysis of the final set of ANNs used to predict recovery times, and a hindcast of the 2011 Joplin Tornado. The final ANNs had the same inputs and training algorithm, but have difference connection weights and neuron biases, and formed an ensemble of ANNs that process data independently to provide outputs that were averaged when used in application for hindcasting the 2011 Joplin tornado.

Table 4-3 List of variables for damage and recovery models

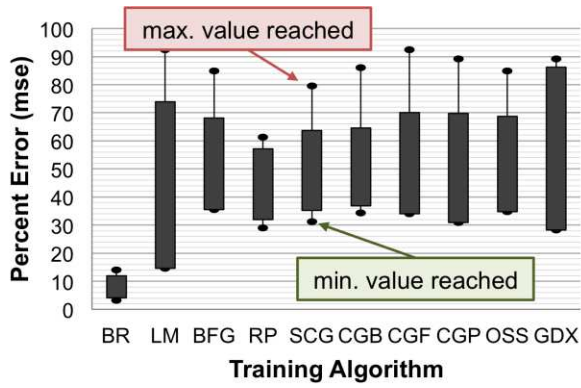
Input Variable	Associated Damage Models	Associated Recovery Models
Hazard <i>(wind type, speed, and event size)</i>	1 2 3 4 5 6 7 8 9 10	1 8 9 10 11 14
Structural <i>(year built, occupancy, roof & wall materials, roof shape, footprint)</i>	1 2 3 4 5 6 7 8 9 10	1 4 5 6 7 8 9 10 11 12 14
Surface Roughness	1 2 3 4 5 6 7 8 9 10	1 2 3 4 8 9 10 11 12 14
Estimated Percent Forested <i>(and Impervious Surfaces)</i>	1 7 8 9 10	1 2 3 4 8 9 10 11 12 14
Tenure <i>(% own, % rent)</i>	1 2 5 8 9	1 2 3 4 5 6 7 8 9 11 12 15
Housing & Population Density	1 7 8	1 2 3 4 5 7 8 9 10 11 12 14
Total Population	1 2 4 5 6 7 8 9 10	1 2 3 4 5 6 7 8 9 10 11 12 14
Age	1 2 6	1 2 3 4 5 6 7 8 10 11 12 14
Race <i>(% Asian, African American, Native American & Hispanic)</i>	1 2 6	1 2 3 4 5 6 7 9 10 11
Industry Employment <i>(extractive and service)</i>	1 2 4	1 2 3 4 5 6 8 9 10 11 12 14
Income <i>(per capita & income: poverty)</i>	1 2 4 9 10	1 2 3 4 5 6 7 8 9 10 11 12 14 15
Add'l Tenure <i>(single female head of household w children, group quarters)</i>		1 2 3 4 5 6 7 8 9 11 12 15
Disability		1 2 3 4 5 6 7 8 9 10 11 12 14 15
Persons over 65 y.o.		1 2 3 4 5 6 7 8 9 10 11 12 14 15
No Vehicle		1 2 3 4 5 6 7 8 9 10 11 12 14
Residence for at least one year		1 2 3 4 5 6 7 8 9 10 12 14 15
Damage State		1 2 3 5 6 7 8 9 10 11 14 15

4.3.1 TRAINING ALGORITHM VARIATIONS

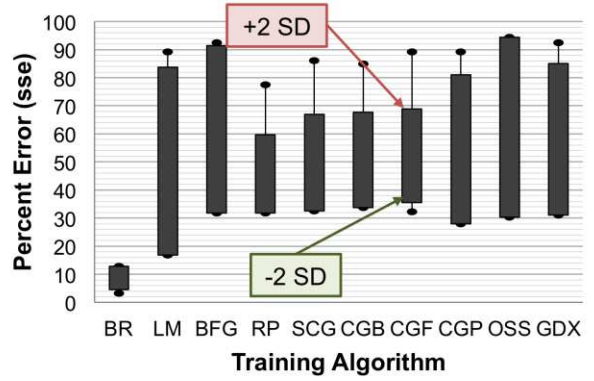
The training algorithms outlined in Table 3-1 represent the core of current training theories used for both the damage and recovery ANN models. Each ANN was “built” once the

lowest possible error (MSE or SSE) was reached through multiple iterations. Each ANN model herein was built a minimum of 50 times (with multiple iterations within each build) to determine a range and subsequent mean for each PCI for training algorithm capability comparisons. To determine if this was enough builds, a coefficient of variation of less than 0.5 with 95% of the data falling within ± 2 standard deviation was used as a mean of determining an adequate sample size of ANN builds and evaluated similar to that of the damage model ANNs.

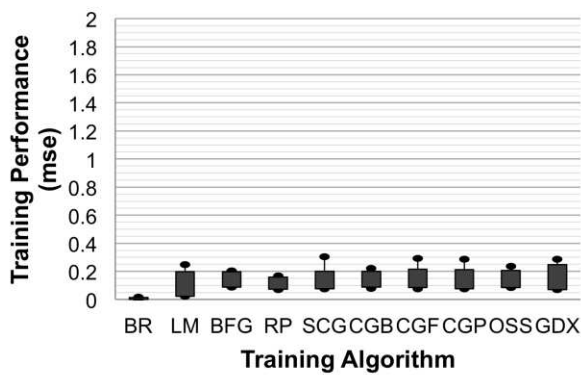
In modeling recovery time, across most algorithms, the PCI's were more desirable with the MSE performance function than the SSE function as shown in Figure 4-15 through the lower percent errors of the MSE functions. The BR training algorithm (with a percent error mode of 7.53% when using MSE) clearly best fit the desired PCIs out of all the training algorithm options by having low percent error and false negative and positive rates, as well as high true positive and negative rates; shown in Figure 4-16. The LM training algorithm (percent error mode of 40.86% for the MSE performance function) was the next best performing algorithm. Similarly, to the damage state modeling analysis, LM was chose to be a form of verification for the BR training algorithm in choosing the most applicable model moving forward.



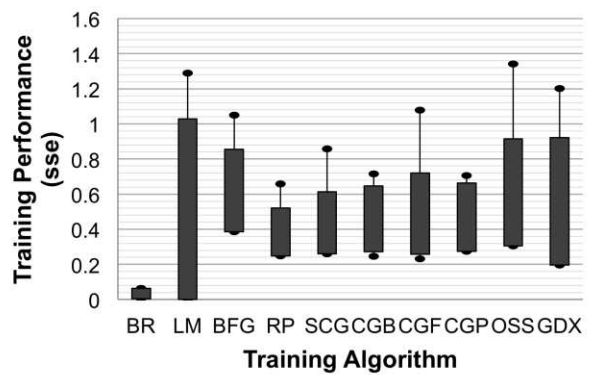
(a)



(b)

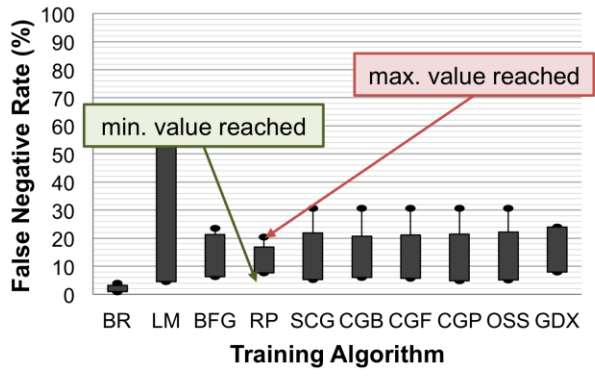


(c)

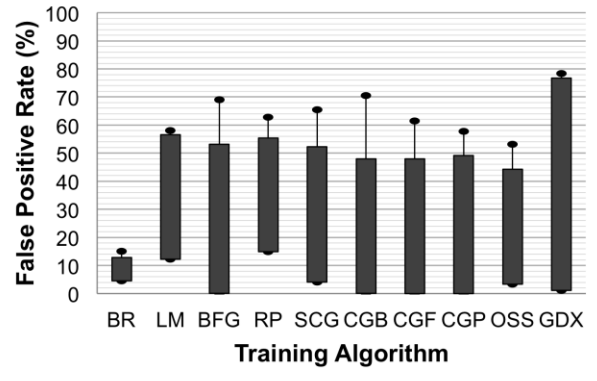


(d)

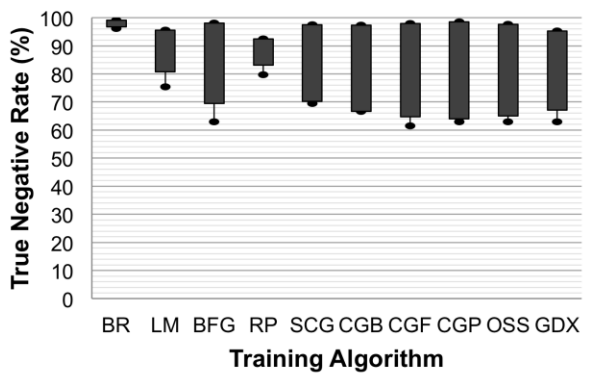
Figure 4-15 (a) Percent error for MSE performance, (b) Percent error for SSE performance, (c) training performance for MSE performance and (d) training performance for SSE performance for the explored training algorithms in modeling recovery time.



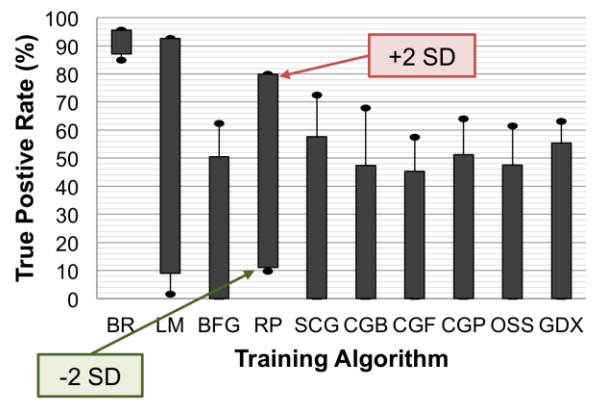
(a)



(b)



(c)



(d)

Figure 4-16 Explored algorithms' (a) FNR, (b) FPR, (c) TNR, and (d) TPR for MSE performance in modeling recovery.

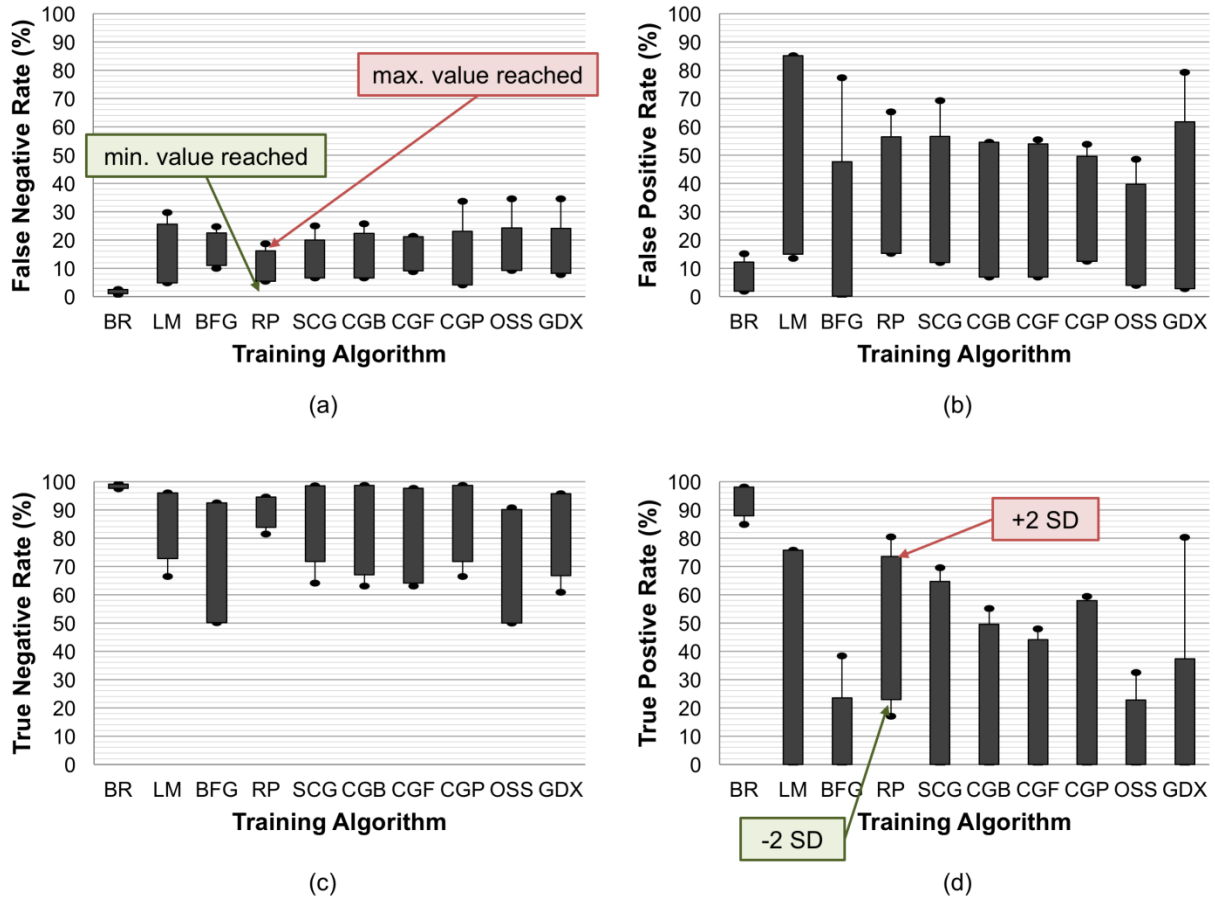


Figure 4-17 Explored algorithms' (a) FNR, (b) FPR, (c) TNR, and (d) TPR for SSE performance.

4.3.2 INPUT VARIABLE VARIATIONS

As with the damage models, multiple recovery models were created in order to further explore relevant variables in determining recovery time. However, instead of a solely structural and hazard model option (DM3), a model focused on social characteristics was created for recovery (RM2). In evaluating how well neural connections were established for different variables, 15 ANNs of varying inputs were built, as outlined in Table 4-3. The results of varying model inputs for both BR and LM training algorithms are shown in Figure 4-18. The resulting best performing models included most sociological, structural, and hazard variables, more so than were required for modeling damage state. While RM8 (all variables minus race), performed the best in establishing patterns between the variables and recovery time, RM2 (primarily social

variables), produced slightly less desirable PCIs. This would suggest that building materials (perhaps availability and ease for construction) do factor into the recovery time. However, RM3, 7, and 11, were some of the poorer performing model structures. RM3 did not include the hazard or structural characteristics. RM7 did not include surface roughness, percent area forested, or the amount of individuals working in extractive or service industries. RM11 did not include the “residence for 1 year” variable, suggesting that, while this variable was not added from the literature, having some form of commitment to a location/community does affect recovery time.

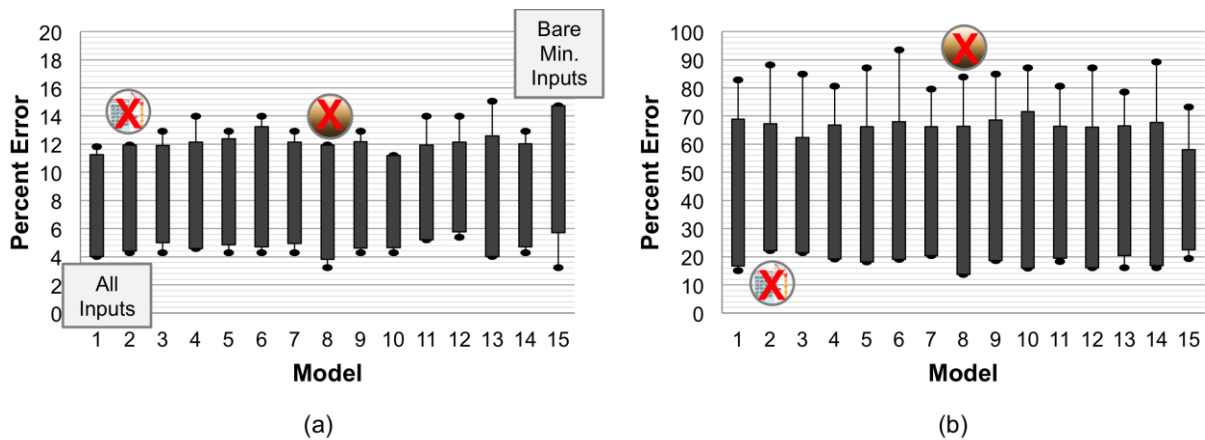


Figure 4-18 Resulting percent error data ranges from 50+ ANN builds for (a) BR and (b) LM, training algorithms, with identifiers for RM2, which doesn't include structural characteristics, and RM8, which negates race.

RM8 was found to be one of the better performing options, comparatively, for both BR and LM training algorithms. Therefore, BR was used for the following assessments and for creating the final model consisting of multiple (designated A through F) ANNs. A model of RM2 was also built for comparison in the following analysis, as well as the graphical analysis, for how connections change when structural variables are introduced. However, it is worth noting that RM2, unlike DM3, was not the poorest performing ANN structure of the model options. Figure 4-19 shows the percent error of the ensemble ANNs A through F for both RMs, as well as the confusion matrices for the lowest percent error ANNs of each model. The confusion matrices show how many data points were correctly placed to their recovery time during training and

testing. These final ensemble ANNs all fell within the 50% lowest possible error from the build analysis, shown in Figure 4-18, and with ROCs clustered primarily in the “true positive” region as shown in Figure 4-20.

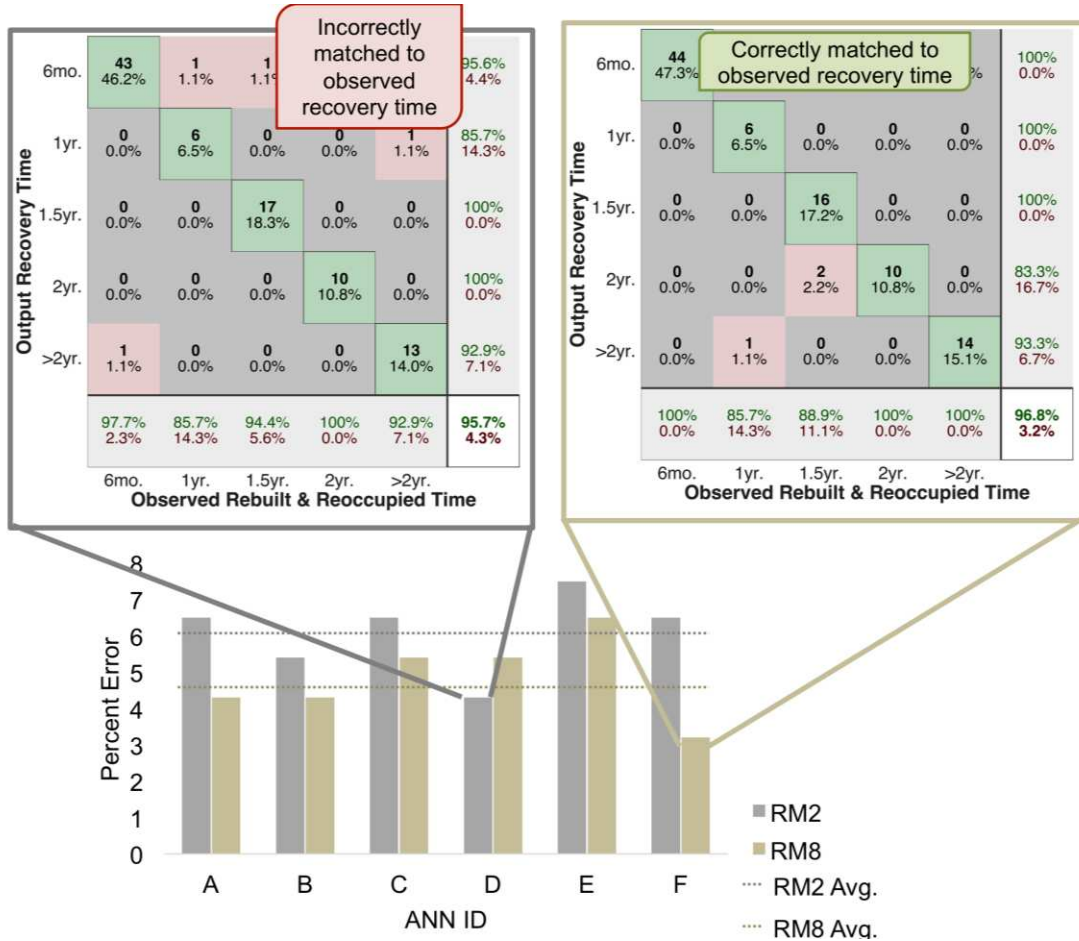


Figure 4-19 Final Ensemble ANNs' build percent error and how that error occurred through the training process as shown by respective confusion matrices.

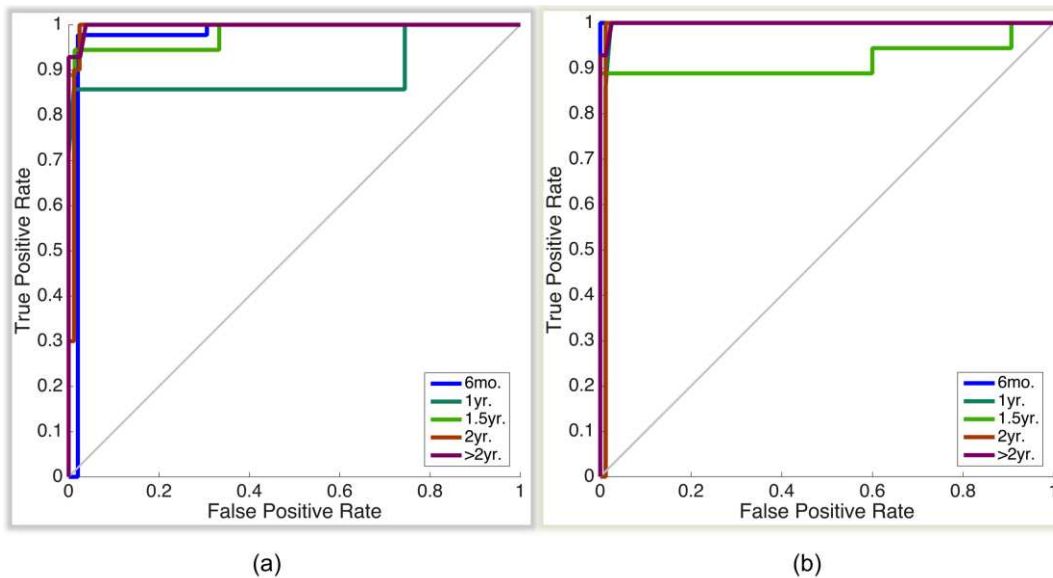


Figure 4-20 ROCs for ensemble ANNs (a) DM3-C and (b) DM8-E.

RM2's percent error was higher for all algorithm types with some having data points output as far off as three damage states. A 3.2% error (BR) was the lowest percent error reached across all algorithms and recovery model builds, and the overall errors reached in modeling recovery time were generally higher than that of the damage state models.

From the above results and analysis, BR was considered the best performing training algorithm with RM8 being the best model input structure. The final machine learning model for predicting a community's building stock recovery time therefore consisted of an ensemble of 6 ANNs requiring RM8 inputs, with 10 hidden neurons, 5 output recovery times, and trained using BR to reach a lowest possible MSE. These final 6 ANNs for RM8 were used for the following graphical analysis and hindcasting the recovery from the 2011 Joplin Tornado. RM2 was also comparatively assessed for the graphical analysis. Since modeling recovery time is still relatively new, there was not a widely accepted and consistent approach to modeling, that has previously been validated against a hindcast, as there was with damage states and the focus on structural components. As a result, recovery from the Joplin tornado was only hindcasted using the best performing model option: RM8.

4.3.3 GRAPHICAL NETWORK ANALYSIS

The graphical analysis of the recovery models was conducted in the same manner as the damage models. In the shortest path analysis, if a relatively strong connection (high weight values) was found in both the combined and averaged approach, then that was considered a finding of this analysis. Similarly, the weaker connections were also evaluated. Figure 4-21 presents the relative results from calculating the shortest path for RM2, primarily social inputs model structure. Note that certain structural parameters, such as size and occupancy, were kept as inputs in RM2, as these were originally considered foundational variables for reconstruction. In RM2, the building size, in terms of footprint area, was linked to a 6mo recovery time, whereas building height was found to strongly link to a 1-year recovery time. Additionally, building damage state was found to strongly connect to a 1.5-year recovery time, population density to 2 years, and area forested to the building taking longer than 2 years to recover (or become abandoned). Weaker connections were found between the amount of people on disability and the income to poverty ratio to a 6-month recovery time. Owning tenure and the wind event type (straight-line or tornadic) were shown to be weakly connected to 1- and 1.5-year recovery times, respectively. Both building height and the amount of people working in the service industry demonstrated a weak connection to determining if the structure would be abandoned in RM2.

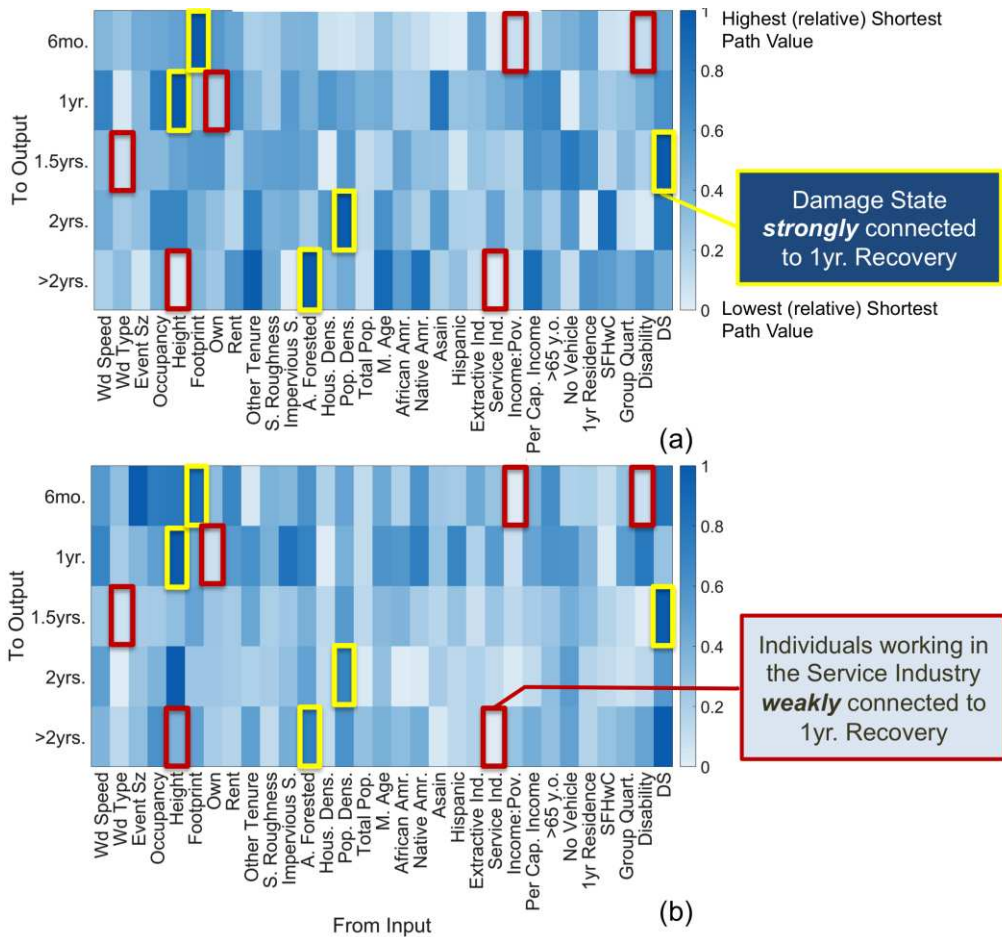


Figure 4-21 Shortest path relative values for RM2 (a) combined ANNs and (b) averaged results from each ANN.

The results from analyzing RM2 provide an initial description of the network connection structure without parameters related to building materials. Figure 4-22 presents the shortest path analysis results after introducing building variables and subtracting out racial variables in the ANN structure to form RM8. While building height still ties strongly to a 1-year recovery time, it has also tied strongly to the 6-month recovery time, which is more intuitive since building height tied strongly to no damage (DS0) in the previous graphical analysis for the damage models. The wind speed and a single female head of household with children were also found to strongly connect to a 1-year recovery time, while the roof shape was strongly connected to an over 2-year recovery or abandonment. Conversely, individuals with disability moved from having a relatively weak connection to 6-month to a 1-year recovery time. The structure's median year

built and occupants working within extractive industries were found to weakly connect to recovery by 1.5 years. While building height remained strongly connected to earlier recovery times and disability weakly connected to earlier recovery times, the remaining strong and weak connections did not suggest any significant shifts in focus. In dropping strong connections from building footprint, damage state, population density, and area forested, strong connections were gained in relation to wind speed, roof shape, and single female head of household with children for RM8. RM2's stronger connections focused more on the area of and surrounding the building, but the inclusion of structural variables does not seem to have replaced those connections with any similar pattern. A similar assessment could be said for the weaker connections, with the exception of the shift from percent of population employed in service industries to percent employed in extractive industries having weak connections.

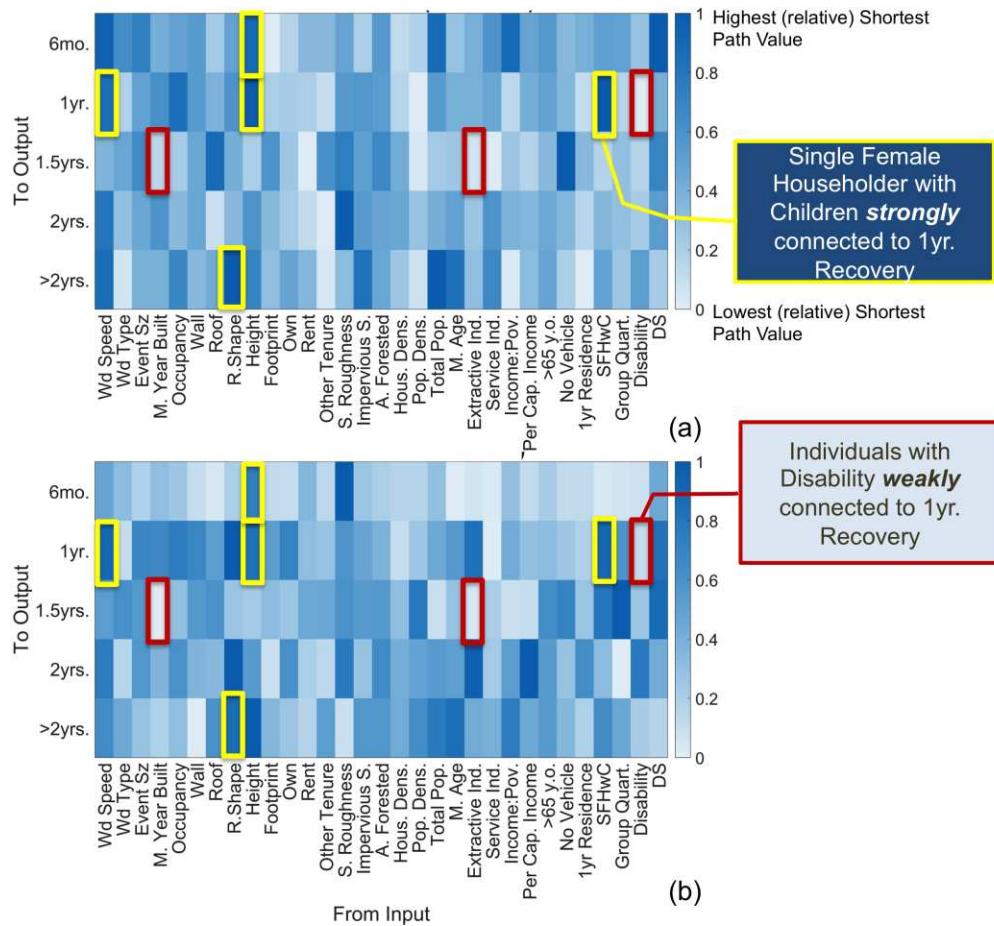


Figure 4-22 Shortest path relative values for RM8 (a) combined ANNs and (b) averaged results from each ANN.

As with the shortest path analysis, the centrality analysis, through the concepts of closeness and degree, was conducted for recovery modeling in the same manner as the damage model analysis. Figure 4-23 shows the centrality scores, plotted as closeness versus degree. RM2 resulted in a combined network where the recovery times of 1 to greater than 2 years were widely influenced by the multiple input variables. The lack of vehicle, other tenure (neither rent nor own), damage state, employment in extractive industries, income to poverty ratio, renting tenure, building occupancy code, and footprint area are also widely connected within the network structure. In combination with the shortest path results, this would suggest that building footprint area and damage state are significant factors in determining recovery time within the RM2 structure. Conversely, owning tenure is a less significant factor in this structure

as it shows a weak connection to a 1-year recovery time and low centrality scores when related to the overall network.

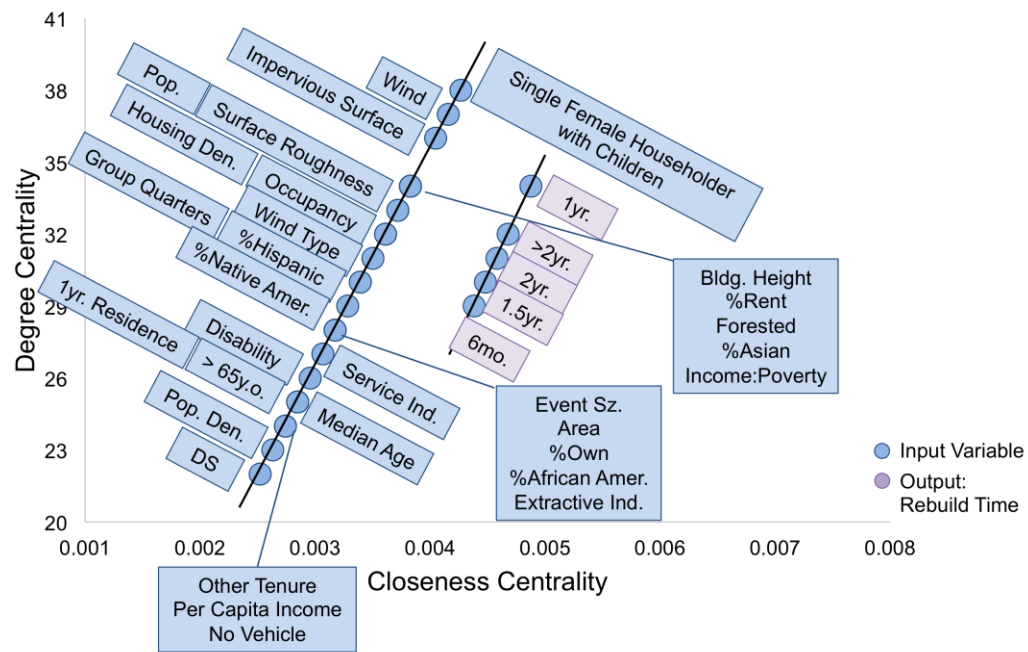


Figure 4-23 RM2 (combined ANN structure) centrality scores as closeness versus degree.

The RM8 centrality scores are shown in Figure 4-24. Single female head of household with children, wind speed, and percent of area consisting of impervious surfaces were all inputs found to be widely connected to the possible recovery times within this network. The 1-year recovery time was also shown to remain a heavily influenced output, indicating that many variables contributed to determining this outcome, as opposed to the 6-month recovery time, which showed a lower degree centrality. In combination with the shortest path results, the wind speed and single female head of household with children variables were found to be overall significant contributors to the time it would take to rebuild and reoccupy a structure following a severe wind event. In RM8, the variables that showed weak connections to specific recovery times did not also rank among the lowest centrality scores. This would indicate that while the number of population employed in extractive industries weakly tied to a 1.5-year recovery time, it also tied relatively well within the entire network overall.

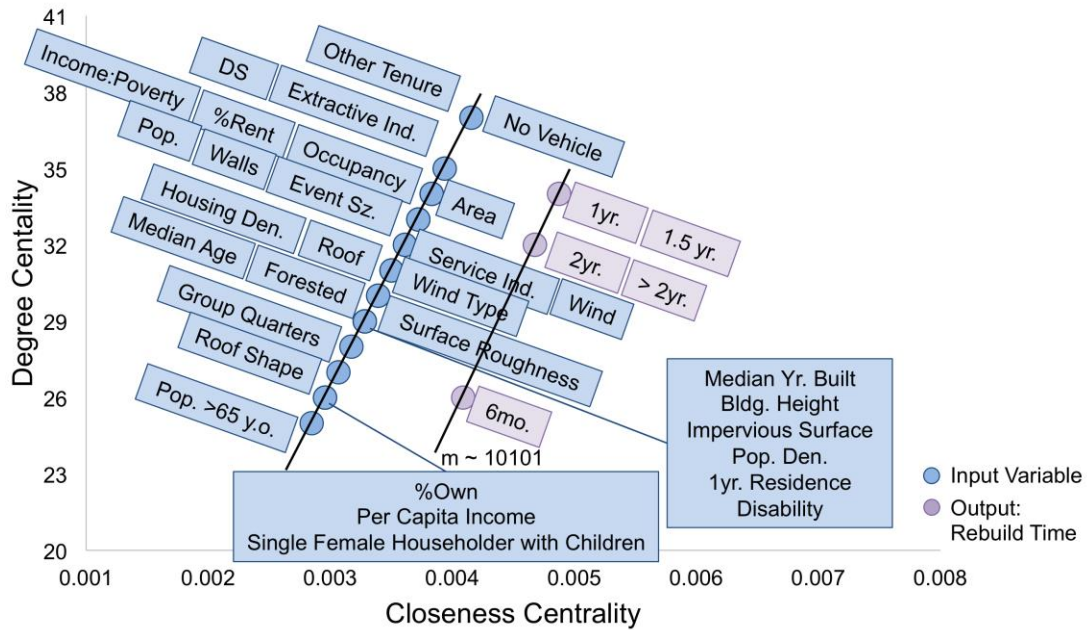


Figure 4-24 RM8 (combined ANN structure) centrality scores as closeness versus degree.

The results from the centrality analysis showed similar organization among both input variables and output recovery times for both RM2 and RM8, indicating that overall connectivity within the network may be similar even with a switched variable hierarchy and differing inputs. Additionally, the shortest path analysis results indicated a remaining importance of wind speed, building height, and roof shape when continuing on from modeling damage state to recovery. Overall, in comparison to modeling damage state, modeling recovery time proved to be a more involved and complex problem due to the overall higher percent errors and similarities in network organization between RM2 and RM8 through shortest path and centrality analyses. The lack of a significant shift in strong network connections and any organizational differences among the centrality plots brings into question how the ANN is built giving the data provided.

4.3.4 HINDCASTING RECOVERY FROM THE 2011 JOPLIN TORNADO

In order to further validate this approach as a method of predicting the time to rebuild and reoccupy a building, the 2011 Joplin, MO Tornado was simulated for RM2 and RM8, then compared to documented recovery of select buildings from video data provided by Kent State University (Curtis and Fagan 2013). The tornado path and intensity was overlaid with the buildings in the area, similar to how the damage hindcast was conducted to include the wind hazard, structural type, and U.S. Census social characteristics.

As was performed with the damage models, the recovery model errors were assessed on a broad scale and a more exact scale. Each building within the video data set was analyzed for whether it was fully recovered (Recovery State 4) by 1-year, 1.5-years, 2-years, or longer. The 6-month recovery data was not available within the actual video data; therefore, the ANN results would subsume 6-month recovery under the 1-year recovery categorization. For the first error assessment, an exact match for each building was assessed for 1-year, 1.5-year, 2-year, and greater than 2-years recovery times. For the second analysis a +/- 6 month error was introduced, such that if the ANN model predicted a 1-year recovery and building actually reached Recovery State 4 by 1.5-years, this was considered a match. This approximated match was used based on the assumption that if a singular building recovered by 10 months or 14 months, the overall impact to the community from such a difference would be minimal. The results are shown in Figure 4-25 with a match percent of 23-42% for the exact match and 76-84% for the approximated match.

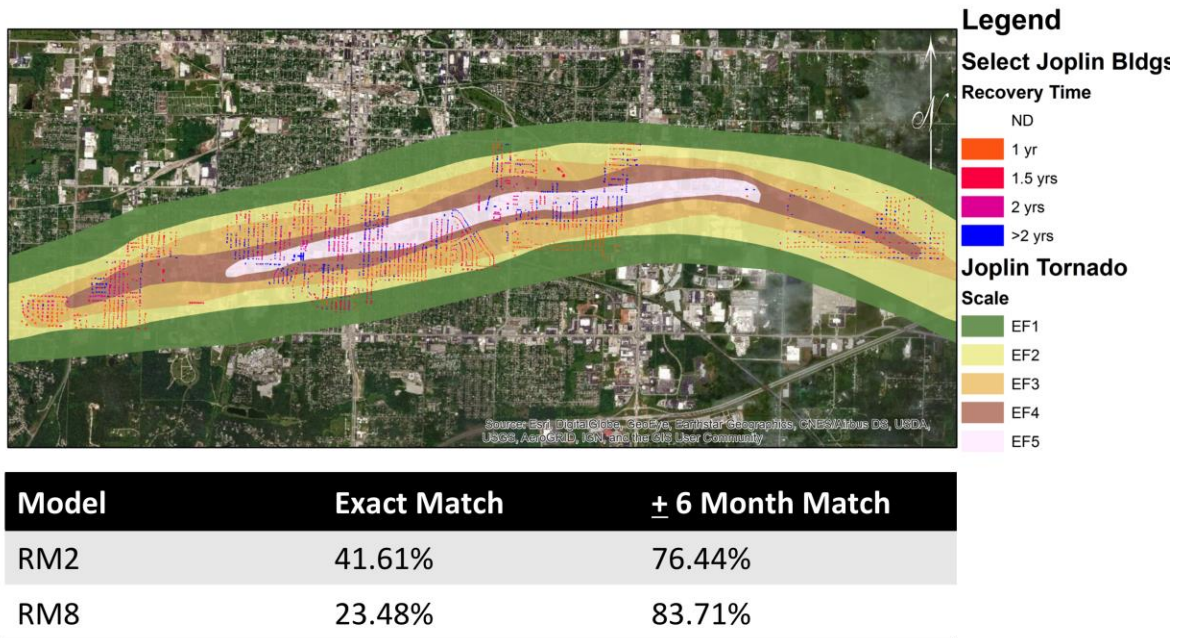


Figure 4-25 Actual recovery time for select buildings within Joplin and the percent errors from hindcasting with RM2 and RM8 for the exact match approach and a +/- 6-month error buffer.

The recovery modeling errors proved to be higher than that of the damage modeling analysis. This was expected since there were differing damage state categorizations across the multitude of post-event assessment surveys, which lead to an error within the known data set, as well as potentially greater uncertainties in categorizing a building’s recovery state over time. Additionally, while DM8 had a slightly lower error than DM3, RM2 resulted in a lower error for the exact match when compared to RM8, with this result switched for the approximated match. However, as with the damage models, the percent error/percent match were close enough such that both models were considered to perform similarly in hindcasting the 2011 Joplin tornado.

Subsequently, an analysis by building type was conducted for both RM2 and RM8 as provided in Table 4-4. As with the damage models, residential (T5) and strip-malls (T6) were better matched to their actual outcomes, specifically for the approximated approach. Residential T5 did not match well for the exact match of RM8, however nearly all possible T5 structures were correctly categorized under the approximated approach. The results from the recovery

hindcasting analysis primarily show sensitivity in modeling by 6-month intervals and should be considered in further recovery modeling development.

Table 4-4 RM8 and RM2 results by building archetype.

Archetype	Exact Match				+/- 6 month match			
	RM8	%Match	RM2	%Match	RM8	%Match	RM2	%Match
1	659	24%	1142	42%	2317	86%	2114	78%
2								
3								
4								
5	0	0%	7	50%	14	100%	14	100%
6	1	6%	11	61%	17	94%	15	83%
7								
8								
9								
10								
11								
12								
13								
14								
15								
16								
17								
18								
19	5	17%	19	63%	24	80%	23	77%

4.4 THE JOPLIN DATA

Thus far, the actual Joplin damage and recovery data has been presented as it pertains to the validation of various modeling approaches. However, this data had patterns of its own to present as well. The total number of buildings within the tornado path, as defined in Attary et al. (2018), was 7,912. However, of those 7,912 buildings, only 2,771 had recovery data recorded for the first two years, which lead to an approximate 35% of affected buildings analyzed for this case study. The majority of the buildings analyzed were residential, specifically, T1 and T5 archetypes, with some business and retail buildings (T6), a hospital (T12), and some office

buildings (T19). Approximately 38% of the residential buildings in Joplin recovered within the first year, while most retail buildings took longer to recover. The hospital building captured in the video data took 2-years to recover. Additionally, most schools were documented as also recovering in 2 years' time (Onstot, 2016).

Most of the buildings with damage data were categorized as DS4 and would have needed to be rebuilt, however, most buildings within the dataset recovered within the first year. At first assessment, this would indicate a correlation between high damage states and quick recovery times. However, by evaluating each DS group individually, as shown in Figure 4-26, it was observed that most DS 1, 2, and 3 buildings, recovered within the first year, with DS1 buildings sometimes needing additional recovery time through 1.5 years. The DS4 buildings were relatively evenly spread out across the 1-year, 1.5-year, 2-year, and longer time frames. Of the over 600 buildings still not yet recovered, only 53 were noted as in the "rebuilding" phase, or RS3, at the two-year mark.

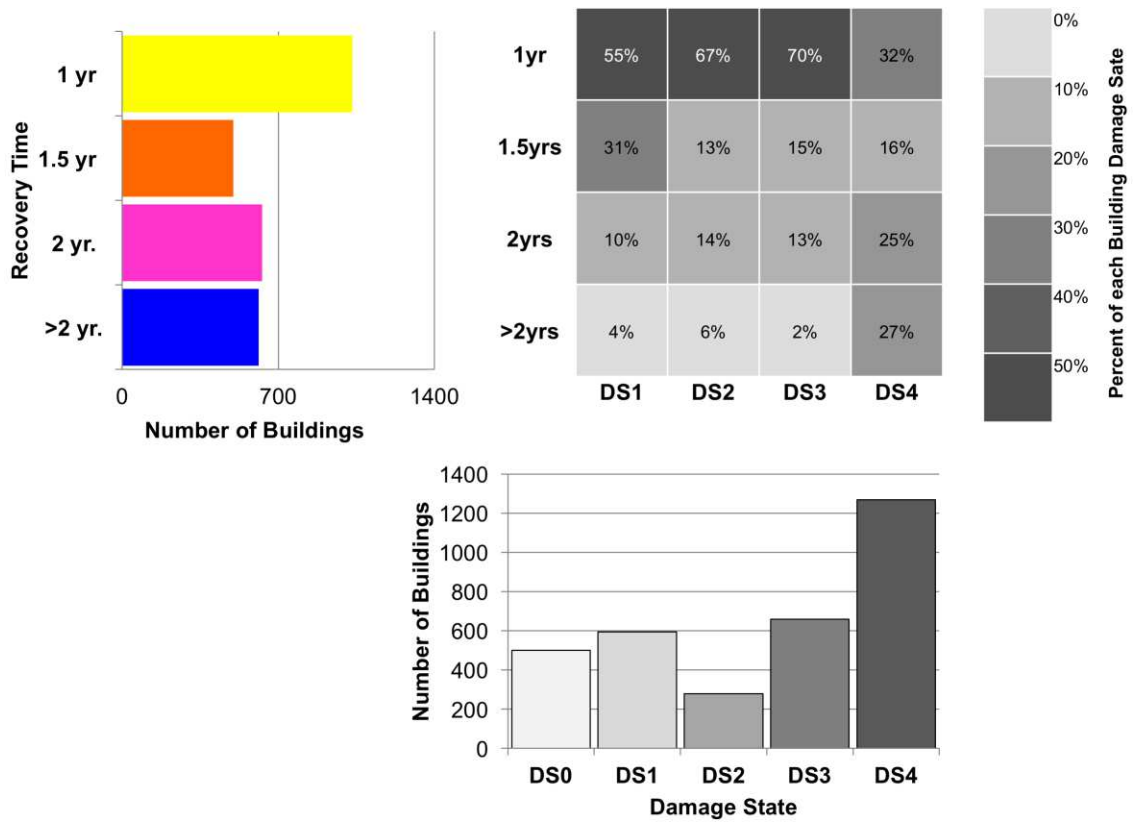


Figure 4-26 Distribution of buildings categorized as being in damage states 0 through 4, recovery time, and how many buildings in each damage state corresponded to each recovery time.

When these recovery times were distributed spatially by neighborhoods (parcels bounded by streets), it was found that the majority of neighborhoods contained buildings that took various time frames to recover. The spatial distribution by neighbors is shown in Figure 4-27. The results of this distribution also indicated that neighbor recovery time did not necessarily contribute to an individual building's subsequent recovery time. In other words, if a building's neighboring structures were all recovered by 1 year, that did not necessarily correlate to that building also recovering within 1 year.

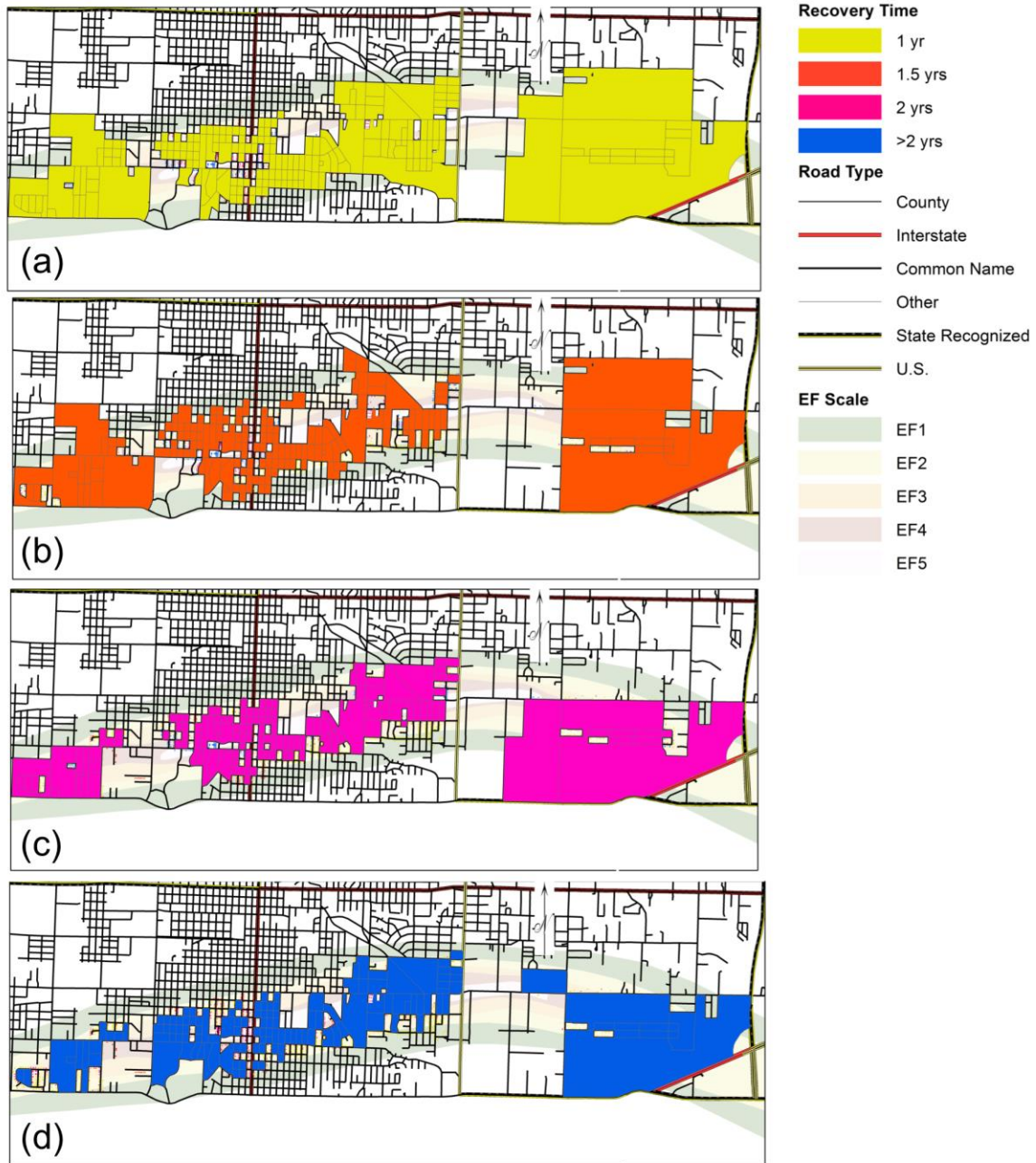


Figure 4-27 Neighborhoods containing structures that were recovered by (a) 1 year, (b) 1.5 years, (c) 2 years, or (d) structures that had not recovered by 2 years.

From here, the neighborhood areas were expanded to Census Block Groups (BG), so as to evaluate any demographics that may correlate to certain recovery times. These BGs were designated Blocks A-N as shown in Figure 4-28a. Figure 4-28b then shows which elementary

school contains attendance from each BG. Note that there are numerous elementary schools, but Joplin High School serves the entire city.

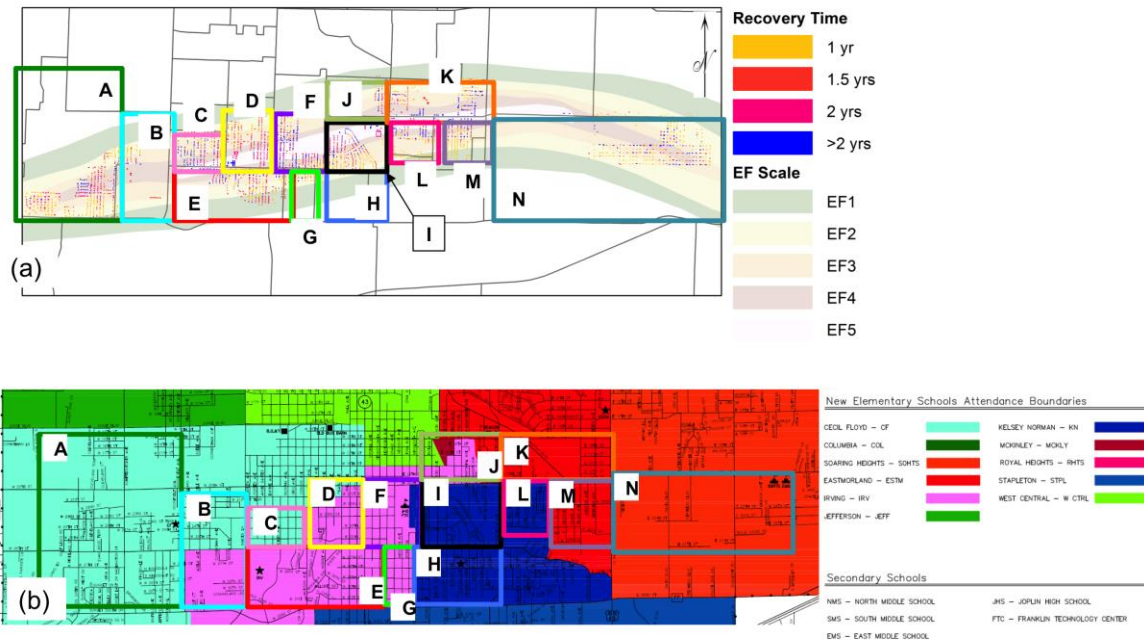


Figure 4-28 Census block group designation (a) for structures with recovery data (Curtis and Fagan 2013; U.S. Census Bureau 2018) and (b) by school district (Joplin Schools 2019).

The damage and recovery patterns were then assessed for each BG using the data in Figure 4-29 & Figure 4-30, respectively. Each BG's damage state distribution and corresponding division by recovery state (Figure 4-30) allowed for evaluation of which areas deviated from the overall pattern previously found in Figure 4-26. Blocks C, D, E, and F showed patterns that indicated slower recovery times. In Block C, DS1 buildings were more spread out across the possible recovery times and a larger percent of structures had not yet recovered by the 2-year mark. This was similar for Blocks D & F, with most DS4 buildings taking at least 2 years to recover, instead of being evenly spread out across the multiple recovery time frames. Block E interestingly had most of DS 3 structures not yet recovered by 2 years, but the DS 4 structures were mostly rebuilt by the 2-year mark. The BGs with some quicker recovery indicators were Blocks B & N, with Block N showing most buildings recovered within the first year across all damage states, and Block B had a larger percentage of DS1 & 2 buildings

recovered by 1 year when compared to the overall community pattern. Blocks K, L, & M showed a mix of quicker recovery for DS1 & 2 (similar to Blocks B & N) but a slower recovery for DS3 & 4 as indicated by the percent of buildings in each damage state recovered by each time step.

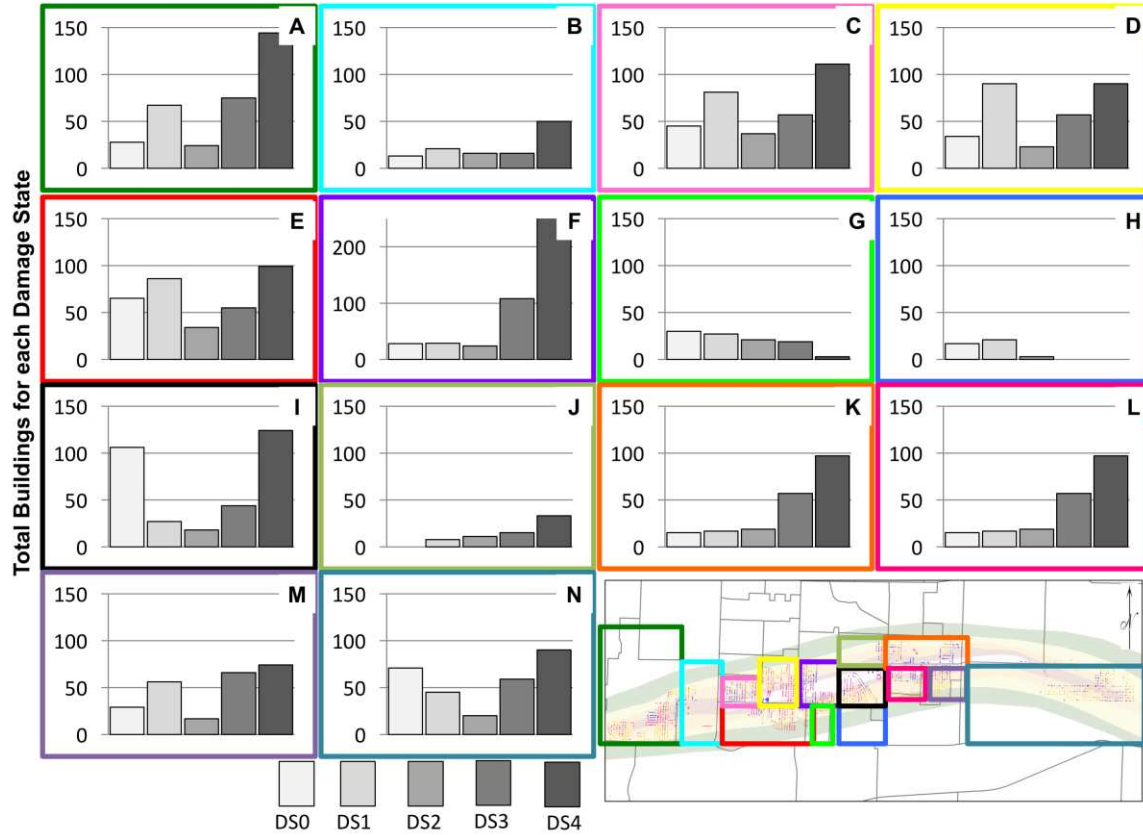


Figure 4-29 Building damage state distribution by census block group.

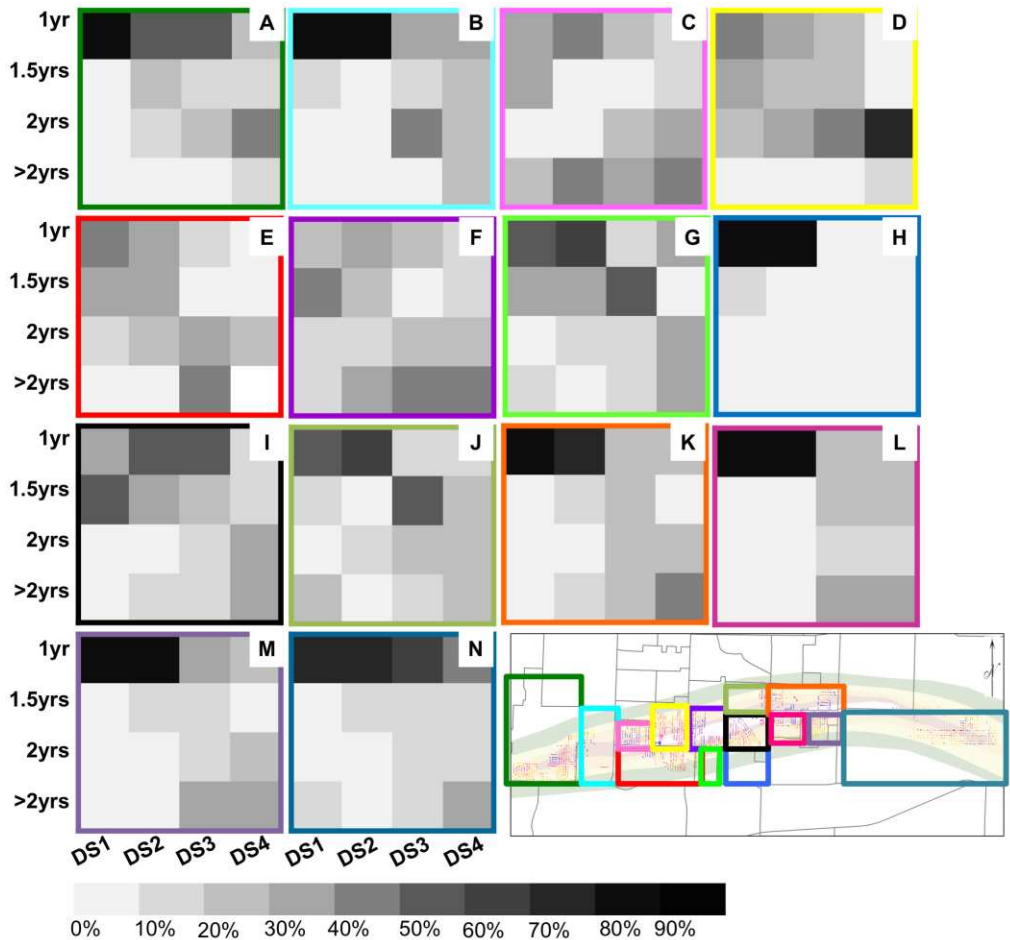


Figure 4-30 Percent of each damage state's buildings corresponding to each recovery time by census block group.

These results prompted an assessment of the BGs demographics and which of the previously studied vulnerability factors correlated to changes in recovery distributions by building damage state. However, not all of the social characteristics are discussed herein as some did not show much correlation and/or were not available in the 2010 ACS for the state of Missouri. For example, one of the most commonly discussed demographics in association with recovery from natural hazard is income. However, as can be seen in Figure 4-31, the per capita income was not very diverse across the Joplin area. Blocks B, C, E, and N all had per capita incomes of less than \$25,000, even though these blocks also showed differing recovery patterns. However, a stronger correlation was found between the Median Year Built of the structures in a BG and slower recovery times. The same BGs that showed slower recovery time

(C, D, E, & F) also had structures of a Median Year Built (YB) prior to 1970. Overall, Figure 4-31 shows the correlation between older structures and slower recovery times, but not a correlation with income.

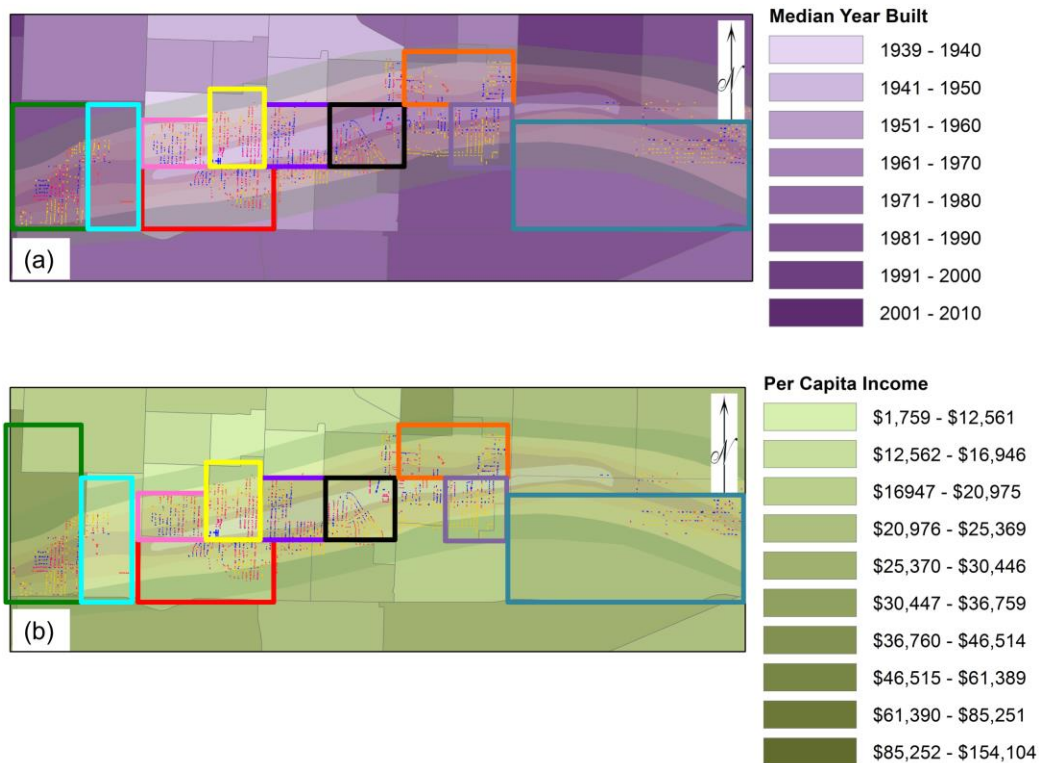


Figure 4-31 Building recovery and corresponding census block group by (a) the structures' median year built and (b) per capita income.

The BGs that showed some tendencies towards quicker recovery times were Blocks B, K, L, M, N, with Blocks K, L, and M containing a higher percentage of DS3 & 4 structures that conversely took longer to recover. There were multiple demographics that were correlated to these areas. Block B, which showed the majority of DS1 & 2 buildings recovering within the first year, also consisted one of the lowest median age BGs as well as a low percentage of individuals who did not have access to a vehicle. Similarly, Blocks K, M, and N, which all showed quicker recovery times for DS1 & 2, also had a low percentage of individuals without a vehicle. These same three BGs actually had a *low* percentage of individuals who neither rented

nor owned that correlated to quicker recovery times. These correlations within the Joplin community are shown below in Figure 4-32.

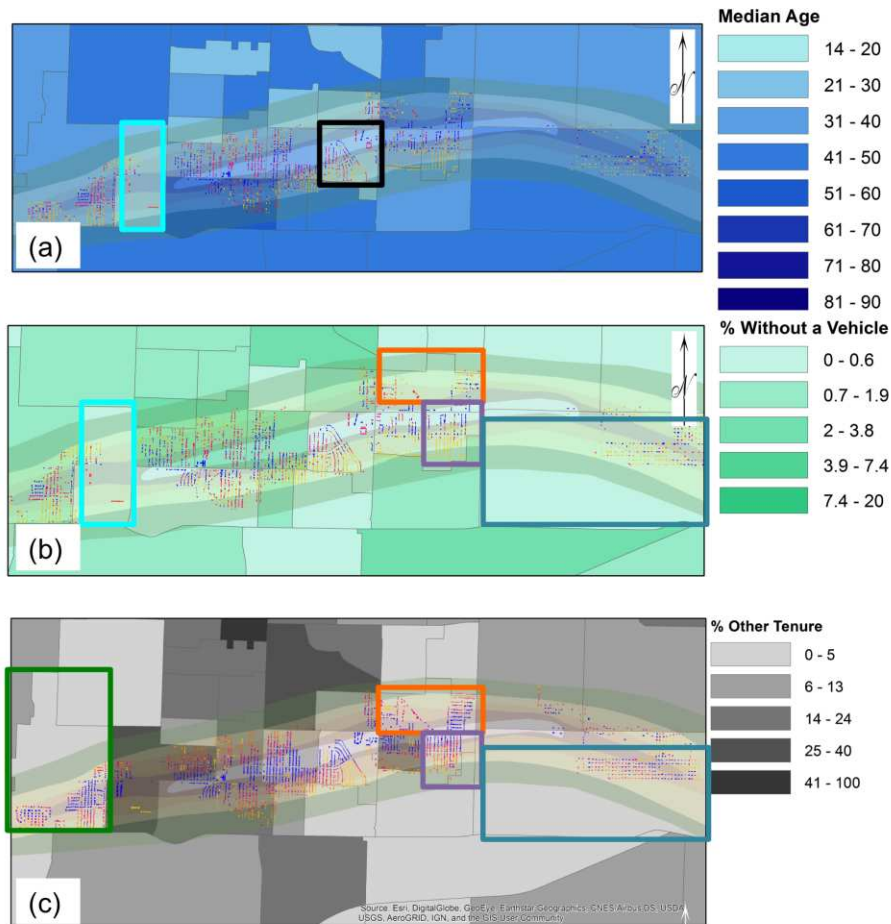
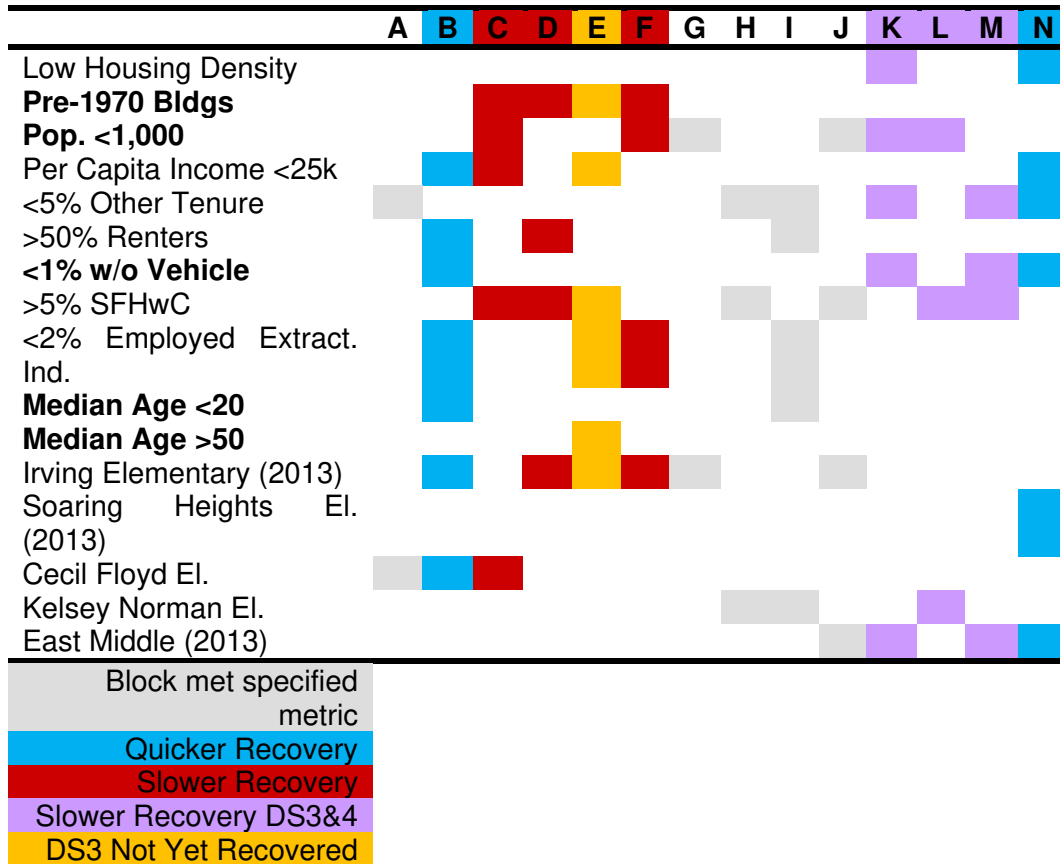


Figure 4-32 Block groups that tended towards quicker recovery times by (a) median age, (b) percentage of individuals who do not have access to a vehicle, and (c) percentage of individuals who neither rent nor own.

A summary of these demographics are provided in Table 4-5. In addition to older structures tying to slower recovery times, a low population count was also found to correlate buildings of more severe damage states (DS3 & 4) to requiring at least 2 years for recovery. Blocks D, E, and F also corresponded to the attendance zone of the Irving Elementary School, which suffered severe damage and was not recovered until 2013 (Onstot, 2016).

Table 4-5 Summary of BG Recovery by select demographics.



4.5 SUMMARY

The build process for the damage and recovery models resulted in the use of BR training with MSE performance evaluation. The final suggested damage model was DM8, which included hazard and structural characteristics as well as percent area forested, housing density, total population, and housing tenure. From the graphical analysis of DM8, wind event size, height, and owning tenure were found to be critical inputs to the network. The results of hindcasting the 2011 Joplin tornado subsequently showed that the use of ANNs is comparable to that of physics-based modeling using fragilities in terms of accuracy. The overall differences between the percent errors for each modeling approach were considered negligible.

For the recovery models, both structural and social variables were also found to be critical in modeling with a wind hazard event. From the graphical analysis, single female head of household with children, building height, wind speed, and employment (industry and income) were highlighted as potential critical variables within a recovery modeling ANN, while a 1-year recovery time was also found to be widely influenced by the input variables. However, the hindcasting results did not show a consistent best performing ANN structure, with overall differences in error also being considered negligible. The changes in the shortest path and centrality analyses for RM2 and RM8 also failed to show patterned changes as the input variables were changed. The Joplin data then showed a correspondence between slower recovery times and census block group median year built and a population under 1,000. The single female head of household demographic within the Joplin area also correlated to slower recovery times specifically for DS3 structures. The lack of agreement, or noticeable pattern differences, among the ANNs evaluated and the Joplin data may suggest either missing variable input data or perhaps that the building recovery process requires further evaluation to improve understanding. The following chapter will further discuss the potential implications of the above results.

CHAPTER 5 IMPLICATIONS OF RESULTS

5.1 THE USE OF ARTIFICIAL NEURAL NETWORKS FOR MODELING SOCIO-TECHNICAL INTERACTIONS

The results of this research have demonstrated a preliminary comparability with physics based approaches, in terms of accuracy, while potentially introducing another option in modeling complex interactions for socio-technical variables. The similar percent errors from real-world use in hindcasting highlight this modeling approach's applicability. However, the similarities of the damage state hindcasting results from both physics-based and ANN methods highlight the question of whether or not one approach is necessarily preferable to the other.

The damage state analysis for the 2011 Joplin tornado yielded results of approximately 40-45% matching for both methods. The 5% additional accuracy from the ANN method could be due to the specific community hindcasted or even considered negligible, which implies the question of why the results were so similar and how the errors could be further reduced, specifically for the ANNs. One of the first considerations to this point would be the amount of data. The damage models were built with 117 data points, while the recovery models were built with 93 data points. While this was the data available for the state of Missouri, the general consideration would typically be that more data points (greater than 100) are better. However, a previous study on sample size and variability of data for the use of neural networks found that this is generally true for highly variable data (Markham and Rakes 1998). For data that is less variable, an ANN may perform just as well as a standard regression analysis. Therefore, for the ANNs discussed herein, this may suggest that the data set was not variable enough to require the use of ANNs or that more than 117 data points were needed. It is worth noting here that the use of data solely from the state of Missouri was decided in the interest of minimizing the potential introduction of complexities related to differing construction practices across states.

This leads into another query as to the possibility of only using data from the 2011 Joplin tornado, where 2,000 of the approximately 3,000 data points could be used to train the network and the remaining used to validate and test the network without an additional hindcast validation. While this would provide more data points to build an ANN, the variability of those data points would be low. The hazard itself was an extreme (and rare) event. Additionally, the social demographics of Joplin, MO are not very diverse (as will be highlighted in the next section). While an ANN trained with more variable data could be used to predict a rarer event falling within the bounds of the training data, an ANN of less variance would not be well suited for predicting less extreme events or for drawing comprehensive conclusions on socio-technical interactions.

Finally, in any modeling approach the resolution at which the model is to be executed will contribute to the resulting errors. Note that for both the damage and recovery ANNs, when the damage states were grouped (DS1&2 and DS3&4) and a +/- 6-month buffer was used, the errors drastically improved. This may similarly relate to creating predictive models at the building level versus a coarser mesh or neighborhood resolution. Not only is there a lack of explicit, correct, data collected relating to a hazard at a specific building, but the structures have also been generalized to fit the construction characteristics of the predefined 19 archetypes. At the building level the number of variables that could contribute to damage state and recovery drastically increases as well as the differences among each variable, whereas at the neighborhood level, an aggregate generalization may provide more feasible data sets. Ultimately, in using ANNs at the building level, given the data variance, the hindcasting results would likely improve if each individual building maintained information on its construction, retrofits, occupancy, usage, and wind speed that could be used to train, validate, and test an ANN. Maintaining a consistent data set, using similar variable values as proposed in Table 3-5 and Table 3-7, may allow for subsequent verification of this modeling approach in the future.

5.2 THE USE OF GRAPH THEORY TO ANALYZE ARTIFICIAL NEURAL NETWORKS

The use of ANNs, and AI in general, has had a “black box” type of implication when applied for modeling use. Inputs are provided to the ANN and in turn the ANN provides outputs without much understanding of what happens in between those two steps. This ultimately introduces the questions: Are the connections being made the “correct connections” and does the use of such modeling impact our understanding of the phenomena being studied? These concerns are certainly valid, especially when AI may perform better at a task than its physics counter parts. This “better” performance may also raise the question of “what were we missing?” Graphical analysis of resulting network patterns provides some insight into these questions.

The damage models built herein provided some specific insight into the relationship between social demographics of a community, structural characteristics of a building subjected to a wind hazard, and the potential for debris impacts. The addition of even some social parameters, such that were added to DM8 in comparison to DM3, ultimately created a more organized network structure. Figure 5-1 further illustrates this more organized structure of the combined six (6) final networks for DM3 and DM8 through the compact nature of the network in a force-directed graph form. Closer clustered nodes/neurons towards the graph center have a higher centrality to the network. The graphical analysis results of DM8 showed a distinct shift from structural materials to building usage once social parameters were added, without losing the importance of critical variables such as building height. In fact the hazard and social demographics appeared more prominent than the standard engineering-related factors.

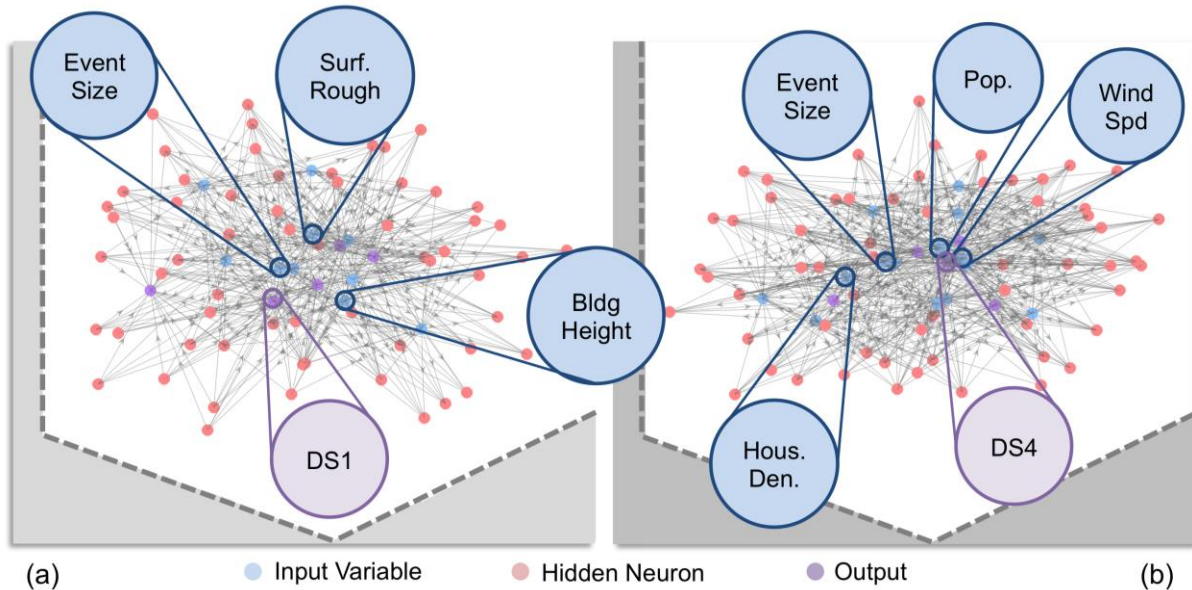


Figure 5-1 3D Force directed graphs of combined network ensembles for (a) DM3 and (b) DM8.

The focus on social demographics and the organization of the output damage state centralities, specifically, also highlight the concept of social vulnerability becoming more vital at the extensive damage point, as was also discussed by Burton (2010). The shortest path analysis of DM8 highlights a strong connection between owning tenure and DS3 (similar to “extensive damage”). The DS4 output neuron was also more connected within the DM8 structure instead of DS1, within the DM3 structure.

The addition of housing density, percent area forested, and tenure to DM8 proved to produce better network connections. The further implications of this stretch to how these parameters affect the resulting outcome. Through sensitivity analyses where each variable was incrementally increased while all other variables remained the same for a hypothetical scenario, the increase of housing density and area forested behaved as expected and resulted in higher damage states. This was essentially confirmation of increased potential for debris impacts resulting in increased damage to a structure. The more interesting variable was that of tenure, as the increase of renting or owning tenure on their own did not provide any distinguishable results. However, the decrease in both of these, therefore the increase in other tenure, such as

government subsidized housing, did show an increase in resulting damage state (Figure 5-2). If all other variables are the same (wind speed and type of building) but the neighborhood has a larger percentage of those classified under “other tenure”, the resulting damage states will be higher. In combination with social vulnerability analyses for owning and renting tenure, this demonstrates further that the building use and maintenance is critical to the resulting damage state from an extreme event. Those who own a building are more likely to keep up with maintenance and invest, if able, in additional measures to further increase the structure’s wind loading resistance. This leaves individuals renting or residing in other structures in more severely damaged buildings.

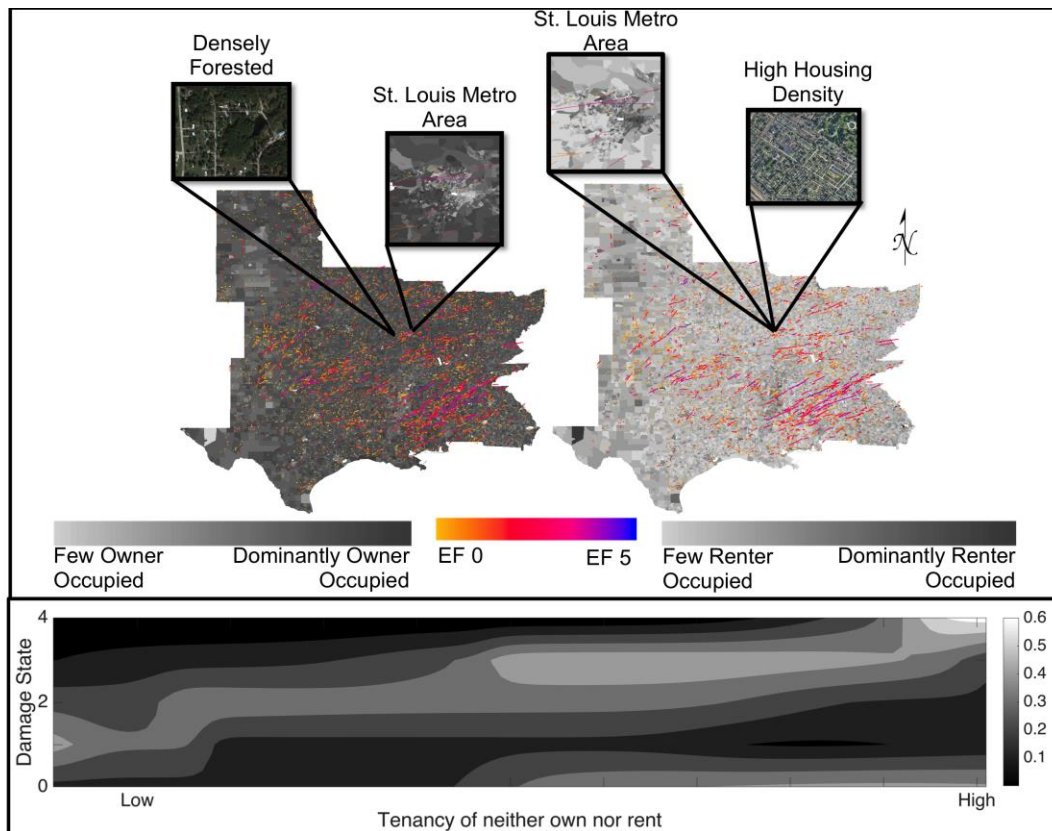


Figure 5-2 The effect of increasing the amount of structures in a neighborhood classified as “other tenure” on resulting damage states and the distribution across tornado alley with satellite image examples of highly forested and high housing density areas.

Following the damage models, the creation of recovery models performed better when parameters such as tenure, housing density, and area forested were included. For example,

RM7 did not include the area forested or housing density and was listed as one of the poorer performing networks. Of the 15 recovery model networks, the two evaluated (RM2 and RM8) did include area forested, housing density, and tenure. However, the differences between these two from the analysis results show more in common than different. The analysis of the damage models resulted in more apparent differences within the ANN building process, the graphical analysis, and the hindcast. RM2 and RM8 mostly showed similar resulting network structures, with both networks showing organization (Figure 5-3). The shift seen in the damage models once social factors were added was not seen in the recovery models once structural characteristics (building materials) were added. Additionally, while both the damage and recovery models showed negligible differences in hindcasting error, the recovery models also switched which model performed slightly better for the exact match and approximated error. Both RM2 and RM8 produced acceptable errors when considering a +/- 6 month approximation and could both be considered viable model structures.

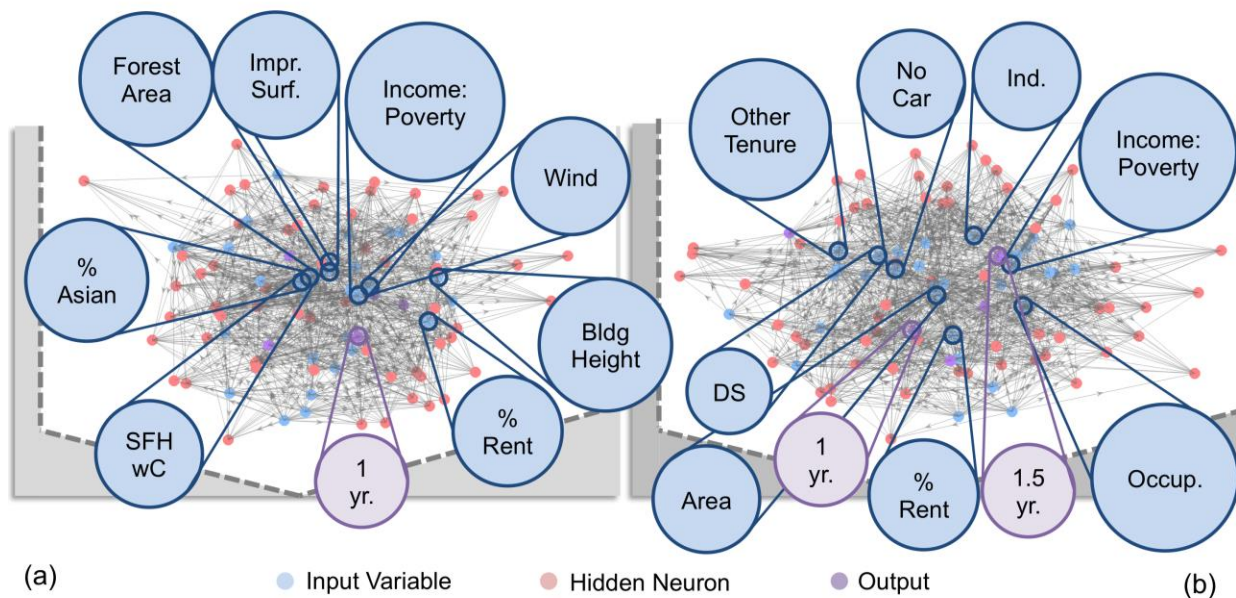


Figure 5-3 3D Force directed graphs of combined network ensembles for (a) RM2 and (b) RM8.

The lack of any significant difference between recovery models in the overall analysis could also indicate missing variables. Either a specific connection type was not captured in the

15 model options, or there were other factors to consider that have not yet been highlighted in the literature. The 15 RMs did not include a specific parameter related to time to obtain building permits and set up construction jobs. The assumption that preceded creating these models was that some social characteristics may inherently overlap with these factors, such as low income or occupation, by tying an ability to manage the system and obtain a permit within a reasonable time frame to a general delay time characterized by social demographics. However, no variables were included on the policy system itself, which could be considered an oversight within this research.

It is also plausible that there are factors that contributed to recovery in past events that cannot yet be captured with a numerical data point. For example, both RM2 and RM8 included the “1 year residency” variable as an attempt to show ties to a community. There is a concept of community mentality that could have a significant effect on how long it would take a community to recover. How close together (socially) is the community? Do they offer to help each other? Is their outlook following an event more accepting or defeatist? These parameters could arguably be more important than any other variables considered herein, but are not easily quantifiable for the purposes of modeling with ANNs.

The potential importance of abstract social concepts, along with the lack of consistent differences between RM2 and RM8, highlighted the low significance of structural characteristics to the recovery process. These characteristics were vital in modeling damage state, or initial impact, but did not appear as critical to modeling recovery time. Within the terms of resilience, this further highlights that the importance of engineering variables exists at the initial impact stage, while the social characteristics are integrated at *all* points along the resilience curve.

5.3 SOCIO-TECHNICAL ASPECTS OF THE 2011 JOPLIN TORNADO DATA AS IT RELATES TO THE ANN ANALYSES

The hindcasting of the Joplin tornado provided a means of evaluating modeling approaches as well as a case study to assess the ANN variable importance findings from the builds and graphical analysis. The general assumption in modeling building damage state has typically been that the more extreme the wind speed is the more damage it will cause. However, by assessing these with the social demographic characteristics identified previously, some discrepancies can be highlighted. For example, note that the first block group (A), highlighted in green, has a majority of its buildings classified as DS4 in Figure 4-29 even though the most intense part (EF5) of the tornado was not present within its boundaries. The only block group that did not have an EF4 or EF5 region of the tornado track was Block G, which did have a very low number of DS4 buildings, while Block N contained mostly an area of EF2 and mostly DS4 or DS0 buildings. Ultimately, in terms of damage state patterns, the resulting data from the 2011 Joplin event did not directly correlate to a wind speed, which would support the hypothesis of introducing building/tree density and social characteristics into modeling building damage states, especially since most of the gathered recovery data was for residential structures and therefore did not contain a variety of building archetypes.

It appeared that areas where damage state patterns diverged from wind speed tracks consisted primarily of a relatively higher population count. There were additional pockets of buildings at higher damage states for lower wind speeds in regions of moderate or high housing density. Contradictory to the results of the ANN analysis, Blocks B & C show pockets of low damage states despite the higher percentage of other tenure structures. However, relatively speaking, the area this tornado struck was not as demographically diverse as other areas of Missouri, which made up the ANN data set. From the selected social demographics shown in Figure 5-4, single female head of household and those working in service industries are the more variable demographics within the Joplin area.

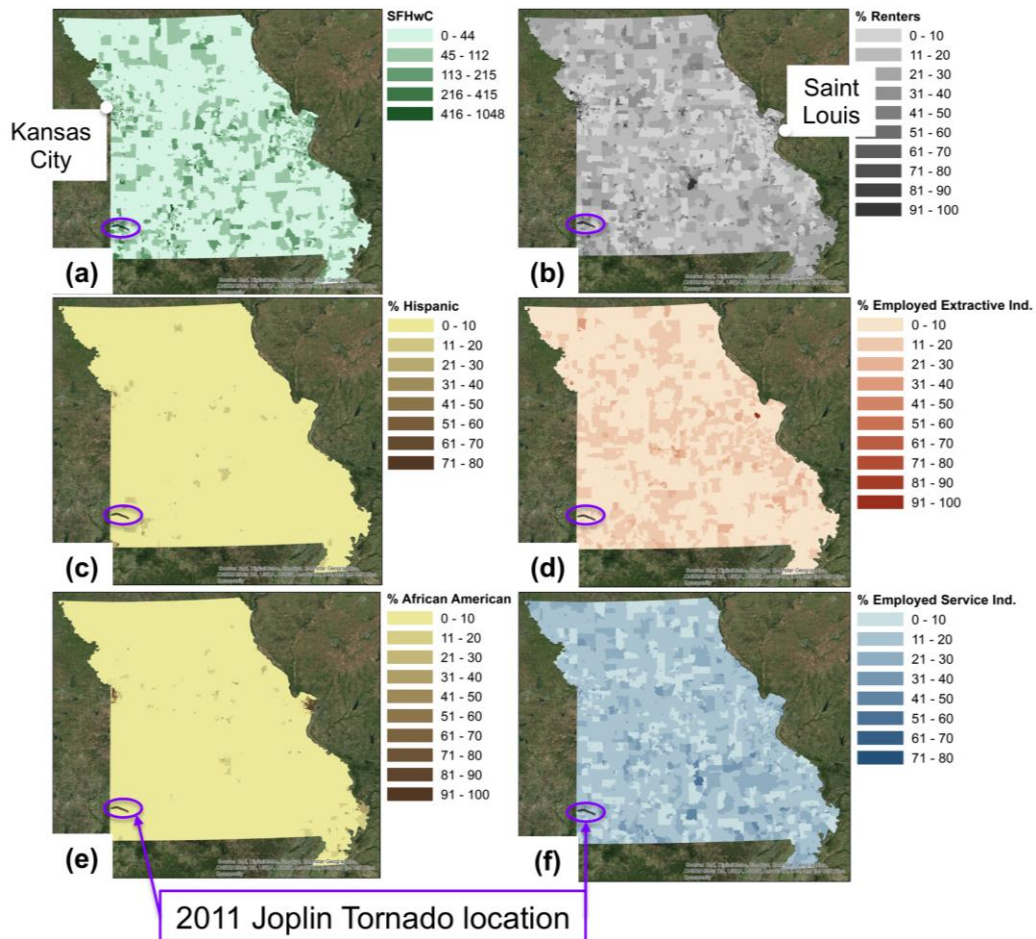


Figure 5-4 Census Block Group distribution of (a) single female head of household with children (SFHwC), (b) renting tenure, (c) Hispanic population, (d) extractive industry employment, (e) African American population, and (f) service industry employment for the state of Missouri.

While industry employment and single female head of household with children were not included in the damage models, they were in the recovery models. Specifically, block groups of greater than 5% single female heads of households with children did correlate to slower recovery times of DS3 buildings (Table 4-5) following the 2011 Joplin tornado. The ANNs showed single female heads of households as a vital variable with strong ties to a 1-year recovery time in RM8. Given the slower recovery times within the block groups of higher concentration of this demographic, this would suggest that the strong tie to 1-year recovery with the ANN refers to a lower number of single female heads of households with children.

Therefore, if a block group has a low number of single female heads of households with children, then there is a strong correlation to recovering within one year.

The ANNs also demonstrated a potentially weak connection between the median year built and a 1.5-year recovery time (RM8), as well as a potentially strong connection between the building damage state and a 1-year recovery time (RM2). Within the Joplin data, older buildings tended towards slower recovery times. Within the RM8 model, this may illustrate a dividing line between 1- and 2-year recovery times as it relates to year built. In other words, the stronger connections within the network to <1.5 years to recover and >1.5 years to recover could correlate to post-1970 structures and pre-1970 structures, respectively. Median year built was not included as a variable within the RM2 structure, which may explain why the strong connection to damage state did not remain for the RM8 structure once structural variables were added, including year built.

While the Joplin data did provide some supporting evidence for the importance of the single female head of household variable and the use of the median year built variable for modeling recovery, the lacking demographic diversity for other variables in this region limited any further analysis. Additionally, 100% of residents in Joplin had wind insurance and this case study has historically been regarded as a quickly recovering community from such an extreme event, which may provide some additional insight into the error sources in hindcasting this event.

5.4 SUMMARY OF FINDINGS AND LIMITATIONS

The results and discussions above highlight findings within the realm of modeling community resilience that could further assist in developing more accurate models through focusing on the factors listed by a categorized importance within the ANNs shown in Table 5-1. An important fraction (I_i) was calculated by multiplying the centrality scores (C and D) with the

shortest past scores (P) for the combined network for each variable (v) and summed across each damage state (DS) such that

$$I_f(v) = \sum_{DS=0}^{DS=4} [P(v)_{DS} \times D_{DS_{in}} \times D(v)_{out} \times C_{DS_{in}} \times C(v)_{out} \times$$

$$R(v)_{DS}] \begin{cases} R = 1.5, \text{strong connection} \\ R = 0.5, \text{weak connection} \\ R = 1, \text{all others} \end{cases}$$

(5-1)

where the R-values are considered for strong/weak connections that were identified in conjunction with the individual network analysis in Figures 4-9, 4-23, and 4-24. The Importance (I) was then calculated by dividing each variable's importance factor by the maximum importance factor (I_M) in the network set, such that

$$I(v) = \frac{I_f(v)}{I_M} \tag{5-2}$$

The general findings are outlined as follows:

- ❖ ANNs using BR were found to be comparable to physics-based methods in terms of hincasting accuracy for damage state and provide an ability capture sociological, structural, and debris potential in a combined model.
- ❖ The combination of total population, building tenure, housing density, and area forested with hazard and structure characteristics produced more cohesive patterns than that of solely structural and hazard characteristics. These models include the presence of social contributions that are not able to be covered within wind codes.
- ❖ Building tenure is a critical variable for modeling damage state and increases in “other tenure” (such as government subsidized housing) increase the resulting damage state.

- ❖ Single female heads of households with children were shown to be a critical variable to recovery, with >5% of the population falling within this demographic indicating slower recovery times.
- ❖ The Median Year Built of structures within a census block group correlates to slower recovery times and may be the driving structural characteristic when combined with socioeconomic demographics for recovery modeling.
- ❖ Top 5 most critical variables for modeling damage states (Table 5-1) Wind Speed, % Owner Occupied, tornadic versus straight-line winds (Wind Type), Building Occupancy Code, and Total Population in census block group.
- ❖ Top 5 most critical *concepts* for modeling building stock recovery (Table 5-1) considering both ANN recovery models and Joplin Data): Wind Speed, Building Height/Categorizations (Occupancy, Damage State, and Median Year Built), area densities (Population, Surface Roughness, Forested Area, Impervious Surfaces, and housing densities), Tenure (rent, own, and other), and SFHwC.
- ❖ Graph theory concepts may provide a means to better understand the “black-box” of AI and could potentially inform physics-based models by highlighting relationships between certain variables.

Table 5-1 Calculated importance (I) values for the variables used in DM8, RM8, and RM2 ANNs.

Damage State Modeling (DM8)		Recovery Modeling			
Importance	Variable	RM8 Importance	Variable	RM2 Importance	Correlation to Joplin
1	Wind Speed	1	Wind Speed	1	
0.902	% Owner Occupied	0.863	Height	0.947	
0.835	Wind Type	0.862	Damage State	0.481	
0.828	Occupancy	0.817	Population	0.385	X
0.770	Population	0.762	No Vehicle	0.374	X
0.724	% Renter Occupied	0.728	Event Size	0.429	
0.706	Roughness	0.724	Occupancy	0.767	
0.703	Event Size	0.644	Roughness	0.649	
0.693	Median Year Built	0.630	Walls		
0.665	Forested	0.594	Forested area	0.914	
0.620	Height	0.594	Roof Shape		
0.579	Roof type	0.583	Service Ind.	0.297	
0.573	Housing density	0.538	Impervious Surfaces	0.810	
0.500	Walls	0.533	Income:Poverty	0.444	
0.495	Roofing	0.502	Roofing		
		0.502	Median Age	0.467	X
		0.480	SFHwC	0.867	X
		0.465	Other Tenure	0.517	X
		0.456	Extractive Ind.	0.378	
		0.431	Footprint	0.691	
		0.427	Median Year Built		X
		0.426	Wind Type	0.399	
		0.365	Over 65 y.o.	0.447	
		0.358	Rent	0.911	
		0.356	Housing Density	0.506	X
		0.320	Group Quarters	0.404	
		0.308	Per Capita Income	0.452	
		0.292	Disability	0.296	
		0.258	1 yr. Residence	0.449	
		0.253	Own	0.514	
		0.174	Population Density	0.401	
			% Asian	0.663	
			% Native American	0.481	
			% African Amer.	0.459	
			% Hispanic	0.312	

These findings were determined with consideration of the errors and limitations for such modeling and analytical approaches. The determination of a building's damage state is, by definition, a qualitative assessment. This resulted in differences across the actual data tallied from post-storm surveys as well as in the data collection for ANN training. The individuals collecting post-survey data and ANN training data were different and would therefore observe images of buildings slightly differently. This is where the approximation error analysis by grouping DS1+DS2 and DS3+DS4 together attempted to consolidate such errors. Similarly, the +/- 6 months approximate analysis for recovery would have consolidated such errors for recovery modeling. In the case of recovery, the Joplin data set, provided by Kent State University, was also post-processed by at least three different researchers, which introduced such error to the hindcast data set. The error contributions of modeling using ANNs primarily resulted from data availability and sampling error since machine learning methods are only as good as the data set available. Data used to build these ANNs included what could be found through publically available data sources, which would leave out more detailed accounts on the individual building level as well policy codes for emergency management by county. The same data may also be skewed as individuals are more likely to document extreme damage and since this data was only gathered for a specific U.S. state. Data was only available in shapefile form from recent years and collected for the state of Missouri, whereas larger data sets are more desirable for machine learning methods. U.S. Census shapefile data had margins of error for each demographic that also carried on into the ANNs. The main sources of error for this research were therefore considered tied to data sampling quality, consistency, and availability.

Data availability was also a limitation of ANN modeling as the models must be built for reasonable application across various locations and hazards. If data was not available for constructing a training data set or if it would not be available if real-world use, it was not used. This included many data points found within the NWS Damage Survey Viewer that did not have images to properly categorize a structure by its building materials. However, the biggest

limitation was brought to attention in the recovery modeling, in that ANNs require quantifiable data. If there was a concept that does not yet have a numerical quantification or has not yet been considered when evaluating community resilience and recovery, it could not be included within the ANNs.

For the graphical analysis, the errors related to the results found could tie to wide array of connection options with an ANN. If 100 people were to solve the same problem and all came to the same solution, the neural pathways activated to reach that solution would likely all differ. The approaches used that involved averaging multiple ANN pathways and combining multiple ANNs into a conglomerate, were performed in an attempt to minimize this error. As a limitation, a feed-forward ANN with a singular hidden layer would be considered a relatively simple graphed network. More complex ANNs (deep learning networks) or other forms of AI could potentially produce differing results. However, it is worth noting that the patterns established were found to be consistent with case studies and logical modeling approaches.

Overall, with these errors considered, the damage model would be an acceptable approach in modeling the impact portion of community resilience. However, the modeling of recovery, while proving relatively applicable due to its acceptable +/-6 month errors, could use more evaluation prior to implementation. This suggestion is based on the lack of discernible differences when using graph theory to evaluate the ANNs as well as the lowest error inconsistencies for the two hindcasting approaches (exact versus +/-6 months), The limitations, in turn call into question how data should be collected and managed in the future. If these methods are to be used, the collection and standardization of building level data post event will be necessary to produce more accurate ANNs in the future.

CHAPTER 6 CONCLUSION AND FUTURE RESEARCH

6.1 SUMMATION

The goal of this research was to create and evaluate ANNs for the use of modeling a community's building stock damage and subsequent recovery from extreme wind hazard events. Overall, the use of ANNs to model building damage could be recommended, however differences in building recovery time modeling do not appear to be well understood enough to recommend using ANNs. The graphical analysis of the final ANNs showed how network connectivity changes as social and structural, or engineering-related, characteristics were combined with hazard intensity. Primarily as social demographics were considered for building damage state, the variable importance shifted from structural components to more of *how* that structure is used and maintained. The recovery models showed less obvious differences as the variables were altered and were even inconsistent within the hindcasting phase. This lack of clear organizational shift suggests that variables may be missing from the ANNs or even perhaps that the modeling problem for building recovery is not yet fully understood on a socio-technical level. However, both the graphical analysis and Joplin case study support the importance of single female heads of households with children, building height, and damage state. Interestingly, higher percentages of single female heads of households and older structures both correlated to slower recovery times in the context of the 2011 Joplin tornado. These findings ultimately suggest that who uses a building mostly dictates its damage and recovery.

6.2 CONTRIBUTION TO COMMUNITY RESILIENCE AND INTERPRETING ARTIFICIAL NEURAL NETWORKS

Modeling community resilience is considered a multidiscipline problem with hazard, engineering, social, and economical aspects. However, currently the initial impact portion of resilience is predicted using individual engineering, social, and economical models, which are first considered independently and then combined. By using ANNs, or other forms of ML, these variables may all be included in one model that allows for simultaneous integration across disciplines in a more cohesive manner. The data variables used to create an ANN also allow for the possibility of expanding beyond the 19+ archetype constraints (and assumptions) of physics-based modeling. The variables, as outlined in previous chapters, are customizable to each building and various demographics pertaining to the location of that building within any community. While the data set used herein was collected for the state of Missouri, it could be expanded to include the rest of the U.S.

However, a typical concern with ANNs is their apparent “black-box” nature. The use of graph theory to understand the internal connections of an ANN may provide a means by which to interpret and evaluate the applicability of ANNs for various problems. Specifically, the analysis conducted herein highlighted relationships between input variables and resulting damage states that researchers desire for socio-technical considerations as well as an organizational structure to the networks. However, the ANNs modeling recovery did not illustrate similar features, leading to doubt in its accuracy and applicability for this specific modeling problem.

The results from a graphical analysis of an ANN may even provide an opportunity in future research as to how engineering and social parameters could be connected within physics-based modeling. By evaluating variable importance in data-driven models, such as ANNs, it may be possible to introduce factors of interest into the fragility building process or even fault-tree analysis. For example, it may be possible to weight the importance of certain

structural variables based on building usage, or social variables. While recovery modeling through ANNs may not be recommended at this time, the findings related to shifting variable importance within an ANN also provide a way forward in understanding which of these variables contribute to recovery and what data is perhaps missing.

6.3 FUTURE APPLICATIONS

The damage model ANNs could likely be applied for real-time events. Modeling damage state through the use of ANNs could also provide a way to streamline the modeling process. Building fragilities for multiple different building types is intensive work and the 19 fragilities provided by Memari (2018) took seven researchers over a year to construct. The ANN models herein, however just require the initial data set that can be compiled by an individual in a matter of months and is less programming-intensive. The structure of the ANNs also allows for flexibility in assigning building types by providing ID codes to the network for specific building materials. Since the graphical analysis of these ANNs highlighted patterns and critical variables in support of past research, the ANNs could be assumed at least as reliable as the current methods. Although, it is worth noting that when hindcasting the 2011 Joplin tornado, the ANN errors were determined through fitting the ID codes to the 19 archetypes defined in previous research work. The error would likely improve if each structure could be coded more specifically than the 19 options.

The recovery models, however, need further work with potential collaboration from multiple county assessor offices and building departments to address missing parameters that would relate to building permit and construction times on the building level. This data was not readily available and should an entire state cooperate in providing such data, the viability of this modeling option could improve. The other aspect of the recovery models that remains difficult to address within any modeling approaches currently explored is that there are potentially some factors that have yet to be quantified in a usable manner. If a community has strong social

connections and a resilient/accepting mentality, the recovery time may improve. However, this is an abstract concept that cannot yet accurately be related to an ANN. There may be other forms of AI that could potentially capture this concept.

6.4 FUTURE RESEARCH

The research discussed herein was intended to provide a step forward in the use of AI for modeling community resilience as well as the use of graph theory to assess that AI similar to how MRIs (or (f)MRIs) and EEGs can be used to better understand the human brain. The next step would be to verify these findings using different AI forms, including ANNs with an increased number of hidden layers, or for the same ANN structure but using different methods to ID structural factors taken from images (change the parameters in Appendix A) or different definitions of recovery states, which may have contributed to some of the issues within the recovery ANNs. A deep learning network would consist of more than one hidden layer and the shortest path analysis would be of primary concern for confirmation within this structure. An unsupervised network may also evolve as new data becomes available and neuron connections could shift, leading to a prospective research question into what made those connections shift. Verifying the results through similar or other forms of AI could also provide an assessment of the uncertainties related to input contributions to the network by addressing the variance in the graphical analysis shortest path and centrality results.

ANNs built to a different scale may also be evaluated for the same variables used herein. For example, instead of an individual building, a single data point in the training set could be a census block group where the individual structural features (and damage state) are aggregated as a representation of the block group. Hindcasting and graphical analysis at this resolution would be of interest in addressing not only model accuracy, but if the same variable connection patterns exist once multiple buildings (or even building clusters) are aggregated up

to coarser resolutions. The block group level could then be expanded to the census tract and county level for further evaluation of these patterns.

Future advancements in AI could provide more options beyond deep learning and neural networks. The analysis conducted herein and future analysis could also aid in altering the mathematical principals for training machine so that they may be better suited for the application of community resilience. For example, after the transfer function is applied, there may be a benefit to applying a shift in the s-curve for certain input neurons to focus the data on social factors or specific structural factors, such as building height. The potential work moving forward could essentially become a looped process in which the AI provides insight into modeling parameters, while physics and case/field study results provide insight into the missing components not being capture by the AI. Subsequently, the importance factors discussed above could be combined with physics-based methods and other modeling types such that social characteristics are applied in conjunction with structural variables.

Overall, the results of this research suggest that applications in AI be constrained to problems where the variables are mostly understood but their interactions are not, or are exceedingly complicated to model. If verified, the results of this research could be best used to communicate socio-technical variable interaction when determining building damage from wind hazards, while highlighting areas of interest for modeling recovery. These modeling variables could even be used within decision-making, development of community resilience plans, and potentially public policy.

REFERENCES

- Achard, S., and Bullmore, E. T. (2007). "Efficiency and cost of economical brain functional networks." *PLoS Comput. Biol.*, 17.
- Ahrens, D. C. (2008). *Essentials of Meteorology. Essentials of Meteorology: And Invitation to the Atmosphere*, (P. Adams, A. Brady, H. Humphrey, B. Broyer, Janet Bollow Associates, and S. Kenter, eds.), Thompson Brooks/Cole.
- Almufti, I., and Willford, M. (2013). *REDiTM Rating System: Resilience-based Earthquake Design Initiative for the Next Generation Buildings*. ARUP Co.
- American Society of Civil Engineers. (2010). *Minimum design loads for buildings and other structures*. ASCE 7-10, Reston, VA.
- Attary, N., van de Lindt, J. W., Mahmoud, H. N., Smith, S., Navarro, C. M., Kim, Y. W., and Lee, J. S. (2018). "Hindcasting community-level building damage for the 2011 Joplin EF5 tornado." *Natural Hazards*, 1–22.
- Bavelas, A. (1950). "Communication patterns in task oriented groups." *Journal of the Acoustical Society of America*, 57, 271–282.
- Baxt, W. G. (1995). "Application of artificial neural networks to clinical medicine." *The Lancet*, 346, 1135–1138.
- Beale, M. H., Hagan, M. T., and Demuth, H. B. (2016). "Neural Network Toolbox (TM) User's Guide." *MathWorks*, (June), 1–558.
- Beale, M. H., Hagan, M. T., and Demuth, H. B. (2018). *Neural Network Toolbox™ User's Guide*. Natick.
- Beauchamp, M. A. (1965). "An improves index of centrality." *Behavioral Science*, 10, 161–163.
- Bellman, R. (1958). "On a routing problem." *Quarterly of Applied Mathematics*, 16(1), 87–90.
- Borden, K. A., and Cutter, S. L. (2008). "Spatial patterns of natural hazards mortality in the

- United States.” *International Journal of Health Geographics*, <<http://www.ij-healthgeographics.com/content/7/1/64>>.
- Bruneau, M., Chang, S. ., Eguchi, R. T., Lee, G. G., O'Rourke, T. D., Reinhorn, A. M., Shinozuka, M., Tierney, K. T., Wallace, W. A., and von Winterfeldt, D. (2003). “A framework to quantitatively assess and enhance the seismic reliance of communities.” *Earthquake Spectra*, 19(4), 733–752.
- Bryant, E. (2005). *Natural Hazards*. Cambridge University Press, Cambridge, United Kingdom.
- Bullmore, E., and Sporns, O. (2009). “Complex brain networks: Graph theoretical analysis of structural and functional systems.” *Nature Reviews Neuroscience*, 10(3), 186–198.
- Buntine, W. L., and Weigend, Andreas, S. (1991). “Bayesian Back-Propagation.” *Complex Systems*, 5, 603–643.
- Burton, C. G. (2010). “Social Vulnerability and Hurricane Impact Modeling.” *Natural Hazards Review*, 11(2), 58–68.
- Cajal, S. R. (1995). *Histology of the Nervous System of Man and Vertebrates*. Oxford University Press, New York.
- CanStockPhoto. (n.d.). “Age illustrations and clipart.” <<https://www.canstockphoto.com/illustration/age.html>> (May 9, 2018).
- Centre for Research on the Epidemiology of Disasters. (2018). “EM-DAT The International Disaster Database.”
- Cimellaro, G. P., Reinhorn, A. M., and Bruneau, M. (2010). “Framework for analytical quantification of disaster resilience.” *Engineering Structures*, Elsevier Ltd, 32(11), 3639–3649.
- ClipartXtras. (n.d.). “28+ Collection of It People Clipart.” <<https://clipartxtras.com/categories/view/44e65324ff0db99c963363de27e786b1482e5ee4/it-people-clipart.html>> (May 9, 2018).
- Constantinescu, R., Lazarescu, V., and Tahboub, R. (2008). “Geometrical Form Recognition

- Using 'One-Step-Secant' Algorithm in Case of Neural Network." *U.P.B. Sci. Bull., Series C*, 70(2), 15–28.
- Curtis, A., and Fagan, W. F. (2013). "Capturing Damage Assessment with a Spatial Video: An Example of a Building and Street-Scale Analysis of Tornado-Related Mortality in Joplin, Missouri, 2011." *Annals of the Association of American Geographers*, 103(6), 1522–1538.
- Cutter, S. L. (1996). "Vulnerability of Environmental Hazards." *Progress in Human Geography*, 20(4), 529–539.
- Cutter, S. L., Barnes, L., Berry, M., Burton, C., Evans, E., Tate, E., and Webb, J. (2008). "A place-based model for understanding community resilience to natural disasters." *Global Environmental Change*, 18(4), 598–606.
- Cutter, S. L., Boruff, B. J., and Shirley, W. L. (2003). "Social Vulnerability to Environmental Hazards." *Social Science Quarterly*, 84(2), 242–261.
- Cutter, S. L., and Emrich, C. T. (2006). "Moral Hazard, Social Catastrophe: The Changing Face of Vulnerability along the Hurricane Coasts." *The ANNALS of the American Academy of Political and Social Science*, 604(1), 102–112.
- Dawson, C. W., and Wilby, R. L. (2001). "Hydrological modelling using artificial neural networks." *Progress in Physical Geography*, 25(1), 80–108.
- Diestel, R. (2017). *Graph Theory*.
- Ellingwood, B. R., Culter, H., Gardoni, P., Peacock, W. G., van de Lindt, J. W., and Wang, N. (2016). "The Centerville Virtual Community: a fully integrated decision model of interacting physical and social infrastructure systems." *Sustainable and Resilient Infrastructure* 2, 1(3–4).
- Ellingwood, B. R., Rosowsky, D. V., Li, Y., and Kim, J. (2004). "Fragility Assessment of Light-Frame Wood Construction Subjected to Wind and Earthquake Hazards." *Journal of Structural Engineering*, 130(12), 1921–1930.
- Ellingwood, B. R., and Tekie, P. B. (1999). "Wind Load Statistics for Probability-Based Structural

- Design." *Journal of Structural Engineering*, 125(4), 453–463.
- Emojipedia. (n.d.). "Emojipedia." <<https://emojipedia.org>> (May 9, 2018).
- Fair, D. A., and et. al. (2007). "Development of distinct cortical networks through segregation and integration." *Proceedings of the National Academy of Sciences*2, 13507–13512.
- Federal Emergency Management Agency (FEMA). (2009). *Multi-hazard loss estimation methodology - Hurricane Model. HAZUS-MH-MR4 Technical Manual*. Washington, D.C.
- FEMA. (n.d.). "Disaster Declarations." <<http://www.fema.gov/disasters>>.
- Flanagan, B. E., Gregory, E. W., Hallisey, E. J., Heitgerd, J. L., and Lewis, B. (2011). "A Social Vulnerability Index for Disaster Management." *Journal of Homeland Security and Emergency Management*, 8(1).
- Fothergill, A., and Peek, L. A. (2004). "Poverty and disasters in the United States: A review of recent sociological findings." *Natural Hazards*, 32(1), 89–110.
- Freeman, L. C. (1979). "Centrality in social networks: Conceptual clarification." *Social Networks*, 1, 215–239.
- GalleryYoPriceVille. (n.d.). "Money." <https://gallery.yopriceville.com/Free-Clipart-Pictures/Money-PNG/Wads_of_Money_Transparent_PNG_Clip_Art_Image#.W4_0162ZOi4> (May 9, 2018).
- Geis, D. (1997). "Disaster Resistant Communities: A Community-Based Approach to Hazard Mitigation." *The CUSEC Journal*, 4(1), 1–2.
- Gill, P. E., Murray, W., and Wright, M. H. (1981). *Practical optimization*.
- Godschalk, D. R. (2003). "Urban Hazard Mitigation: Creating Resilient Cities." *Natural Hazards Review*, 4(3), 136–143.
- Goodman, R., Speers, M., McLeroy, K., Fawcett, S., Kegler, M., and Parker, E. (1998). "Identifying and defining the dimensions of community capacity to provide a basis for measurement." *Health Education & Behavior*, 25, 258–278.

- Google. (2018). "Google Maps."
- Gordon, J. (1978). *Structures*. Penguin Books, Harmondsworth, U.K.
- Hall, S. G., and Ashley, W. S. (2008). "Effects of Urban Sprawl on the Vulnerability to a Significant Tornado Impact in Northeastern Illinois." *Natural Hazards Review*, 9(November), 209–219.
- He, Y., Chen, Z., and Evans, A. C. (2008). "Structural insights into aberrant topological patterns of large-scale cortical networks in Alzheimer's disease." *Journal of Neuroscience*, 28.
- Herseth, A., and Ashley, E. (2013). *FEMA Mitigation Assessment Team Program: Observations and Recommendations Since Hurricane Andrew*. Digital Hurricane Consortium.
- Holling, C. (1973). "Resilience and Stability of ecological systems." *Annual Review of Ecology and Systematics*, 4, 1–23.
- Holmes, J. D., and Syme, M. J. (1994). "Wind Loads on steel-framed low-rise buildings." *Steel Construction (Australian Institute of Steel Construction)*, 28, 2–12.
- IBC. (2007). "Chapter 3: Use and Occupancy Classification." *Oregon Structural Specialty Code*.
- Joplin Schools. (2019). "Attendance Zones." http://www.joplinschools.org/departments/transportation/attendance_zones.
- Jungnickel, D. (2005). *Graphs, Networks and Algorithms*. Springer-Verlag, Berlin.
- Kelley, T. (2011). "Joplin Tornado Damage Photos."
- Koliou, M., van de Lindt, J. W., McAllister, T., Ellingwood, B. R., Dillard, M., and Cutler, H. (2018). "State of the Research in community resilience: Progress and challenges." *Journal of Sustainable and Resilient Infrastructure*, (January).
- Kuligowski, E. D., and Jorgensen, D. P. (2014). *Technical Investigation of the May 22, 2011 Tornado in Joplin, Missouri*.
- LeCun, Y. A., Bottou, L., Orr, G. B., and Müller, K. R. (2012). "Efficient backprop." *Lecture Notes in Computer Science (including subseries Lecture Notes in Artificial Intelligence and Lecture Notes in Bioinformatics)*, 7700 LECTU, 9–48.

- Lee, K. H., and Rosowsky, D. V. (2005). "Fragility assessment for roof sheathing failure in high wind regions." *Engineering Structures*, 27(6), 857–868.
- Lee, T. L. (2006). "Neural network predication of a storm surge." *Ocean Engineering*, 33(3–4), 483–494.
- Lin, P., and Wang, N. (2016). "Building portfolio fragility functions to support scalable community resilience assessment." *Sustainable and Resilient Infrastructure*, 1(3–4), 108–122.
- Lin, P., and Wang, N. (2017a). "Stochastic post-disaster functionality recovery of community building portfolios I: Modeling." *Structural Safety*, Elsevier Ltd, 69, 96–105.
- Lin, P., and Wang, N. (2017b). "Stochastic post-disaster functionality recovery of community building portfolios II: Application." *Structural Safety*, Elsevier Ltd, 69, 106–117.
- van de Lindt, J. W., Dao, T., Graettinger, A. J., Prevatt, D. O., Gupta, R., and Culbourne, W. (2013). "Dual objective-based tornado design philosophy." *Journal of Structural Engineering*, 139(2), 251–263.
- van de Lindt, J. W., Ellingwood, B. R., Gardoni, P., Lee, J. S., McAllister, T., Cox, D., Cutler, H., and Peacock, W. G. (2019). "The Structure of the Interconnected Networked Community Resilience Modeling Environment." *ICONHIC*, Chania, Greece.
- Livingston, I. (2017). "A look at tornadoes by rating." *U.S. Tornadoes*.
- Mahmoud, H., and Chulahwat, A. (2018). "Spatial and Temporal Quantification of Community Resilience: Gotham City under Attack." *Computer Aided Civil and Infrastructure Engineering*, 33, 353–372.
- Maloney, T. D., Ellingwood, B. R., Mahmoud, H., Wang, Y., and Lin, P. (2018). "Performance and risk to light-framed wood residential buildings subjected to tornadoes." *Structural Safety*, 70, 35–47.
- Markham, I. S., and Rakes, T. R. (1998). "The effect of sample size and variability of data on the comparative performance of artificial neural networks and regression." *Computers Ops Res.*, 25(4), 251–263.

- Marquardt, D. W. (1963). "An Algorithm for Least-Squares Estimation of Nonlinear Parameters." *J. Soc. Indust. Appl. Math.*, 11(2).
- Mathworks. (n.d.). "traingdx."
- McAllister, T. (2018). "Community Resilience Planning Guide." *Community Resilience*.
- McDonald, J. R. (2002). "Development of an enhanced Fujita scale for estimating tornado intensity." *21st Conf. on Severe Local Storms*, American Meteorological Society, Austin, TX, 174–177.
- Mehta, K. C., McDonald, J. R., and Minor, J. E. (1981). "Procedure for predicting wind damage to buildings." *J. Struct. Div.*, 107(11), 2089–2096.
- Memari, M., Attary, N., Masoomi, H., Mahmoud, H., van de Lindt, J. W., Pilkington, S. F., and Ameri, M. (2018). "Minimal Building Fragility Portfolio for Physics-based Damage Assessment of Communities Subject to Tornadoes." *Journal of Structural Engineering*.
- Micheloyannis, S., and et. al. (2006). "Small-world networks and disturbed functional connectivity in schizophrenia." *Schizophr. Res.*, 87, 60–67.
- Miles, S. B., and Chang, S. E. (2011). "ResilUS: A Community Based Disaster Resilience Model." *Cartography and Geographic Information Science*, 38(1), 36–51.
- Missouri Spatial Data Information Service. (n.d.). "Data on MSDIS."
- Møller, M. F. (1993). "A Scaled Conjugate Gradient Algorithm for Fast Supervised Learning." *Neural Networks*, 6, 525–533.
- Morrow, B. H. (1999). "Identifying and mapping community vulnerability." *Disasters*, 23(1), 1–18.
- National Association of Home Builders (NAHB). (2003). *Roof sheathing connection toleranced*. NAHB Research Center, Upper Marlboro, MD.
- National Institute of Standards and Technology (NIST). (2006). *Product List File: Generic Asphalt Shingles*.
- National Institute of Standards and Technology (NIST). (2017). "Community Resilience."
- National Severe Storms Laboratory. (n.d.). "Severe Weather 101 - Tornadoes."

- <https://www.nssl.noaa.gov/education/svrwx101/tornadoes/>.
- National Weather Service. (n.d.). "The Enhanced Fujita Scale."
- National Weather Service. (2018). "Damage Survey Viewer."
<http://apps.dat.noaa.gov/stormdamage/damageviewer/> (Feb. 2, 2018).
- Neal, R. M. (1992). *Bayesian Training of Backpropagation Networks by the Hybrid Monte Carlo Method. Tech. Rep. CRG-TR-92-1*, Toronto, Ontario, Canada.
- Nicholls, R. J., and Small, C. (2002). "Improved Estimates of Coastal Population and Exposure to Hazards Released." *Eos*, 83(28), 301–305.
- NIST. (2011). "May 22, 2011 Joplin, MO Tornado Study."
- Norris, F. H., Stevens, S. P., Pfefferbaum, B., Wyche, K. F., and Pfefferbaum, R. L. (2008). "Community resilience as a metaphor, theory, set of capacities, and strategy for disaster readiness." *American Journal of Community Psychology*, 41(1–2), 127–150.
- Onstot, L. I. (2016). *Joplin , Missouri hit by EF-5 Tornado on May 22, 2011*. Joplin, MO.
- Pilkington, S. F., and Mahmoud, H. N. (2016). "Using Artificial Neural Networks to Forecast Economic Impact of Multi-Hazard Hurricane-Based Events." *Journal of Sustainable and Resilient Infrastructure*, 1(1).
- Pilkington, S. F., and Mahmoud, H. N. (2017a). "Real-Time Application of the Multi-Hazard Hurricane Impact Level Model for the Atlantic Basin." *frontiers in Built Environment: Wind Engineering and Science*.
- Pilkington, S., and Mahmoud, H. (2017b). "Spatial and temporal variations in resilience to tropical cyclones along the United States coastline as determined by the multi-hazard hurricane impact level model." *Palgrave Communications*, 3(1).
- Powell, M. J. D. (1977). "Restart procedure for the conjugate gradient method." *Mathematical Programming*, 12, 241–254.
- Riedmiller, M. (1994). *Rprop - description and implementation details*.
- Ritchie, H., and Roser, M. (2018). "Natural Disasters." *Our World in Data*.

- Rubinov, M., and et. al. (2007). "Small-world properties of nonlinear brain activity in schizophrenia." *Human Brain Mapping*.
- Sabidussi, G. (1966). "The centrality index of a graph." *Psychometrika*, 31, 581–603.
- Scales, L. E. (1985). *Introduction to non-linear optimization*. Springer-Verlag New York, Inc., New York, NY.
- Shamseldin, A. Y. (1997). "Application of a neural network technique to rainfall-runoff modelling." *Journal of Hydrology*, 199, 272–294.
- Sherrieb, K., Norris, F. H., and Galea, S. (2010). "Measuring Capacities for Community Resilience." *Social Indicators Research*, 99(2), 227–247.
- Simmons, K. M., and Sutter, D. (2005). "Protection from nature's fury: Analysis of fatalities and injuries from F5 tornadoes." *Natural Hazards Review*, 6(2), 82–87.
- Sporns, O. (2002). "Graph Theory Methods for the Analysis of Neural Connectivity Patterns." Bloomington, IN, 169–18.
- Standohar-Alfano, C. D., van de Lindt, J. W., and Ellingwood, B. R. (2017). "Vertical Load Path Failure Risk Analysis of Residential Wood-Frame Construction in Tornadoes." *Journal of Structural Engineering*, 143(7).
- Stenabaugh, S. E., and Kopp, G. A. (2012). "Failure vs . Flight : An experimental study of wind speeds associated with roof failures of houses." *Forensic Engineering*, 9, 851–860.
- Storm Prediction Center. (2015). "10 Costliest U.S. Tornadoes since 1950."
- Supekar, K., Menon, V., Rubin, D., Musen, M., and Greicius, M. D. (2008). "Network analysis of intrinsic function brain connectivity in Alzheimer's disease." *PLoS Comput. Biol.*, 4(1000100).
- Sutley, E. J., and Hamideh, S. (2017). "An interdisciplinary system dynamics model for post-disaster housing recovery." *Sustainable and Resilient Infrastructure*, 3(3), 109–127.
- Svozil, D., Kvasnicka, V., and Pospichal, J. (1997). "Introduction to multi-layer feed-forward neural networks." *Chemometrics and Intelligent Laboratory Systems*, 39, 43–62.

- Swanson, L. W. (2003). *Brain Architecture*. Oxford University Press.
- The Federal Emergency Management Agency. (2016). "Damage assessment operations manual - A guide to assessing damage and impact." 121.
- U.S. Census Bureau. (2018). "TIGER/Line® Shapefiles and TIGER/Line® Files." <<https://www.census.gov/geo/maps-data/data/tiger-line.html>> (May 1, 2018).
- Unanwa, C. O., and McDonald, J. R. (2000). "Building Wind Damage Prediction and Mitigation Using Damage Bands." *Natural Hazards Review*, 1(November), 197–203.
- Wang, Y., Wang, N., Lin, P., Ellingwood, B. R., Mahmoud, H., and Maloney, T. D. (2018). "De-aggregation of community resilience goals to obtain minimum performance objectives for buildings under tornado hazards." *Structural safety*, 70, 82–92.
- Werbos, P. J. (1990). "Backpropagation Through Time: What It Does and How to Do It." *Proceedings of the IEEE*, 78(October), 1550–1560.
- Widrow, B., Rumelhart, D. E., and Lehr, M. A. (1994). "Neural Networks: Applications in Industry, Business and Science." *Communications of the ACM*, 37(3), 93–105.
- Yau, S. C., Lin, N., and Vanmarcke, E. (2011). "Hurricane Damage and Loss Estimation Using an Integrated Vulnerability Model." *Natural Hazards Review*, 12(November), 184–189.
- Zubrick, S., and National Weather Service. (2012). "June 29, 2012 Derecho."

APPENDIX A: ARTIFICIAL NEURAL NETWORK VARIABLES

Table A-1 Building code (surface roughness and occupancy) key for ANN inputs.

Parameter	Code Notation	Brief Description	ANN Notation
Surface Roughness Categories	B	Urban and suburban areas, wooded areas, or other terrain with numerous closely spaced obstructions having the size of single-family dwellings or larger.	2
	C	Open terrain with scattered obstructions having heights generally less than 30 ft (9.1 m). This category includes flat open country, grasslands, and all water surfaces in hurricane prone regions.	3
	D	Flat, unobstructed areas and water surfaces outside hurricane prone regions. This category includes smooth mud flats, salt flats, and unbroken ice.	4
IBC Use and Occupancy			
Assembly	A-1	Assembly uses, usually with fixed seating, intended for the production and viewing of the performing arts or motion pictures. (Theaters, concert halls, TV studios admitting an audience)	303.2
	A-2	Assembly uses intended for food and/or drink consumption. (Restaurants, Bars, Banquet halls, casinos)	303.3
	A-3	Assembly uses intended for worship, recreation, or amusement, and other assembly not classified elsewhere in Group A. (Bowling alleys, community halls, gyms, lecture halls, libraries, museums, churches, billiards, waiting areas in transportation terminals).	303.4
	A-4	Viewing of indoor sporting events (tennis courts, swimming pools, arenas)	303.5
	A-5	Viewing of outdoor sporting events (stadiums, grandstands, amusement park structures)	303.6
Business	B	The use of building or structure or a portion thereof, for office, professional or service-type transactions, including storage of records and accounts. (Airport traffic control towers, animal hospitals, banks, salons, car wash, civic admin, clinic outpatient, educational occupancies for students above 12th grade, data processing, food processing, cafeterias < 2500 sqft, labs, post offices, professional services).	304.1

Parameter	Code Notation	Brief Description	ANN Notation
Education	E	The use of a building or structure or a portion thereof, by six or more persons at any one time for educational purposes through the 12th grade. Includes occupancy of more than five children 2.5 years of age or older who receive education or personal care for fewer than 24 hours per day (day care).	305.1
Factory	F-1	Moderate hazard. (Aircraft appliances, athletic equipment, automobiles, bakeries, beverages over 16% alcohol, bicycles, boats, business machines, cameras and photo equipment, canvas, rugs, construction or agriculture machinery, disinfectants, dry cleaning, furniture, laundries, machinery, fabrics, television filming w no spectators, paper mills, film or printing, textiles, tobacco, wood)	306.2
	F-2	Low-hazard. Industrial uses that involve the fabrication or manufacturing of non-combustible materials that during finishing, packing, or processing do not involve a significant fire hazard. (Beverages with < 16% alcohol, brick and masonry, foundries, glass products, gypsum, ice, fabrication and assembly of metal products)	306.3
High Hazard	H	The use of a building or structure, or a portion thereof, that involves the manufacturing, processing, generation or storage of materials that constitute a physical or health hazard in quantities in excess of those allowed in control areas complying maximum allowable quantity limits.	
	H-1	Detonation hazard: Explosives, organic peroxide (Class UD), Oxidizer (class 4), Unstable reactive (Classes 4 & 3).	307.3
	H-2	Deflagration hazard or hazard from accelerated burning: Combustible dust, combustible liquid, cryogenic flammable, flammable gas, flammable liquid, organic peroxide (Class I), Oxidizer (Class 3), Pyrophoric, Water reactive (Class 3).	307.4
	H-3	Readily support combustion or pose a physical hazard: Combustible fiber, combustible liquid, consumer fireworks, cryogenic oxidizing, explosives (Division 1.4), flammable liquid, flammable liquid combination, flammable solid, organic peroxide (Class II & III), oxidizer (Class 2), Oxidizing gas, unstable reactive (Class 2), water reactive (class 2).	307.5
	H-4	Health hazards: corrosives, toxic materials	307.6

Parameter	Code Notation	Brief Description	ANN Notation
	H-5	Semiconductor fabrication facilities and comparable research and development areas in which hazardous production materials are used and the aggregate quantity of material is in excess.	307.7
Institutional	I-1	Occupancy shall include buildings, structures, or portions thereof for more than 16 persons, excluding staff, who reside on a 24-hour basis in a supervised environment and receive custodial care. (Alcohol/drug centers, assisted living, care facilities, group homes, halfway houses)	308.3
	I-2	Occupancy shall include buildings and structures used for medical care on a 24-hour basis for more than five persons who are incapable of self-preservation. (Foster case, Detox facilities, hospitals, nursing homes, psychiatric hospitals).	308.4
	I-3	Occupancy shall include buildings and structures that are inhabited by more than five persons who are under restraint or security. (Correctional centers, detention centers, jails/prisons, reformatories).	308.5
	I-4	Day care facilities (more than five persons who receive custodial care for fewer than 24 hours per day).	308.6
Mercantile	M	The use of building or structure or portion thereof for the display and sale of merchandise, and involves stock goods, wares or merchandise incidental to such purposes and accessible to the public. (Department stores, markets, drug stores, motor fuel-dispensing facilities, retail stores, sales rooms)	309.1
Residential	R-1	Occupancies containing sleeping units where the occupants are primarily transient in nature. (Hotels, boarding houses, congregate living facilities with more than 10 occupants)	310.3
	R-2	Occupancies containing sleeping units or more than two dwelling units where the occupants are primarily permanent in nature. (Apartment houses, non-transient boarding houses with more than 16 occupants, convents, dorms, frats and sororities, non-transient hotels, live/work units, monasteries, vacation timeshare properties)	310.4

Parameter	Code Notation	Brief Description	ANN Notation
	R-3	Houses. Occupancies where the occupants are primarily permanent in nature and not classifies as R-1, R-2, R-4, or I. (Buildings that do not contain more than two dwelling units, non-transient boarding houses with <16 occupants, transient boarding houses with <10 occupants, care facilities for <5 persons receiving care, lodging houses with <5 guest rooms)	310.5
	R-4	Occupancy shall include buildings, structures or portions thereof for more than five but not more than 16 persons, excluding staff, who reside on a 24-hour basis in a supervised residential environment and receive custodial care. (drug centers, congregate care facilities, group homes, halfway houses, social rehab facilities)	310.6
Storage	S-1	Moderate-hazard. Buildings occupied for storage uses that are not classified as S-2. (Aerosols, aircraft hangar, bags, bamboos, books and paper in rolls or packs, boots and shoes, indoor dry boat storage, glues, grains, clothing materials, sugar, tires, upholstery, wax candles)	311.2
	S-2	Low-hazard. Buildings used for the storage of noncombustible materials such as products on wood pallets or in paper cartons with or without single thickness divisions or in paper wrapping. (Asbestos, beverages <16% alcohol, cement in bags, chalk and crayons, dairy products, dry cell batteries, electrical coils, empty cans, food products, glass, ivory, metals, parking garages, stoves, talc and soap stones, washers and dryers)	311.3
Utility and Miscellaneous	U	Buildings and structures of an accessory character and miscellaneous structures not classified in any specific occupancy. (Agriculture buildings, aircraft hangars, accessory to a one- or two- family residence, barns, carports, fences taller than 6 ft, silos, greenhouses, livestock shelters, private garages, retaining walls, sheds, stables, tanks, towers)	312.1

Table A-2 Building materials and shapes key for ANN inputs.

Parameter		$\sim E$ (GPa)	Example Descriptors	ANN Notation
Materials (ordered by modulus of elasticity)	Open (N/A)	0	Stadiums	0
	Brick/ Clay	2	Brick veneer/façade, mortar connections. Typically older buildings. Older culverts.	1
	Asphalt	3	Roof shingles	2
	PVC & Plastic	3	Water pipes & house siding	3
	BUR	4	Built-Up Roofing	4
	Wood/Timber	11.3	Wood studs, drywall, wood paneling, wood shingles. Typically wont exceed 4 stories.	5
	Unreinforced Masonry (URM) or Tilt-ups	17	Concrete blocks (CMU). Typically older buildings.	6
	Concrete/ Masonry (reinforced)	30	Poured concrete walls, basements, concrete blocks	7
	Other Metals	69	Aluminum sheets, corrugated siding, metal connection brackets/nails. Typically storage facilities. Some transmission towers.	8
	Glass	75	Mainly windowed façade.	9
	Steel	200	I-beams, gusset plates, roof joists, iron pipes, transmission towers. (use "89" after a decimal point)	10 or 89
	Manufactured home		Trailers, mobile homes	0.5
Roof type/ shape (ordered by peaks)	Open	NA		0
	Flat		Same story level	1
			Various stories	1.numberofstories
	Domed		Single	2
			Multiple	2.numberofdomes
	Stepped			

Parameter		$\sim E$ (GPa)	Example Descriptors	ANN Notation
Roof type/ shape <i>(ordered by peaks)</i>	Monoslope	NA	(theta <10)	4.1
			(theta >10)	4.2
	Sawtooth		Multi-Monoslope	5.numberofslopes
	Gable		(theta <7)	6.1
			(theta >7)	6.2
	Hip			7
	Mansard			8
	Gambrel			9
	Intersecting (Gable)		Multiple (theta <10)	10.1.numberofgables
	Multiple (theta >10)	10.2.numberofgables		
Intersecting (hip)	Multiple	11.numberofhips		
Footprint Area	Extra-Small	NA	Shed, mobile home, equally small house	1
	Small		Average size house, small office	2
	Medium		Multi-person home, avg. size business office, small strip mall	3
	Large		Mall, big box, industrial buildings	4
	Extra-Large		Airports, stadiums	5

APPENDIX B: ITERATIVE ANALYSIS RESULTS FOR MODIFYING TRAINING ALGORITHM AND MODEL INPUTS

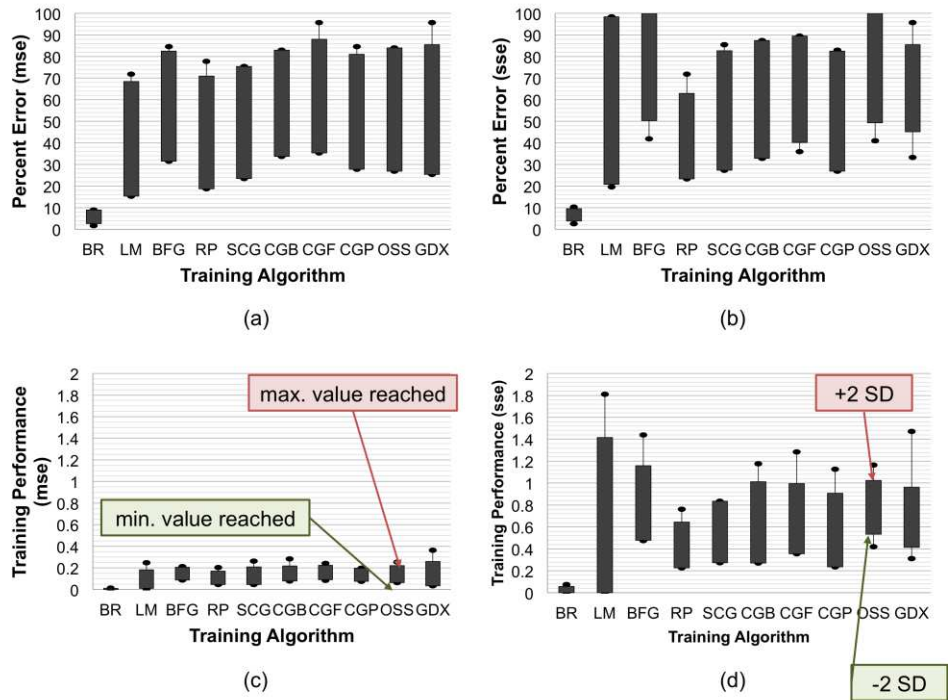


Figure B-1 DM explored algorithms' (a) percent error with MSE, (b) percent error with SSE, (c) training performance of MSE, and (d) percent error of SSE.

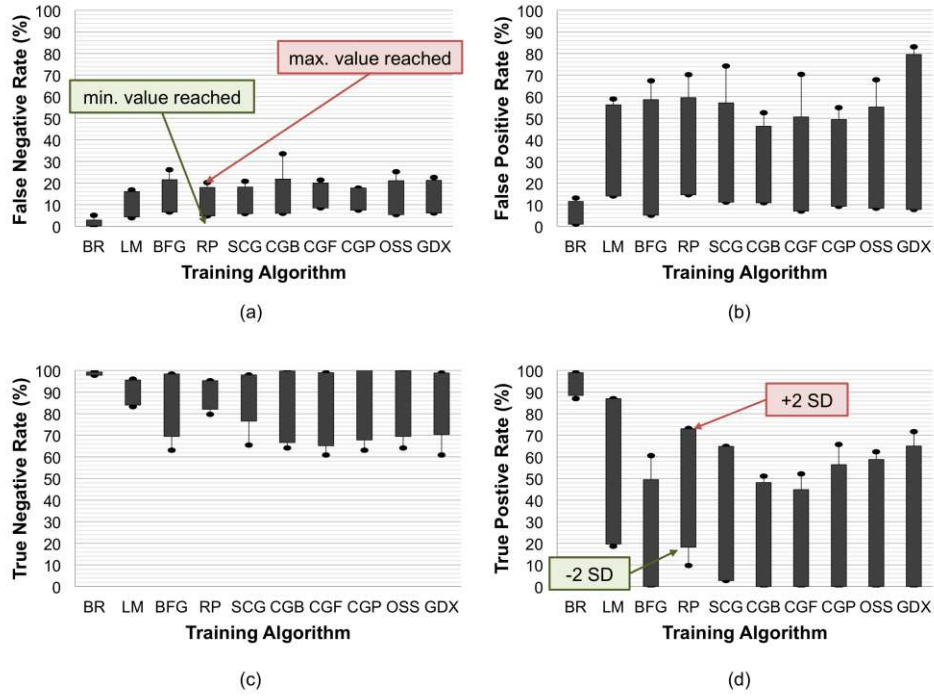


Figure B-2 DM explored algorithms' with MSE (a) FNR, (b) FPR, (c) TNR, and (d) TPR.

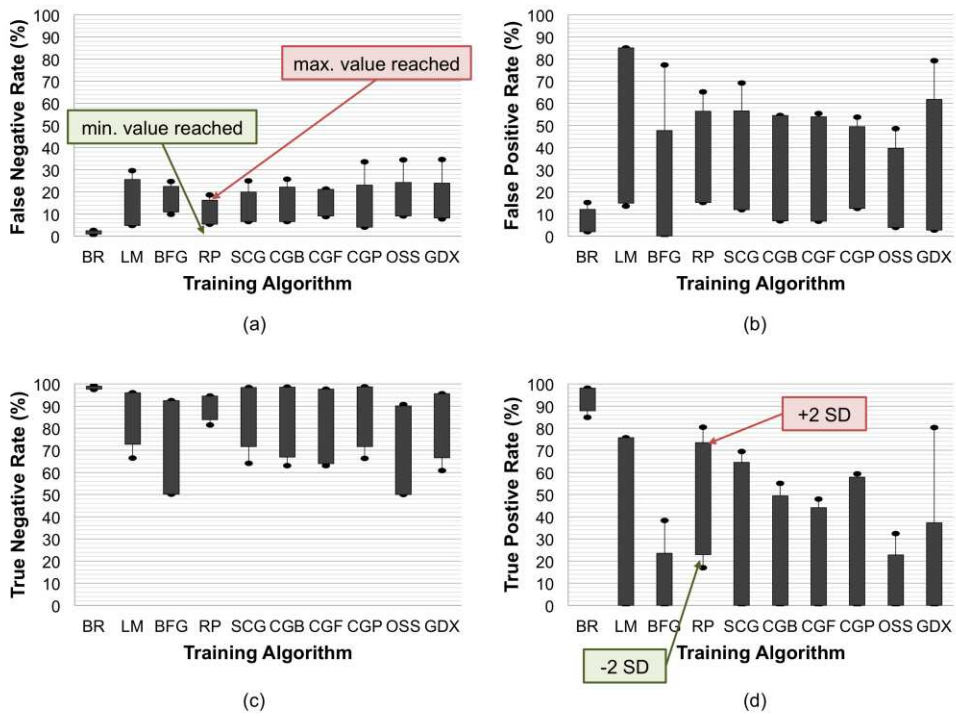


Figure B-3 DM explored algorithms' with SSE (a) FNR, (b) FPR, (c) TNR, and (d) TPR.

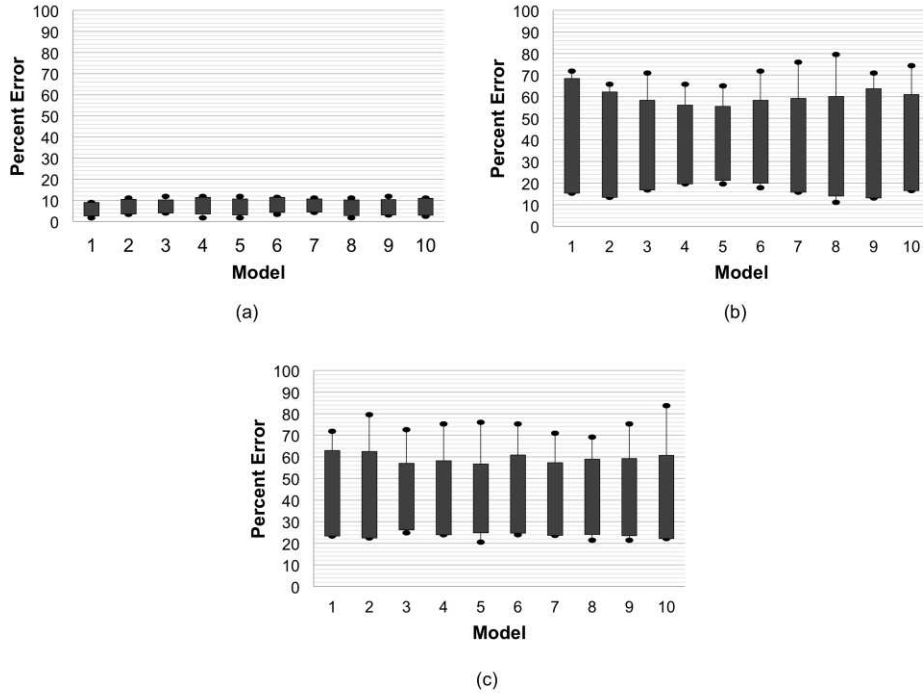


Figure B-4 Various DMs' percent error for (a) BR, (b) LM, and (c) RP training algorithms.

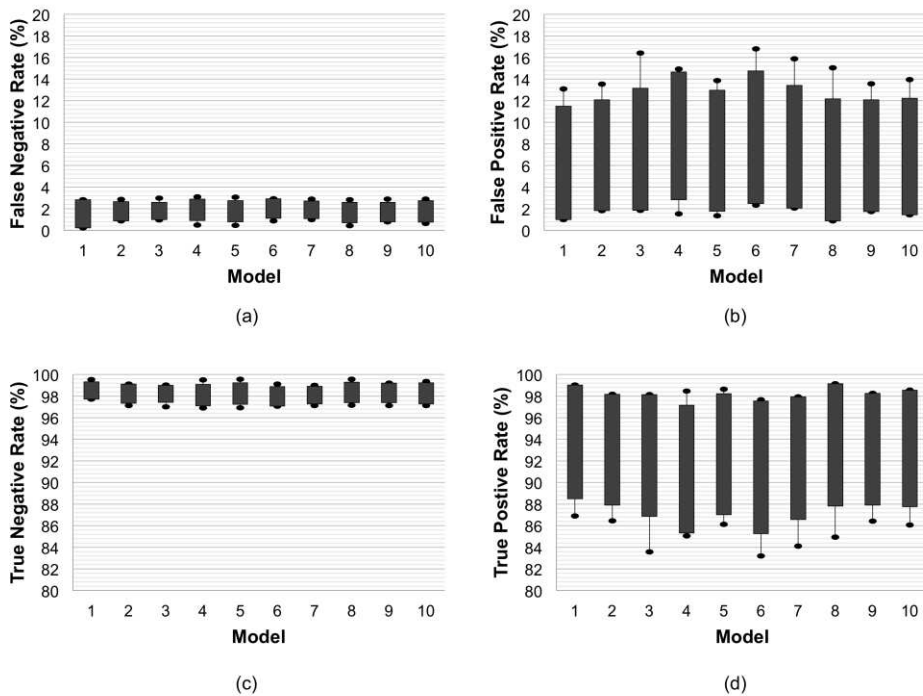
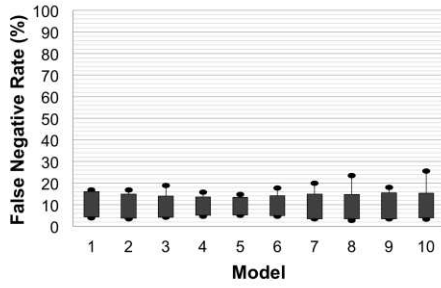
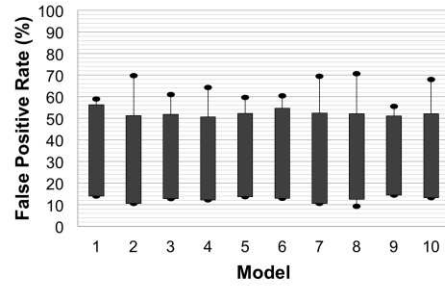


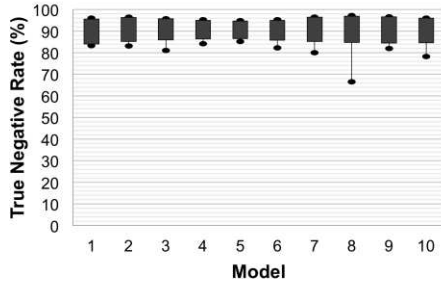
Figure B-5 Various DM (a) FNR, (b) FPR, (c) TNR, and (d) TPR for BR.



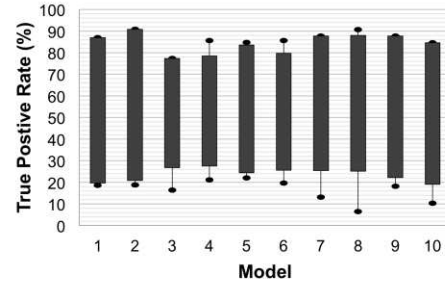
(a)



(b)

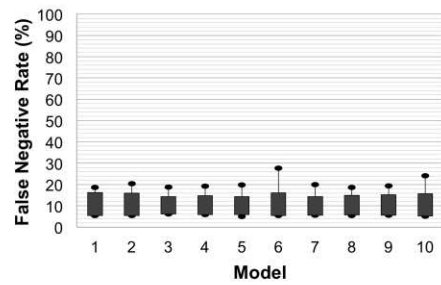


(c)

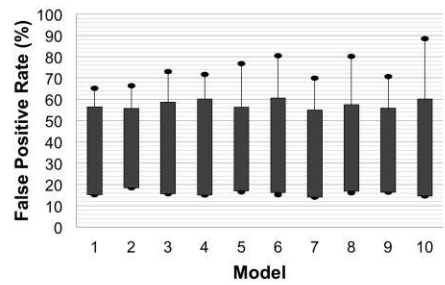


(d)

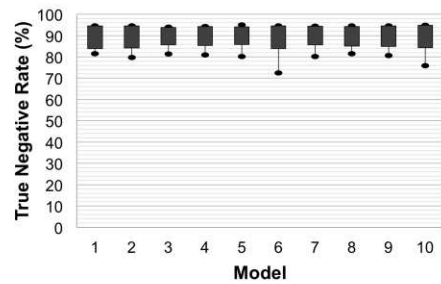
Figure B-6 Various DM (a) FNR, (b) FPR, (c) TNR, and (d) TPR for LM.



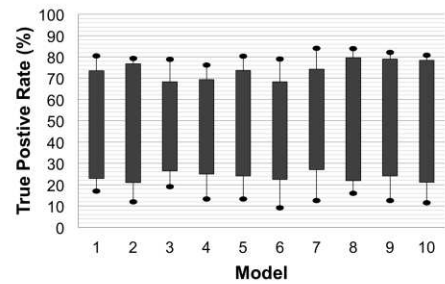
(a)



(b)



(c)



(d)

Figure B-7 Various DM (a) FNR, (b) FPR, (c) TNR, and (d) TPR for RP.

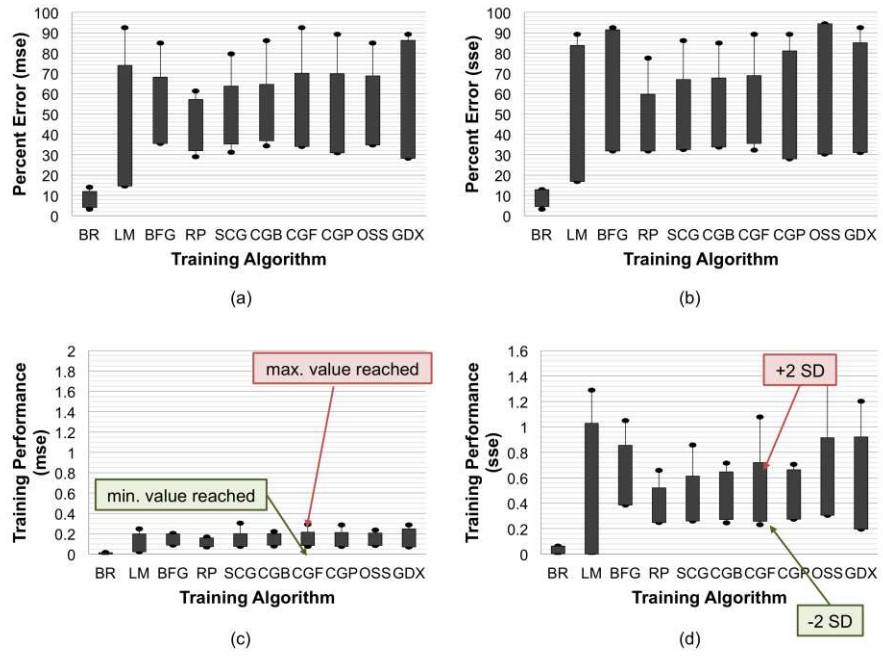


Figure B-8 RM explored algorithms' (a) percent error with MSE, (b) percent error with SSE, (c) training performance of MSE, and (d) percent error of SSE.

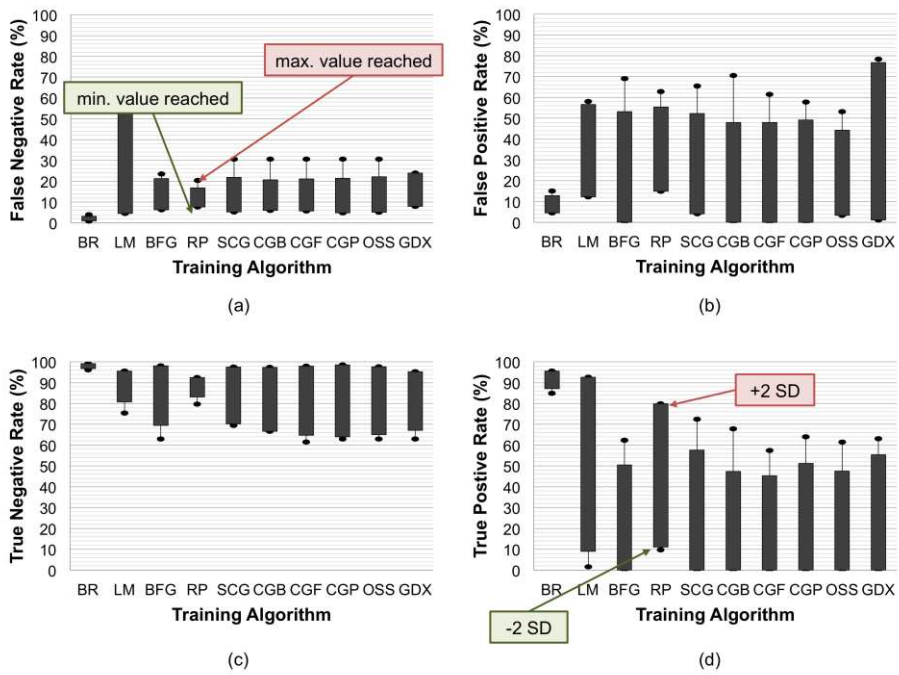
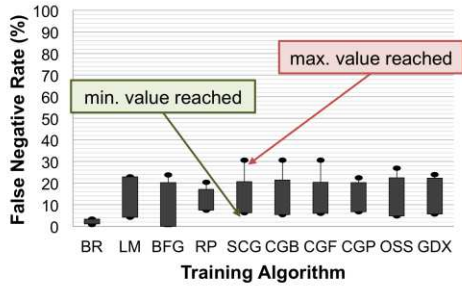
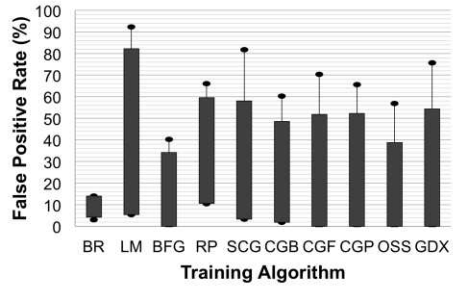


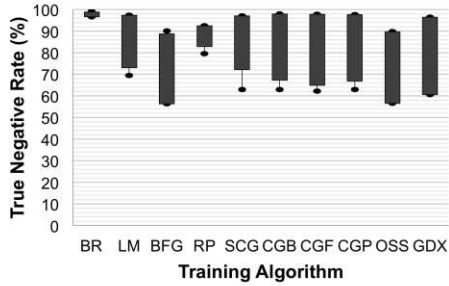
Figure B-9 RM explored algorithms' with MSE (a) FNR, (b) FPR, (c) TNR, and (d) TPR.



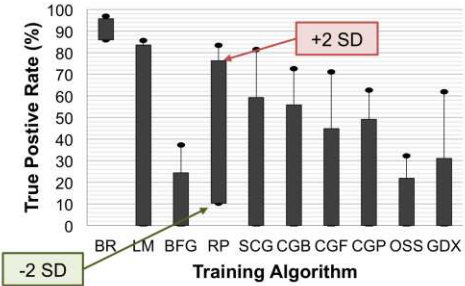
(a)



(b)

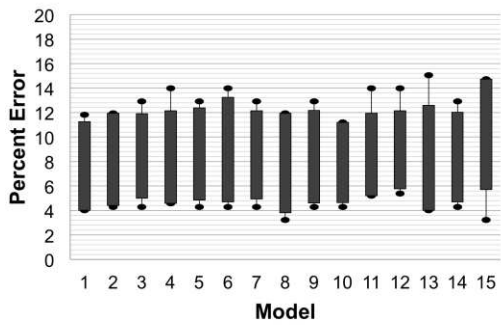


(c)

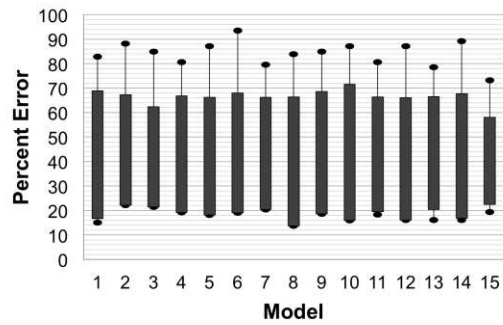


(d)

Figure B-10 RM explored algorithms' with SSE (a) FNR, (b) FPR, (c) TNR, and (d) TPR.

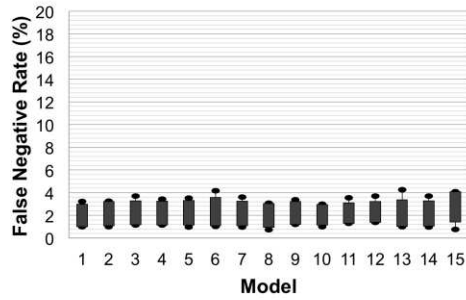


(a)

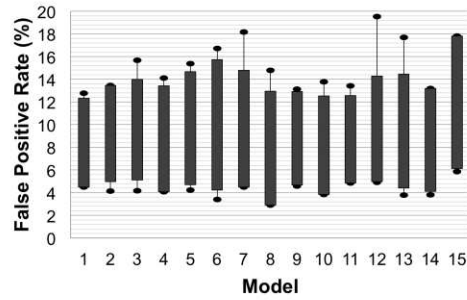


(b)

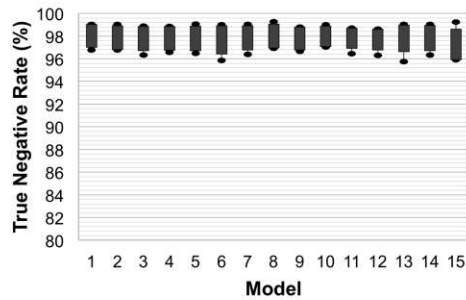
Figure B-11 Various RMs' percent error for (a) BR and (b) LM training algorithms.



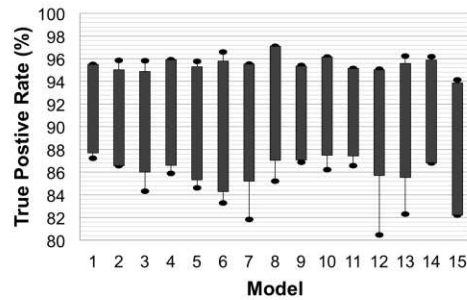
(a)



(b)

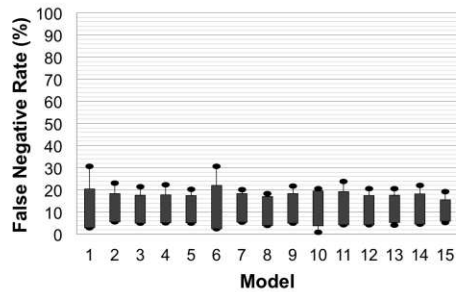


(c)

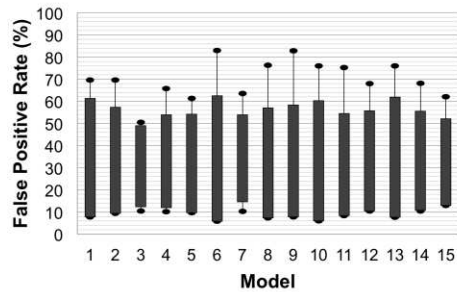


(d)

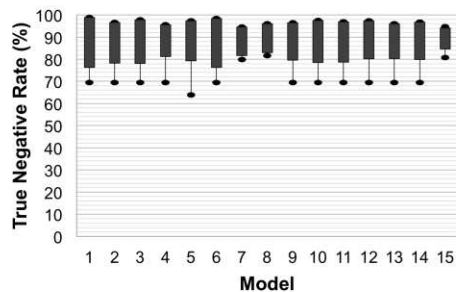
Figure B-12 Various RM (a) FNR, (b) FPR, (c) TNR, and (d) TPR for BR.



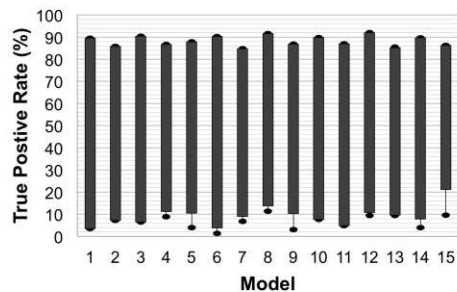
(a)



(b)



(c)



(d)

Figure B-13 Various RM (a) FNR, (b) FPR, (c) TNR, and (d) TPR for LM.